ATMOSPHERE-LAND SURFACE FLUXES AND CONTINENTAL BOUNDARY LAYER MOISTURE RECYCLING: INSIGHTS FROM STABLE WATER ISOTOPE RATIOS IN SOIL, SURFACE VAPOR AND PRECIPITATION AT A MID-LATITUDE TALL-TOWER SITE

By

ALEYA KAUSHIK

B.Sc., St. Stephen's College, 2002

M. Sc., Indian Institute of Science, 2005

M. Sc., Stony Brook University, 2011

A thesis submitted to the

Faculty of the Graduate School of the

University of Colorado in partial fulfillment

of the requirement for the degree of

Doctor of Philosophy

Department of Atmospheric and Oceanic Sciences

2018

This thesis entitled:
Atmosphere-Land Surface Fluxes and Continental Boundary Layer Moisture Recycling: Insights From Stable Water Isotope Ratios in Soil, Surface Vapor and Precipitation at a Mid-Latitude Tall-Tower Site
written by Aleya Kaushik
has been approved for the Department of Atmospheric and Oceanic Sciences

_____
Julie K. Lundquist

_____
David C. Noone

Date_____

The final copy of this thesis has been examined by the signatories, and we find that both the content and the form meet acceptable presentation standards of scholarly work in the above mentioned discipline.

Kaushik, Aleya (Ph. D., Atmospheric and Oceanic Sciences)

Atmosphere-Land Surface Fluxes and Continental Boundary Layer Moisture Recycling: Insights From Stable Water Isotope Ratios in Soil, Surface Vapor and Precipitation at a Mid-Latitude Tall-Tower Site

Thesis directed by Professor David C. Noone

Atmosphere-land surface exchanges represent the largest uncertainties in climate models used to make projections about future hydroclimate. Measurements of stable isotope ratios in water can be exploited to better understand mechanisms controlling land surface-atmosphere water fluxes, as they provide more process-level information than bulk water. This thesis examines mechanistic controls on boundary layer moisture cycling using four years of meteorological and stable isotope ratio measurements of water (δD and δ^{18}O) in vapor, precipitation, vegetation and soil from the Boulder Atmospheric Observatory (BAO), a 300-meter tall-tower site in Erie, Colorado.

First, near-surface water isotope ratios in vapor, precipitation and soil were used to evaluate the net ecosystem exchange of water at BAO. Stable water vapor isotope ratio profiles coupled with soil water isotope ratio and meteorological measurements constrained surface evaporation models to weight the contributions of rainfall, surface water vapor exchange and sub-surface vapor diffusion to soil water isotope ratios. A multi-year time series allowed for validation of model parameters, such as kinetic fractionation factor, that are not easily measurable. Results show a strong evaporative contribution from sub-surface vapor, and less diffusive control on evaporative exchange than previously thought. Reconciling isotope-derived evapotranspiration partitioning

with an isotope-independent method highlighted mechanisms and model parameterizations that are relevant for correct latent heat flux partitioning.

Next, boundary layer rain re-evaporation was measured using stable water isotope ratios in precipitation and vapor coupled with disdrometer measurements of raindrop size. Precipitation isotopes represent an integrated condensation history of the water parcel, controlled by air mass source, temperature and continental recycling along the parcel back-trajectory. Vapor isotopes show seasonality, which reflects air mass source and surface evaporative exchange. Results show that temperature equilibration explained 80% of the isotope correlations, however, the correlation for summer rainfall was much lower at 50%. Isotope-enabled models that explicitly used weighted drop size distribution information significantly improved the prediction of rainfall isotope ratios for summer rainfall, which has implications for improving representations of rainfall evaporation in isotope-enabled climate models.

These results provide critical observational constraints for further refinement of climate models that will ultimately be used to predict future biogeochemical and hydroclimate changes.

CONTENTS

TABLES

CHAPTER II

FIGURES

CHAPTER I

Introduction

1. Statement of the problem

The moisture balance of the continental boundary layer plays an important role in regulating the exchange of water and energy between the land surface and atmosphere. Water vapor is the most abundant greenhouse gas in the atmosphere, and while bulk water movement is well simulated in climate models, regional predictions of future hydroclimate rely on the ability to differentiate between contributing fluxes – e.g. from soil moisture, evapotranspiration, precipitation, infiltration and boundary layer remoistening from evaporating rainfall (Henderson-Sellers et al., 2004). Reducing the uncertainties associated with individual processes would greatly improve model representations of the water cycle and will be essential for evaluating the future strength of water vapor feedbacks and simulations of precipitation changes (Guo et al., 2006; Koster et al., 2016).

Land surface parameterization schemes in climate models specify the exchanges of mass, energy and momentum between the atmosphere and the continents, and soil moisture is known to play an important role in regulating these surface energy fluxes and land-atmosphere feedbacks (Eltahir, 1998; Guo et al., 2006; Koster et al., 2006; Small & Kurc, 2003). Near-surface moisture is controlled by a number of factors, including precipitation, infiltration and evapotranspiration. However, identifying the relative contributions of precipitation, infiltration and sub-surface exchange processes to evapotranspiration has remained challenging and leads to divergence between model simulations that can be difficult to reconcile without observational evidence of the partitioned flux terms (Good et al., 2012; Haverd et al., 2011; Rothfuss et al., 2012; Sutanto et al., 2014).

Away from the land surface in the convective boundary layer, a key feature of moisture cycling is the degree of recycling and remoistening from rain evaporation as evaporating raindrops can have a direct influence on heat and moisture budgets (Emanuel et al., 1994). Evaporating raindrops have also been linked to the formation and maintenance of downdrafts in storm systems (Bony et al., 2008; Emanuel, 1991). However, the degree to which rain evaporation contributes to moisture recycling is uncertain (van der Ent et al., 2010; Worden et al., 2007). Land-atmosphere interactions play a crucial role in moderating continental moisture fluxes (Koster et al., 2004; Seneviratne et al., 2013). Climate models simulating these interactions show a wide range of possible outcomes for land-atmosphere couplings and feedbacks (Guo et al., 2006; Koster et al., 2006; Seneviratne et al., 2010; Wei & Dirmeyer, 2010). Water vapor feedbacks are especially important in arid and semi-arid regions of the world, where water recycling and the associated greenhouse effect of water vapor can be very sensitive to humidity changes (Eltahir, 1998; Risi et al., 2010).

In order to improve understanding of the individual water cycle processes occurring in the convective boundary layer, from below the soil surface to cloud base, this thesis employs the use of stable water isotope ratio tracers. The successful use of these tracers in hydrological studies relies on the small mass differences between regular water molecules ($H_2{}^{16}O$) and the heavy isotopologues of water (HDO and $H_2{}^{18}O$), where one atom is substituted by its heavier counterpart (D or ^{2}H in place of H, and ^{18}O in place of ^{16}O). Stable water isotopologues undergo the same reactions and progress through the same pathways as regular water, but the small differences in molecular mass lead to measurable isotopic fractionations for which isotopic mass balances can be solved alongside mixing calculations to partition components. The ratio of the heavy to light isotopologue changes during phase changes (evaporation and condensation), while it is conserved

during mixing and advection. Measurements of stable isotope ratios in water can therefore be exploited to better understand the evolution of moisture processes and mechanisms controlling atmosphere-land surface water fluxes.

2. Isotope ratios and land surface exchange

Stable water isotope ratios have been used in localized watershed studies to ascertain and partition source water (Dawson, 1996; Limm et al., 2009) as well as to evaluate surface water budgets (Henderson-Sellers et al., 2004). At regional scales, knowledge of isotope fluxes has helped in the assessment of continental rainfall recycling (Risi et al., 2010) and mechanisms controlling remoistening of the troposphere (Berkelhammer et al., 2012; Gat & Airey, 2006; Noone, 2012). At global scales, water isotope ratios have been used to explore global land-atmosphere interactions (Hoffmann et al., 2000; Werner et al., 2011) and to reconstruct past environmental conditions such as ambient temperature and relative humidity (Helliker & Richter, 2008). The use of stable isotopes in reconstructing past temperatures has recently been called into question though, because the sensitivity of model-predicted isotope ratios to temperature varies depending on advective versus eddy moisture fluxes and distance from evaporation source (Hendricks et al., 2000; Jouzel et al., 1997). Understanding the processes that set sub-surface soil water isotope ratios can prove extremely useful for refining paleoclimate interpretations of stable oxygen and hydrogen isotope-based proxies and for drawing conclusions about whether or not these proxies reflect precipitation inputs or, alternatively, evaporative exchange.

The isotopic composition of water moving through the land-surface system is modified by the isotope fractionation that accompanies the phase transitions of water, primarily evaporation (Gat, 1996). Evaporation can play a dominant role in dryland ecosystems (Risi et al., 2010; Wang et al., 2012). Other changes in the isotopic composition in the terrestrial part of the water cycle

result from mixing with water bodies and from selective pools of water being involved in runoff generation or groundwater recharge (Barnes & Allison, 1988; Gehrels et al., 1998; Mathieu & Bariac, 1996). In addition, there are latitudinal and seasonal differences in the isotopic composition of precipitation (Berkelhammer et al., 2012; Buenning et al., 2012; Dansgaard, 1964), as well as large differences of the isotope composition within a rain shower or between showers of different intensity or water yields (Coplen et al., 2008; Lee et al., 2007). Processes involved in regional convective boundary layer moisture cycling are depicted in Figure 1, accompanied by notes on the isotopic effects of these processes.

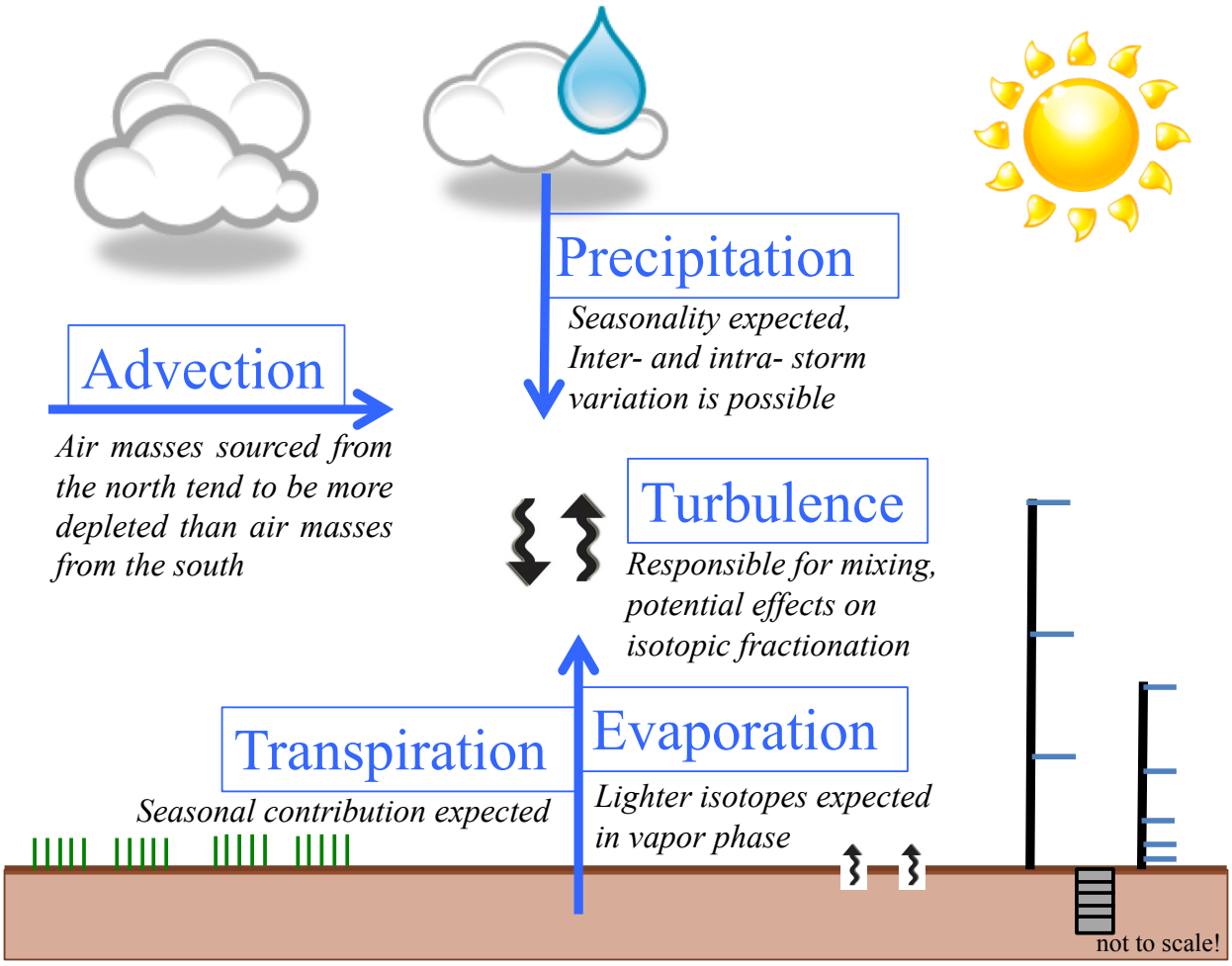

Figure 1: Key processes involved in moisture cycling in the convective boundary layer. This depiction pertains to the Boulder Atmospheric Observatory, a semi-arid grassland tall-tower

site in Erie, Colorado. Observations of co-located sources and fluxes were taken from 2012-2016 at three heights on the tall tower (100, 200 and 300 m), five heights on a 10-m tower (0.43, 0.88, 1.94, 3.94 and 8.4 m) and at 8 depths below the soil surface (2.5, 5, 10, 15, 35, 34, 70 and 85 cm).

Methods for determining the evaporative flux from isotope measurements include the Keeling mixing model approach (Keeling, 1958), the flux gradient method (Yakir & Wang, 1996), and the relaxed eddy accumulation technique (Bowling et al., 1999). More recently, the eddy covariance techniques have been used to deduce the isotopic composition of evapotranspiration (Griffis et al., 2010; Williams et al., 2004). The development of instruments making high-frequency (0.1-1 Hz) isotopic measurements of water vapor using laser absorption spectroscopy has emerged as a valuable tool in recent years (Gupta et al., 2009; Helliker et al., 2002; Lee et al., 2006; Tremoy et al., 2011) to complement eddy covariance techniques. Successful field campaigns have been conducted using these laser-based isotopic analyzers (Berkelhammer et al., 2013; Lai & Ehleringer, 2011; Noone et al., 2013; Welp et al., 2012), however, logistical problems still remain for conducting long-term field campaigns at sites with co-located meteorological measurements which are essential for the successful application of these techniques.

In addition, the one missing piece in most studies of evaporative flux is data about soil moisture, and in particular depth-resolved water isotope ratios. Due to practical difficulties involved in sampling, soil evaporation isotopic composition has been modeled rather than measured. The most commonly used model is the Craig-Gordon model (Craig & Gordon, 1965; Gat, 2008; Horita et al., 2008; Tanny & Cohen, 2008). In limited comparisons with data, significant deviations have been noted between observations and expected Craig-Gordon model results (Braud et al., 2009a, 2009b) and error estimates of up to 30% have been reported for the evaporative flux (Rothfuss et al., 2010). It would be invaluable to better validate the assumptions

about the fundamental exchange processes that underlie the Craig-Gordon model formulation for isotopic exchange because use of appropriate parameterizations would ultimately reduce uncertainty in land-surface schemes.

3. Isotopic exchange during precipitation

Evaporating raindrops are a key component of boundary layer moisture budgets, however, the mechanisms associated with moistening and drying are both poorly observed and modeled. Rain evaporation can have a direct influence on heat and moisture budgets (Emanuel et al., 1994), and are also linked to maintaining downdrafts in convective systems (Emanuel, 1991). Precipitation isotope ratios have long been used to interpret past climate, but correct reconstructions require a more detailed understanding of the moisture transport and exchange processes that predominantly control isotope signatures. Tropical rainfall isotope ratios are often interpreted as being the result of the "amount effect" (Dansgaard, 1964; Rozanski et al., 1993), but details of the contributing processes (which include condensation, downdraft moisture recycling, mesoscale organization, regional rain evaporation) are difficult to observe directly (Conroy et al., 2016). Satellite observations of HDO have been used recently to improve representations of large-scale mixing and deep convection in atmospheric general circulation models (Frankenberg et al., 2013; Galewsky et al., 2016), but these lack observational verification for mid-latitude sites. In addition, parameterizations in these models are based on average raindrop sizes and there is no verification that these calculations work across the drop-size distribution and under differing synoptic conditions.

4. Objectives

This dissertation examines which physical processes are controlling water exchange between the land surface and the atmosphere using soil water, water vapor and precipitation isotope ratio

data collected from 2012-2016 at the Boulder Atmospheric Observatory (BAO) tall-tower site in Erie, Colorado (40.050N, 105.003W, 1584 m a.s.l.). For more site details and operational history, the reader is referred to the website http://www.esrl.noaa.gov/psd/technology/bao/site/ and to Wolfe & Lataitis (2018). Co-located measurements of soil moisture, soil temperature and water isotope ratios in surface vapor are part of a long-term continuous measurement time series that was developed and maintained at this site. In addition to soil and water isotope information, ancillary meteorological data were collected from a flux tower on-site that measured air temperature and relative humidity at two heights (2 m and 10 m). This flux tower was also set up to perform eddy covariance measurements of wind, water and carbon dioxide fluxes. Meteorological data at the height of 300 m above-ground were obtained from NOAA. Locations of the met flux and isotope towers relative to the tall-tower are shown in Figure 2. The isotope and flux tower are 150 m apart.

Figure 2: Towers at the BAO site from which measurements were made.

The problem of surface latent heat flux partitioning is tackled in Chapter 2. We test several specific mechanisms and models for evaluating evapotranspiration and find that existing isotope-based methods overestimate the transpiration portion of evapotranspiration due to inaccurate

accounting of sub-surface and fractionation processes. We reconcile a revised transpiration fraction with an isotope-independent method based on gross primary productivity (Berkelhammer et al., 2016; Zhou et al., 2014) and find that contrary to existing literature, 58-84% of evaporation at this semi-arid site can be non-fractionating. This is theoretically possible through complete removal of water from soil layers, where the isotope molecules are simply moved entirely from liquid to vapor phase. This would account for an overestimation of the transpiration fraction as non-fractionating processes have historically been solely assigned to transpiration. Overall this leads to anomalously weaker than expected fractionation associated with evaporation, and this weaker fractionation is found to occur not only at the daily model time step scale, but also for bulk fluxes at synoptic scales as well as isotope climatology on seasonal scales.

The role of rain evaporation in the boundary layer moisture recycling is examined in Chapter 3. Stable water isotope ratio measurements in precipitation and vapor provide insight into air mass sources and event-based moisture dynamics, e.g. condensation history and separation of drizzle events from convection. Seasonality in vapor and precipitation isotope ratios were consistent with rain falling through an unsaturated atmosphere at the semi-arid site, and near-surface humidity was strongly correlated to isotope ratio signatures. Profiles of water vapor isotope ratios from the surface to the top of the 300 m tower are used to examine rain evaporation and ambient exchange that accompanies falling raindrops. Raindrop populations measured using a Parsivel disdrometer (that captures rain drop size and velocity) were used to evaluate existing models of rain evaporation.

An integral component of the National Science Foundation funding for this project included an outreach program at local schools in the St. Vrain Valley School District. Results from deployments and samples collected at these schools and direct connections to BAO research are

given in Appendix A. Finally, perspectives on future work are offered, including the extension of this work to other sites within the National Ecological Observation Network and coupling water isotope ratio observations to other land surface flux measurements to provide hydrological constraints on biogeochemical cycling.

CHAPTER II

Reconciling evapotranspiration partitioning models with evidence of anomalously low isotopic fractionation during evaporation in semi-arid landscapes

1. Introduction

The water balance of the continental convective boundary layer plays an important role in regulating the exchange of water and energy between the land surface and atmosphere. Soil moisture is known to moderate surface energy fluxes and land-atmosphere feedbacks (Eltahir, 1998; Guo et al., 2006; Koster et al., 2006; Small & Kurc, 2003). Accurately modeling land-atmosphere fluxes requires an improved understanding of how moisture sources in the continental boundary layer are partitioned between advective and local land surface fluxes such as evaporation and transpiration. Identifying the relative contributions of precipitation, infiltration and sub-surface exchange processes to evapotranspiration has remained challenging and leads to divergence between model simulations that can be difficult to reconcile without observational evidence of the partitioned flux terms (Good et al., 2012; Haverd et al., 2011; Rothfuss et al., 2012; Sutanto et al., 2014).

Stable oxygen and hydrogen isotope ratios in water have been used to explore global and local land-atmosphere interactions (e.g., Hoffmann et al., 2000; Werner et al., 2011, Kanner et al., 2014). The isotopic composition of water moving through the land-surface system is modified by isotopic fractionation that accompanies the phase transitions of water, primarily evaporation (Gat, 1996). This provides a tool with which to assess the explicit dependence of isotope ratios on landscape processes (Wang et al., 2012; Kanner et al., 2014). Instruments capable of making high-frequency (0.1-1 Hz) isotopic measurements of water vapor using laser absorption spectroscopy

have emerged as a valuable tool (Lee et al., 2006; Gupta et al., 2009; Zhang et al., 2010; Tremoy et al., 2011) and have been used successfully in short-term campaigns to deduce the isotopic composition of evapotranspiration (Dubbert et al., 2013; Griffis et al., 2010; Hu et al., 2014; Lai & Ehleringer, 2011; Noone et al., 2013; Williams et al., 2004) and understand environmental controls on scaling fluxes from leaf to canopy (Berkelhammer et al., 2013; Welp et al., 2012).

While the total isotopic evapotranspiration flux can be directly measured, isotopic ratios of component fluxes need to be modeled. The most commonly used model is the Craig-Gordon model (Craig & Gordon, 1965; Gat, 2008; Horita et al., 2008; Tanny & Cohen, 2008). In limited comparisons with data, significant deviations have been noted between observations and expected Craig-Gordon model results (Braud et al. 2009a, 2009b), with up to 30% error estimates reported for contributions of evaporative flux to the total evapotranspiration (Good et al., 2012; Rothfuss et al., 2010, 2012). Some of this error is attributable to processes such as sub-soil water vapor diffusion and exchange, which are not taken into account by the Craig-Gordon model. Tang & Riley (2013) noted that inclusion of sub-surface water vapor exchange in a process model, National Center for Atmospheric Research's Community Land Model Version 4 (NCAR CLM4), improved estimates of bare-soil evaporation, and they suggested that their approach is likely to be verifiable using depth-resolved soil water and water δ^2H (hereafter δD) and $\delta^{18}O$ profiles. However, sampling soil moisture, and δD and $\delta^{18}O$ in particular, is difficult and not commonly done beyond short-term campaigns.

An additional complication arises from limitations in the theoretical bases for accounting for isotopic fractionations due to changes in temperature, turbulence and molecular diffusion. Equilibrium fractionation between liquid and vapor states is well established for temperatures ranging from 0 to 100 °C (Merlivat, 1978; Horita & Wesolowski, 1994; Barkan & Luz, 2007), but

kinetic fractionation associated with molecular diffusion is less well described because the pathways of vapor through the vadose zone and canopy are tortuous. In addition, kinetic fractionation applies to both liquid and vapor diffusion within soil matrices. Various methods can be used to calculate a kinetic fractionation factor (Brutsaert, 1982; Barnes & Allison, 1984; Mathieu & Bariac, 1996; Lee et al., 2009) but verification of these schemes has been limited without long-term field observations. A common assumption is that turbulent transport does not fractionate, whereas molecular diffusion does, yet theoretical models that relate total mass transport to the proportion of diffusive versus turbulent exchange, which is necessary to estimate the kinetic fractionation factor, cannot be validated.

Transpiration is often considered to be net non-fractionating when at steady state, i.e. the isotope ratio of transpiration flux is equal to that of soil water prior to being drawn up by roots (Farquhar & Lloyd, 1993). Under steady state conditions, bulk leaf water becomes enriched in heavy isotopologues relative to soil water to exactly balance the fractionation which accompanies phase change in the leaf chloroplast and subsequent kinetic effects as water molecules diffuse from the stomata to the canopy airspace above. Conversely, evaporation has been viewed as net fractionating, and using a simple Craig-Gordon approach, results in δD and $\delta^{18}O$ soil water values becoming progressively higher over time. If, however, one considers that evaporation in a dry environment can result in near complete removal of layers of water from the soil, one may posit a situation in which evaporation similarly results in no net fractionation if all of the liquid is completely moved into vapor phase. This distinction becomes particularly important in light of results that show the choice of kinetic fractionation factor can greatly influence model outcomes (Dubbert et al., 2013).

Here we use data from a multi-year field experiment designed to test which mechanisms are

controlling water exchange between the soil and the atmosphere using water isotope ratio tracers. The analysis seeks to: (1) evaluate the basic mechanisms associated with isotopic enrichment in upper soil relative to recharge of soil water by infiltration of precipitation, (2) provide an evaluation of existing approaches to determine an appropriate choice of kinetic fractionation factor, and (3) test the relative contributions of fractionating and non-fractionating processes to soil evaporation at this semi-arid site. We demonstrate the need to account for sub-surface vapor exchange and discuss the implications of these results on traditional isotope-based approaches for determining ecosystem water partitioning. A series of steady state and mass conservation considerations offer an alternate explanation that, contrary to previous assumptions, soil evaporation in semi-arid environments can be considered to be non-fractionating under certain conditions. This alternate approach for partitioning evapotranspiration reconciles shortcomings in the isotopic method which otherwise has higher transpiration contributions to latent heat flux estimations compared to other methods.

2. Methods

2.1 Field site and measurement techniques

Measurements were made at the 300-m-tall Boulder Atmospheric Observatory (BAO) tall-tower site in Erie, Colorado (40.050N, 105.003W, 1584 m a.s.l.). For more site details and operational history, the reader is referred to the website http://www.esrl.noaa.gov/psd/technology/bao/site/ and to Wolfe & Lataitis (2018). Soil moisture and temperature were measured using Campbell Scientific model probes CS616 and 107 respectively. Soil probes were installed in August 2011 and allowed to equilibrate for 6-8 months before data were used for scientific analysis. Wind and humidity/temperature measurements were

made with Met One 010C/020C and Vaisala HMP 155 instruments respectively. Eddy covariance measurements were taken with a Campbell Scientific EC150 open-path gas analyzer for carbon dioxide and water coupled with a CSAT3A 3-D sonic anemometer for wind measurements, installed at 10 m on a meteorological tower. Eddy covariance measurements were used to derive the sensible and latent heat fluxes, calculated as 30-minute averages using a 1-hour window on either side of the middle point.

In addition to meteorological, flux and soil moisture and temperature measurements, a Picarro L2120-i water vapor isotope analyzer, capable of measuring $^{2}H/^{1}H$ and $^{18}O/^{16}O$, was installed in a temperature-controlled laboratory on-site. Stable isotope values are expressed in permil units (‰) and are referenced to the international standard Vienna Standard Mean Ocean Water (VSMOW):

$$\delta\ (‰) = \left(\frac{R}{R_{std}} - 1\right) \times\ 1000 \qquad (1)$$

where R is the isotopic ratio of the sample (e.g. D_{spl}/H_{spl} or $^{18}O_{spl}/^{16}O_{spl}$) and R_{std} is the isotopic ratio of the standard VSMOW [$R_{std}(D) = 1.558\text{x}10^{-4}$, $R_{std}(^{18}O) = 2.005\text{x}10^{-3}$].

Deuterium excess, "D_{excess}", is defined as:

$$D_{excess} = \delta\text{D} - 8*\delta^{18}\text{O} \qquad (2)$$

and is a useful diagnostic for tracing kinetic processes. Lighter isotopologues preferentially escape the evaporation zone because of kinetic effects, and due to mass differences, D escapes faster than ^{18}O. This leaves residual water with low D_{excess} values and, by mass balance, a positive anomaly in the vapor phase.

2.1.1 Stable isotope ratio measurements

Isotope ratios in water vapor were measured sequentially at eight heights (0.43 m, 0.88 m,

1.94 m, 3.94 m, 8.40 m, 100 m, 200 m, 300 m) at approximately 0.5 Hz. The design of the measurement system follows Berkelhammer et al. (2016a, 2016b) and Tremoy et al. (2011). For May 2012-June 2013, the isotopic analyzer sampled water vapor from each height for 15 minutes before switching to the next sampling line. From June 2013 to November 2016, the sampling interval was 10 minutes for each line. The last 5 minutes of data from each inlet were used to construct mean values to avoid memory effects (Bailey et al., 2015; Berkelhammer et al., 2016a). Isotopic measurements were calibrated with reference to VSMOW by introducing a pair of secondary standard waters, chosen to bracket observations, approximately every 6 hours using the commercially available Standards Delivery Module from Picarro Inc. Following Bailey et al. (2015) and Berkelhammer et al. (2016a, 2016b), isotopic data were also corrected for humidity-dependent isotope bias and instrument drift, and specific humidity was calibrated using a dew point generator. After calibration and corrections, average standard errors for the 5-minute blocks of vapor measurements were 0.49‰ for δD and 0.07‰ for δ^{18}O. All secondary standards used in the field and in the laboratory below were tied to the International Atomic Energy Agency scale with mass spectrometer determinations at the Stable Isotope Laboratory, Institute of Arctic and Alpine Research, Boulder, CO.

2.1.2 Precipitation and soil water isotope ratios

Bulk precipitation samples were collected at the site approximately weekly from May 2013 to October 2015 using a 1-liter separatory funnel filled with ~150 ml mineral oil to prevent evaporation of collected rain water. Liquid samples were analyzed following the procedure given by Noone et al. (2013). Shallow soil cores (0-30 cm in 5 cm intervals) and vegetation samples were taken at approximately weekly intervals from May to October (2012-2014) for water isotope

ratio measurements. The predominant vegetation at this site is Downey brome (cheatgrass) which typically grows 4-30 inches tall during summer months. 0-30 cm soil at BAO is approximately 30% clay, 40% silt and 30% sand and has a bulk density of 1.18 ± 0.05 g cm^{-3}.

Soil and vegetation was then frozen until cryogenic extraction was performed on a vacuum line based on the procedure outlined by West et al. (2006). Recent literature has highlighted cryogenic extraction methods as being appropriate only for sampling the mobile pool of water available in soil (Newberry et al., 2017). This is consequential because the authors hypothesize that evaporation is sourced from mobile water, while transpiration is sourced from bound water. However, Vargas et al. (2017) found that mobile and bound water pools equilibrate up to 99% in soils, and therefore the cryogenic extraction technique does sample all available soil water. Isotope ratios of the resultant liquid samples were measured on a laboratory Picarro L2120i water isotope analyzer using a LEAP PAL autosampler system. Observed standard deviations for liquid sample replicates were 0.16‰ for δD and 0.06‰ for δ^{18}O.

2.2 Modeling evapotranspiration fluxes

2.2.1 Observational estimates of the isotopic ratio of evapotranspiration

The isotope ratio of evapotranspiration flux was obtained using the near-surface profile, e.g., Noone et al. (2013). This is similar to the "Keeling plot" approach which was developed to use isotopic composition and bulk concentration of CO_2 to quantify respiration sources (Keeling, 1958), and is still widely applied in terrestrial carbon research (Pataki et al., 2003; Munksgaard et al., 2013). It has also been applied to water vapor measurements for short field measurement periods (Berkelhammer et al., 2016; Noone et al., 2013; Wang et al., 2010; Yepez et al., 2003). Traditionally, the isotope ratio is plotted on the y-axis, and the inverse of the concentration of the

species of interest is plotted on the x-axis (e.g., isotope ratio R vs $1/q$ where q is H_2O concentration). Miller and Tans (2003) showed that regression errors are reduced if analysis is performed on plots of $R*q$ vs q and so we adhere to this method following Noone et al. (2013) for further calculation of Keeling plot values. Hereafter, this is also referred to as the "profile method".

2.2.2 A bulk flux framework for evaluating isotopic evapotranspiration

A starting point for considering bulk evapotranspiration fluxes begins with the Langmuir linear-resistance model, which is the basis for isotopic approaches to modeling evaporation and transpiration (Craig & Gordon, 1965; Gat, 1996; Horita et al., 2008). Let us assume that the evapotranspiration from the ecosystem as a whole is captured by defining an effective source for evaporating water (represented by the isotope ratio R_{eff} in equation 3 below; Figure 1a). Following Craig & Gordon (1965) and using the Langmuir linear-resistance model, we may write an equation where the kinetic effect on isotope ratios of soil water is governed by an effective kinetic fractionation factor (α_{k-eff} in equation 3 below) and the isotopic ratio of the evapotranspiration flux at the land-atmosphere interface (R_{ET}) is then written as:

$$R_{ET} = \frac{\boldsymbol{\alpha}_{k-eff} \times \left(R_{eff} - R_{vap} \times h \right)}{(1-h)} \qquad (3)$$

R_{ET} is calculated using the Keeling approach applied to five measurement heights from 0.43 m to 8.40 m, R_{vap} is the isotopic ratio of the surface vapor at 8.40 m and h is ratio of ambient vapor pressure to saturation vapor pressure calculated at the soil evaporating surface. Saturation vapor pressure at the soil evaporating surface was calculated using temperature measurements from an Campbell Scientific IR sensor (downward pointing SI-111 measuring infrared temperature at the soil surface). We use the lowest five tower heights so as to accurately assess evapotranspiration at the surface. Rearranging equation (3) we obtain:

$$R_{vap} * h = -\left(\frac{1}{\alpha_{k-eff}}\right) * (1-h) * R_{ET} + R_{eff} \qquad (4)$$

The parameters R_{eff} and α_{k-eff} can be estimated via equation (4) as the coefficients of the regression $R_{vap} * h$ versus $(1-h) * R_{ET}$ for a number of consecutive days. We performed this calculation using 3-day running means and weighted the final α_{k-eff} values by latent heat flux measured by eddy covariance. Three days is the minimum requirement to generate a centered-in-time solution to equation (4), and this short time period retains synoptic variability in the results. Testing performed with longer time periods reduces the standard error on calculations of α_{k-eff} but does not change the final interpretation of the results. It is essential to weight by latent heat flux to ensure that the isotope ratio derived is relevant for the total mass flux over the time period analyzed. This relatively simple bulk approach is used to estimate net ecosystem kinetic fractionation factor values under different soil wetness and turbulence regimes.

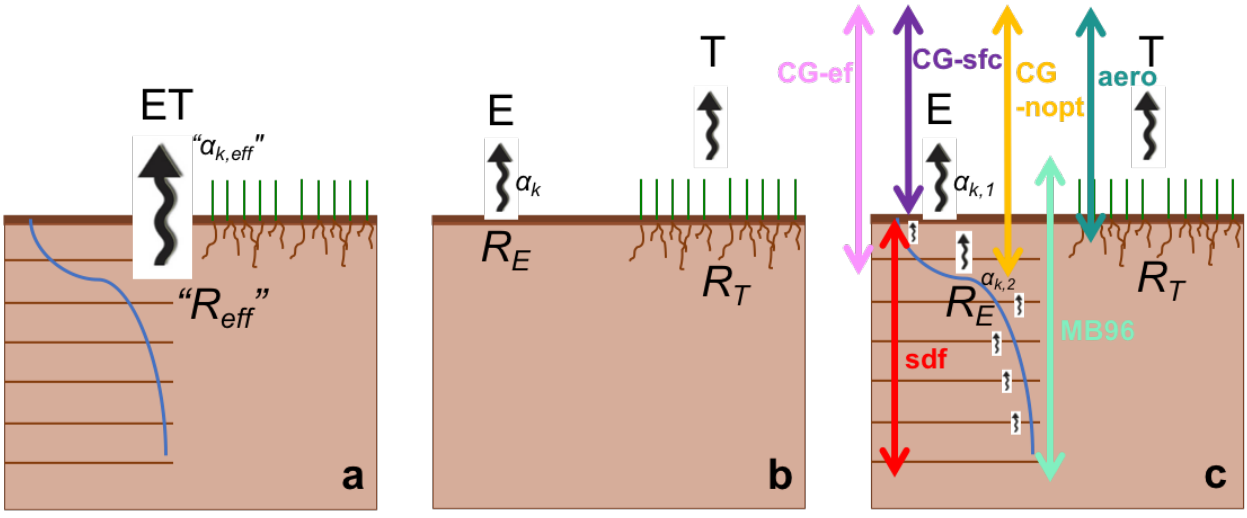

Figure 1: Schematic of approaches for determining the contributions to total evapotranspiration flux. (a) "Effective source" approach where both R_{eff} and α_{k-eff} can be determined through a simple linear regression knowing the humidity and isotope ratio values for the lowest atmospheric layer and the surface evapotranspiration flux value from the profile method; the blue line depicts an example water profile, (b) Two-stream method where R_E

is the isotope ratio of the surface soil layer and R_T is the isotope ratio of the root weighted soil column, (c) Explicitly resolving below-ground processes by dividing the soil column into layers; R_E is now the isotope ratio of the evaporation horizon and R_T is the same as in (b). Colored arrows depict scheme choices for modeling ET flux, showing approximate locations best represented with model parameters described in Table 1. Detailed descriptions for each model are given in section 2.2.3.

2.2.3 Modelling isotopic ratios of evapotranspiration

The isotopic ratio of the evapotranspiration flux can be decomposed as follows:

$$R_{ET} = R_E(1 - f_T) + R_T f_T \qquad (5)$$

where R_{ET} is the isotopic ratio of the evapotranspiration flux described above, R_T is the isotopic ratio of the transpiration flux and f_T is the transpiration fraction (Figure 1b). R_E is calculated from equation (6) below. We calculated R_T as a weighted average of the soil column water isotope ratios corresponding to approximate rooting depths of plants at the BAO site. Rooting depths were determined by digging into the soil to gauge the depth of grass roots during the summer season. In all digs, roots were between 10 and 25 cm. Soil core water isotope ratios for these depths were therefore weighted by water content to calculate the most likely pools accessed for transpiration. The underlying assumptions are that transpiration fluxes are approximately at steady state around midday, and that root-weighted soil water can be used as an approximation for xylem water (i.e. R_T). The steady-state assumption does not hold true through the full diurnal cycle (Farquhar & Cernusak, 2005) but is a reasonable basis for calculating surface fluxes around midday (Dubbert et al., 2013; Welp et al., 2008).

The Craig-Gordon (hereafter CG) model was originally designed to estimate equilibrium and kinetic fractionation during evaporation from the ocean surface (Craig & Gordon, 1965). It is also commonly used in land-surface flux calculations (Gat, 1996; Haverd & Cuntz, 2010; Henderson-Sellers et al., 2006; Horita et al., 2008; Soderberg et al., 2011) and numerical model alternatives

based on the CG model have been developed (Lee et al., 2009; Mathieu & Bariac, 1996; Melayah et al., 1996; Riley et al., 2002; Wong et al., 2017). Following Gat (1996):

$$R_E = \frac{\alpha_{k-CG} \times \left[\frac{R_{soil}}{\alpha_{eq}} - R_{vap} \times h \right]}{[1-h]} \qquad (6)$$

where R_E is the isotopic ratio of the evaporative flux from equation (5), α_{k-CG} is the kinetic fractionation factor, α_{eq} is the equilibrium fractionation factor, R_{soil} is the isotopic ratio of the soil water undergoing evaporation, R_{vap} is the isotopic ratio of the vapor and h is the ratio of ambient vapor pressure to saturation vapor pressure at the soil evaporating surface. We use measurements from 8.40 m for R_{vap} and h. For model calculations, we used averaged values (~1200-1500 local time), selecting time periods where maximum evapotranspiration occurs, and based on observations of u_* > 0.25 m/s, indicating that a turbulent mixing regime was well established. The dependence of α_{eq} on temperature has been characterized in laboratory measurements (Horita & Wesolowski, 1994).

A significant source of uncertainty arises from the choice of the kinetic fractionation factor, as there is disagreement on the correct formulation to use (e.g., Braud et al., 2005; Horita et al., 2008; Rothfuss et al., 2012). α_{k-CG} is commonly parameterized as:

$$\alpha_{k-CG} = \left(\frac{D_i}{D_{h2o}} \right)^n \qquad (7)$$

where D_i is the molecular diffusivity of the isotopologue (either HDO or $H_2{}^{18}O$), D_{h2o} is the molecular diffusivity of water ($H_2{}^{16}O$) in air. There is a range of values in the literature for the ratio of D_i/D_{H2O} (Merlivat, 1978; Cappa et al., 2003; Barkan & Luz, 2007). We use values from Barkan & Luz (2007) which are in excellent agreement with the original values proposed by Merlivat (1978) (D_i/D_{h2o} = 0.9723 for $H_2{}^{18}O/H_2{}^{16}O$ and D_i/D_{h2o} = 0.9755 for $HD^{16}O/H_2{}^{16}O$). The

value of n remains ambiguous, and is often taken to be 2/3, motivated by turbulence theory (Brutsaert, 1975), yet values ranging from 0 to 1 are theoretically possible. From a mechanistic standpoint, the use of n parameterizes kinetic effects from diffusion (n = 1, i.e. pure diffusion) versus turbulent or other advective transport (n = 0, i.e. no kinetic effect). Recent studies have provoked discussion about the value of n (Braud et al., 2005; Dubbert et al., 2013; Horita et al., 2008). Isotopic evaporation model parameterizations of n or α_k are associated with physical variables, and a summary of the models and mechanisms tested in this paper are given in Table 1 and described below.

The CG view invokes the presence of diffusive exchange adjacent to the boundary (i.e. the land surface) in the "laminar layer". In the analysis that follows we test the assumptions of the CG model in three ways: (i) we assume the soil surface is the source of water for evaporation (CF-sfc); (ii) we assume the subsurface evaporation horizon is the source for evaporation (CG-ef); (iii) in addition to (ii), we also assume that near complete removal of water from this layer results in evaporation either having no kinetic fractionation, which implies n = 0 in equation (7), or having a weaker kinetic fractionation than expected (CG-nopt; where nopt indicates an optimal choice of n between 0 and 1).

Modifications to n and α_k may be based on below-ground soil water content (Mathieu & Bariac (1996), hereafter 'MB96') and/or above-ground aerodynamic roughness lengths and friction velocities (this study, based on Brutsaert (1982) and Lee et al. (2009) hereafter 'AERO'). The first (MB96) calculates n using soil water content to simulate dry layer development, which reflects a change in soil porosity:

$$n'_{\mathrm{K}} = \frac{(\theta_s - \theta_r)n_a + (\theta_{sat} - \theta_s)n_s}{(\theta_{sat} - \theta_r)} \qquad (8)$$

where θ_s is the soil surface volumetric water content (taken to be observations from soil moisture

probes at 2.5 cm depth), θ_{sat} is the saturated water content (which we assume to be a conservative estimate of 0.35, based on Braud et al., 2005), θ_r is the residual volumetric water content (which we take to be data for the lowest soil moisture sensor at 85 cm, well below the depth at which isotope ratio fluctuations are observed). n_a and n_s are the atmosphere- and soil-controlled exponents of diffusivity, respectively, and when the soil is saturated ($\theta_s = \theta_{sat}$), $n'_{\mathrm{K}} = n_a$, i.e. the exchange is atmosphere-controlled. n_a (=0.5) and n_s (=1) are extreme values of n used to account for soil dryness. α_{k-MB96} is calculated from equation (7) using $n = n'_{\mathrm{K}}$.

A complementary approach (AERO) calculates a net kinetic effect using aerodynamic and canopy resistances at the land-atmosphere interface. Following Berkelhammer et al. (2016a) and Lee et al. (2009) and using the molecular diffusivities from Barkan & Luz (2007), the kinetic fractionation factor for evaporation is calculated from a resistance-weighted mean of several contributions:

$$\epsilon_{k-AERO} = \frac{\frac{2}{3}Ar_{subcanopy} + Ar_{soil}}{r_{atmosphere} + r_{subcanopy} + r_{soil} + r_{litter}} \qquad (9)$$

where A is 28.5 for δ^{18}O and 15.1 for δD. r_{soil} is assumed to have a constant value of 500 s m^{-1} (Berkelhammer et al., 2016a; Lee et al., 2009). Following Oleson et al. (2010) and Wong et al. (2017) and noting that the BAO site has 1-2 cm of dry grass matting, r_{litter} is calculated as:

$$r_{litter} = \left(\frac{1}{0.004u_*}\right)(1 - e^{-0.5}) \qquad (10)$$

The calculations of $r_{subcanopy}$ and $r_{atmosphere}$ follow Berkelhammer et al. (2016a):

$$r_{atmosphere} = r_{boundary} - r_{total} \qquad (11)$$

$$r_{total} = \frac{1}{uT_c} \qquad (12)$$

$$T_c = \frac{k^2}{log(z_m - d)/z_o - \phi_m log(z_m - d)/z_q - \phi_h} \qquad (13)$$

$$r_{boundary} = \frac{b}{2} L \frac{I_w^{0.5}}{u} \quad (14)$$

$$r_{subcanopy} = \int_0^{canopy} \frac{dz}{K} \quad (15)$$

In the above equations, u is the wind speed (m s^{-1}) measured by an anemometer at the reference height (10 m), T_c is the transfer coefficient, k is the von Karman constant (equal to 0.4), z_m is the reference height (10 m), d is the displacement height (m), z_o is the momentum roughness (set to 0.1 times the average canopy height of 0.5 m), z_q is the humidity roughness (set equal to $z_0/\exp(2)$), $\phi_{m/h}$ are the integral similarity functions for momentum and heat, b is the boundary layer resistance coefficient (set to 283 $s^{-0.5}$ m^{-1}), L is the leaf area index (set to 1.88 for the semi-arid BAO site), I_w is the leaf dimension (set to 0.05 m), K is the eddy diffusivity (m^2 s^{-1}), dz (m) is the length of the canopy air space and the integral in equation (15) is calculated from the soil surface across the canopy air space. ϵ_{k-AERO} is related to the fractionation factor α_{k-AERO} using:

$$\alpha_{k-AERO} = \frac{\epsilon_{k-AERO}}{1000} + 1 \quad (16)$$

This approach is consistent with a more detailed mechanistic model that has previously been used at this site (Wong et al., 2017).

In addition to the two models described above, we test a third method which highlights the potential role of sub-surface diffusion (hereafter 'SDF'). Depth-resolved soil water isotope ratio sampling is essential for this method, and our observations enable us to set up and validate a simple 1-D soil column model to simulate diffusion within a sub-saturated soil matrix. The soil matrix at BAO is predominantly unsaturated, with soil moisture profile observations showing that the evaporation front was deeper in summer months around 25 cm and shallower in spring and fall around 17 cm. The soil column model was set up from 0-1 m at 1 cm resolution and interpolated

soil water isotope ratio and temperature values were used to initialize the calculation at each model depth. Gas phase fluxes at each depth were calculated based on the gas phase transport described in Mathieu & Bariac (1996). At every soil level, we calculate the vapor diffusion based on concentration differences in adjacent layers and ultimately couple this to the evaporative flux at the soil surface through atmospheric turbulent exchange processes.

Figure 1c shows a schematic description of these isotopic modeling approaches for calculating evapotranspiration flux, and Table 1 summarizes the physical attributes tested by the different model choices. These models, while based on physical processes, can be difficult to validate because of the number of assumptions involved. Optimizing either the value of the exponent '*n*' (i.e. $\boldsymbol{\alpha_k}$) or the transpiration fraction $\boldsymbol{f_T}$ could lead to vastly different conclusions about the agreement of any given model with observations. Making use of the four-year data set collected at BAO, $\boldsymbol{R_T}$ and $\boldsymbol{R_E}$ can be computed from these different models and compared to $\boldsymbol{R_{ET}}$ calculated from the gradient Keeling approach. The importance of accurate estimates of $\boldsymbol{\alpha_k}$ and the appropriate physical model on the derived transpiration fraction is described under different soil wetness regimes to enable a test that yields the most likely simultaneous estimate of $\boldsymbol{f_T}$ and $\boldsymbol{\alpha_k}$.

Model	**Physical attributes**
CG-sfc	Surface is the source of water for evaporation (Craig & Gordon, 1965)
CG-ef	Evaporation horizon is the source of water for evaporation [this study, based on Craig & Gordon (1965)]
CG-nopt	*n* is optimized in α_k calculation for source water as in CG-ef, i.e. evaporation from the evaporation horizon [this study]
MB96	α_k is based on soil moisture parameters at three depths (Mathieu & Bariac, 1996)

AERO	α_k is based on aerodynamic resistance parameters [this study, based on Brutsaert (1982), Lee et al., (2009), Oleson et al., (2010)]
SDF	α_k is a combination of sub-surface properties; +AERO adds surface layer resistance parameters [this study, based on Mathieu & Bariac (1996) and Tans (1998)]

Table 1. A summary of the different evaporation models and physical attributes of these models tested in this study.

2.2.4 Modeling evapotranspiration using gross primary productivity

The GPP method uses the non-linear relationship between vapor pressure deficit and carbon-water coupling to estimate T/ET scaled to the total ET flux (Zhou et al., 2014). Following Berkelhammer et al. (2016a), we plotted ET versus GPP x $VPD^{0.5}$, which normalizes the ET fluxes to VPD and linearizes the relationship between GPP and ET. GPP was calculated based on Reichstein et al. (2005). Data were processed using the REddyProc package available at https://www.bgc-jena.mpg.de/bgi/index.php/Services/REddyProcWebRPackage.

I then divided the GPP range into 0.1 normalized bins and fit a curve corresponding to the minimum ET for each bin (where the minimum was defined as the lowest 5th percentile to account for measurement errors). From this, transpiration fraction is calculated as the ratio between the observed and minimum ET:

$$\frac{T}{ET} = \frac{min_{GPP}\|ET\|}{ET_{flux}} \qquad (17)$$

Neither the isotope-based nor the GPP method can be immediately considered to be a measure of truth. However, broad agreement between them would offer some degree of confidence via simple consensus. The success of the GPP method for T/ET partitioning (Berkelhammer et al., 2016a) makes it a valuable isotope-independent comparison tool.

3. Results

3.1 Seasonality of isotopic ratios

Observations of the seasonal cycles of isotopologues are shown in Figure 2. Higher $\delta^{18}O$ and lower D_{excess} values in soil water and surface water vapor in summer months reflect a strong contribution from local evaporative sources, namely bare soil evaporation at this midlatitude semi-arid site (Gat, 2000). This analysis is consistent with similar studies highlighting the role of locally derived vapor contributions in summer months when continental circulation is weak (Zimmermann et al., 1967, Rozanski et al., 1993). Flux footprint analyses for measurements at 8.4 m at the BAO site, based on Schuepp et al. (1990), reveal that for well-mixed turbulent regimes where u_* is greater than 0.25 m/s, the distance where the peak flux contribution comes from is ~120 m away from the 10 m tower, and 90-95% of the cumulative flux contribution is obtained from a 5-12 km radius around the tower. Local sources ~120 m away are mostly semi-arid grassland much like the tower site, and contribute significantly to the background atmospheric moisture in summer.

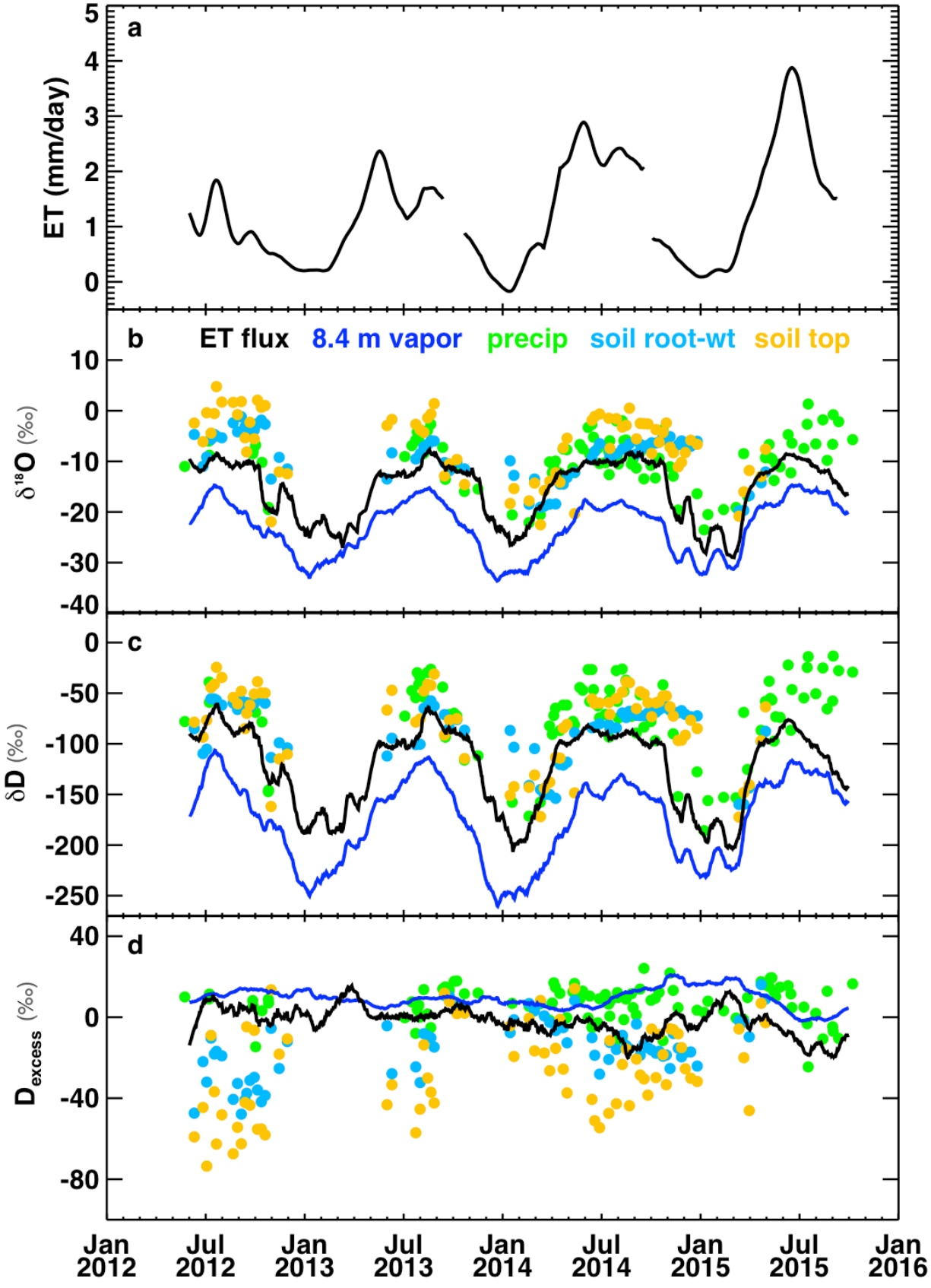
a
ET (mm/day)
5
4
3
2
1
0
b
ET flux
8.4 m vapor
precip
soil root-wt
soil top
δ18O (‰)
10
0
-10
-20
-30
-40
c
δD (‰)
0
-50
-100
-150
-200
-250
d
Dexcess (‰)
40
0
-40
-80
Jan 2012
Jul 2012
Jan 2013
Jul 2013
Jan 2014
Jul 2014
Jan 2015
Jul 2015
Jan 2016

Figure 2: (a) Evapotranspiration (ET) in mm/day plotted as 30-day running mean of daily total ET (standard error = 0.05 mm/day); Isotope ratios of (b) $\delta^{18}O$, (c) δD and (d) D_{excess} for 2012-2015 showing precipitation (green), 8.4 m vapor (blue line), ET flux (black line) from profile method calculations, root-weighted soil water (cyan) and soil top layer (orange). Isotope ratio ET and 8.4 m vapor lines are plotted as 30-day running means of midday averages. Standard errors were 0.16 ‰ for δD/0.06 ‰ for $\delta^{18}O$ for preciptation and soil water measurements, and 3.0 ‰ for δD/0.4 ‰ for $\delta^{18}O$ for isotope ratio ET flux.

The transition from winter maximum to summer minimum in soil water D_{excess} values corresponds well with steep declines in soil moisture during extended arid periods in early-late summer, showing a direct physical connection between moisture recycling and surface layer water isotope ratios. This is also evident from an examination of soil moisture and isotope ratios from soil water core samples from 2012-2014 (Figure 3). In days following precipitation events, the 0-30 cm soil column, and particularly the near-surface 0-15 cm layer, show more negative D_{excess} values in residual soil water, which are indicative of strong drying by evaporation. Transpiration is thought to be mostly unfractionated with respect to uptake at the roots (Farquhar & Lloyd, 1993) and therefore should not have any effect on the midday soil water D_{excess} values shown in Figure 3.

Figure 4 shows soil water isotope ratios sampled from 0-30 cm plotted alongside the summer and winter precipitation isotope values. The close correspondence between the deep soil (below 20 cm) and precipitation values shows that the isotopic signature of the soil column is initially set by the incoming precipitation. The local meteoric water line at this site has a slope of 7.09 ± 0.24 (5.95 ± 0.35 in summer and 8.17 ± 0.52 in winter; the errors reported here refer to inter-annual variability). Deviation of the slope from the global average meteoric water line slope of about 8 is indicative of arid conditions and rainfall with a higher degree of re-evaporation in summer months. In winter, high D_{excess} values in snow combined with reduced evaporation account for a higher slope value (Gat (1996) and references therein). Deviation of sample points off the

local meteoric water line, i.e. shallower slopes for the near-surface soil layers (above 15 cm), indicate the dominance of an evaporation signal near the surface.

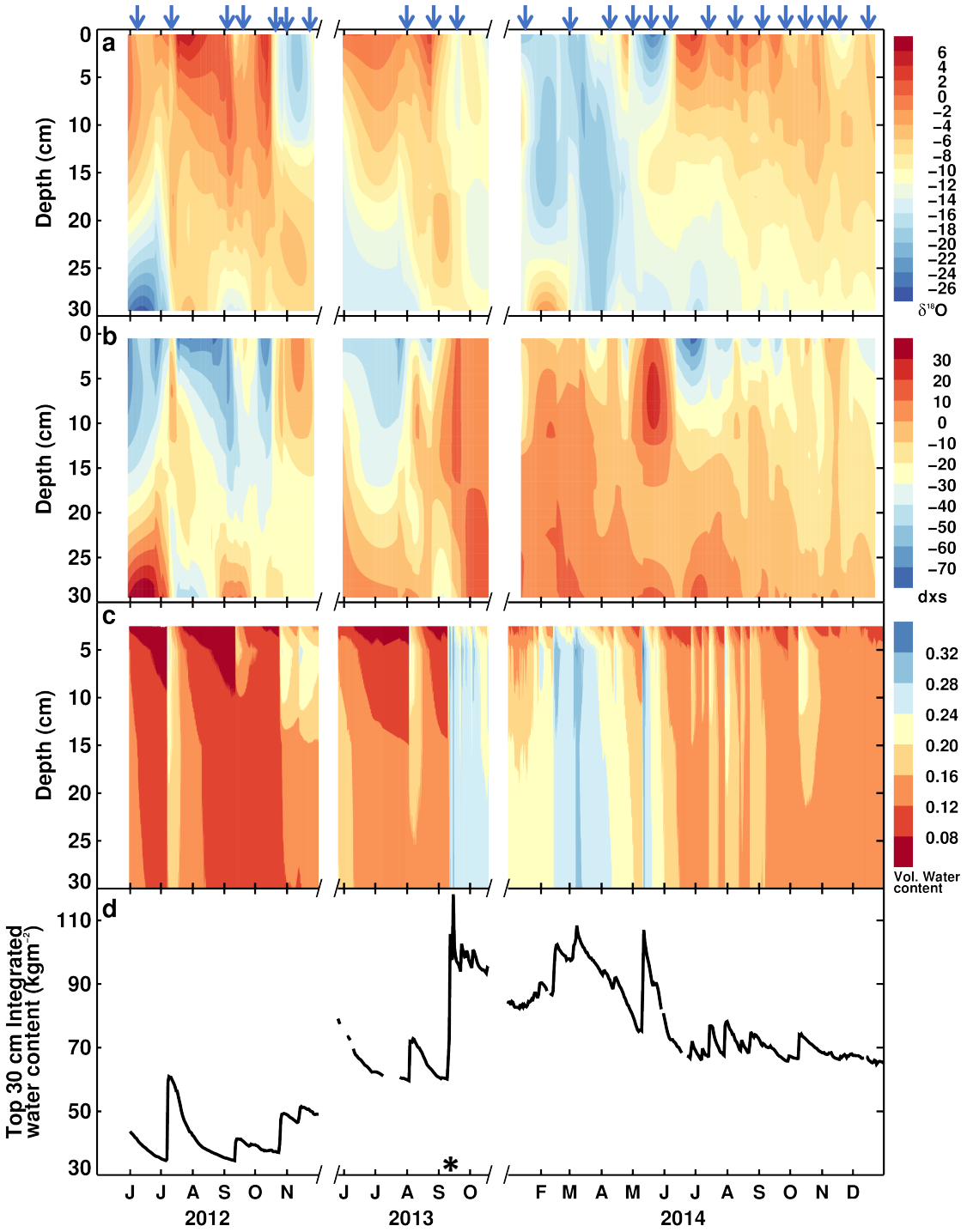

Figure 3: 2012-2015 soil water and isotope ratio observations for (a) $\delta^{18}O$ (‰), (b) D_{excess} (‰), (c) Volumetric Water Content and (d) Top 30 cm total integrated column water content (kg/m^2). Rapid dry-down is evident from the progressive depletion in D_{excess} values following precipitation events (indicated by blue arrows). In September 2013 (indicated by *), the high water content and D_{excess} values were the result of a record rain event in which ~7 inches of rain were recorded at BAO between Sep 9 and Sep 16. The isotopic signature of this deluge is clearly visible in early 2014 as the soil column takes several months to dry out such a large input. Soil moisture probes were calibrated using volumetric water content measured from the soil cores taken for water isotope analysis.

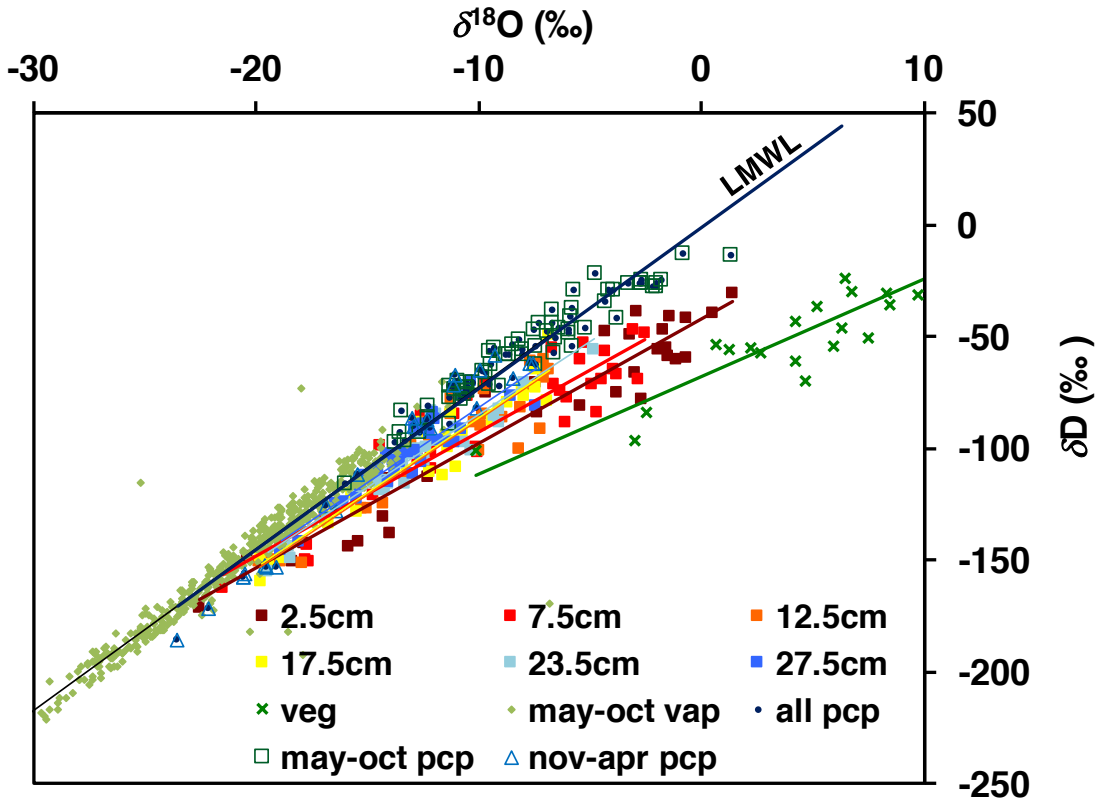

Figure 4: Stable isotope ratios (δD and $\delta^{18}O$) of liquid water in soil layers (2.5 cm to 27.5 cm), vegetation, May-Oct 8.5 m vapor, May-Oct and Nov-Apr precipitation. The slope of the local meteoric water line (LMWL, slope = 7.09) indicates a trend towards evaporative enrichment at the BAO site. This trend is more pronounced in May-Oct precipitation (slope = 5.95) vs Nov-Apr precipitation (slope = 8.17). Soil layers show decreasing slopes towards the surface as surface soil layers dry out faster than deeper soil layers.

3.2 Evaluation of surface flux isotope ratios

Figure 2 shows the isotope ratios of key ecosystem components of interest for evaluating ET. The soil values in particular are important drivers for model estimations described below. In addition to seasonal cycles being evident in all components, a gradient in enrichment is seen from the soil surface (most enriched) to the 8.4 m vapor (least enriched). There are periods in Figure 2 when the isotopic composition of ET flux overlaps with precipitation values and the alignment or difference between these two sets of values points to different mechanisms controlling the isotope ratio of the ET flux. Figure 5 shows the modeled isotope ratios of different methods to evaluate the evaporation flux (colored dots, corresponding to R_E in equation 6) compared to the observed ET flux from the profile method (solid black line), alongside total daily precipitation and soil water content observations. The root-weighted soil water values correspond to a fully non-fractionating system (corresponding to R_T in equation 5). This best describes the ET flux under wet conditions (where the column integrated water content exceeds 200 kg/m^2; RMSE$_{\delta 18O}$ = 1.9‰, RMSE$_{Dexcess}$ = 3.7‰). Higher water content values (>220 kg/m^2) correspond to spring snowmelt and several days of heavy rainfall in September 2013 and May 2015. Summer dry soil conditions typically correspond to 80-200 kg/m^2 column integrated water content, and under drier conditions, it is values from the SDF or CG-nopt models that are closest to the observed ET flux (RMSE$_{\delta 18O}$ = 3.4‰ and 3.0‰, RMSE$_{Dexcess}$ = 5.9‰ and 5.5‰, for SDF and CG-nopt respectively). This implies that vapor diffusion within the soil matrix and/or weaker kinetic fractionation are likely important under drier conditions.

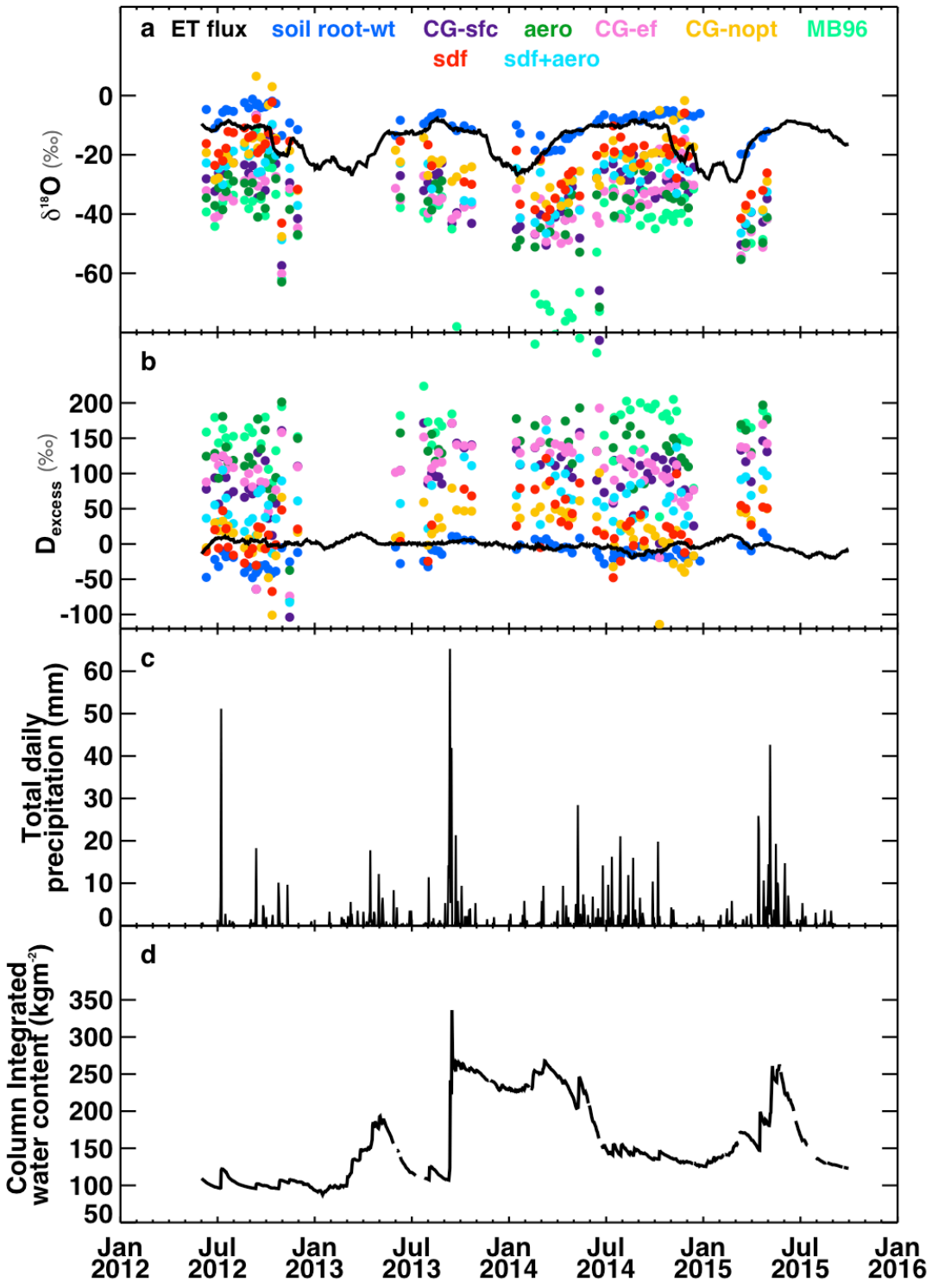

Figure 5: 2012-2015 BAO data for evapotranspiration (ET) flux isotope ratios of (a) $\delta^{18}O$ and (b) D_{excess} from profile method calculations and ET flux predicted from fully non-fractionating (evaporation fraction = 0, i.e. full transpiration, 'soil root wt') and fully fractionating

(evaporation fraction = 1, i.e. full evaporation) model choices (described in Table 1 and illustrated in Figure 1), (c) Total daily precipitation (mm), (d) Total column integrated water content (kg/m^2) for 0-1 m. A close correspondence between fully non-fractionating models and ET flux is evident during periods of high soil moisture content.

3.3 Consequence of fractionation on partitioning

Model	$f_{T,18O}$	$f_{T,D}$	$f_{T,dxs}$
CG-sfc	0.73 ± 0.03	0.58 ± 0.05	0.75 ± 0.03
CG-ef	0.78 ± 0.03	0.62 ± 0.04	0.80 ± 0.03
CG-nopt (n=0.2)	0.64 ± 0.05	0.58 ± 0.05	0.58 ± 0.05
MB96	0.79 ± 0.03	0.61 ± 0.04	0.86 ± 0.02
AERO	0.78 ± 0.03	0.59 ± 0.05	0.83 ± 0.02
SDF	0.64 ± 0.06	0.60 ± 0.06	0.58 ± 0.06
SDF+AERO	0.69 ± 0.05	0.61 ± 0.05	0.68 ± 0.04

Table 2. Transpiration fractions calculated from all the models described summarized in Table 1, using $H_2{}^{18}O$, HDO and D_{excess} values for May-Oct 2012-2015. Error values are quoted as 1 standard deviation error on the estimates.

Transpiration fraction (f_T) values calculated from individual isotope ratios δD and δ^{18}O, and from D_{excess}, for the growing season (May-Oct) for 2012-2015 for all modeled R_E are summarized in Table 2. The computed f_T values can differ substantially depending on which isotope quantity is chosen, but if a particular model accurately captures exchange processes then the choice of α_k parameterization in that model should give the same value of f_T from both isotopes separately, as well as from D_{excess}. The closest match between the three f_T predictions are for the CG-nopt model (0.60 ± 0.03) using a value of n = 0.2 in the calculation of α_k from equation (7), and for the SDF model (0.61 ± 0.03). These average f_T values fall within the range of values reported in the meta-analysis of semi-arid grassland environments (Schlesinger & Jasechko, 2014; Yepez et al., 2005). The reason why a low value of n = 0.2 is an appropriate choice is justified below. In practice, the

value is based on optimal selection that simultaneously minimizes the error between observed and modeled values for both $\delta^{18}O$ and D_{excess}. Both of these results point to mechanistic controls on evaporation in semi-arid environments, i.e. that evaporation is sourced from near complete evaporation of layers of water at the evaporation horizon with weaker net kinetic fractionation (and thus a lower n exponent than the traditional 2/3 value), and that diffusion plays an important physical role in transporting sub-surface water vapor in a near-steady state.

Figure 6a illustrates the performance of different evaporation models in predicting f_T under varying soil moisture conditions. For most models, as the soil dries out, a lower degree of transpiration is predicted (i.e. a higher degree of evaporation relative to transpiration). This is in contrast to assessments of transpiration fraction from gross primary productivity (GPP), which predict higher transpiration fractions under drier conditions. This is because during dry spells plants can access water at lower depths and of lower matric potential and thus maintain higher transpiration rates, while evaporation should comparatively decrease under drier conditions (Maxwell & Condon, 2016). It should be noted that the f_T values predicted by the CG-nopt, SDF and SDF+AERO models under dry conditions approximately match the magnitude of the same values from the GPP method, strengthening the case for the mechanistic controls mentioned above.

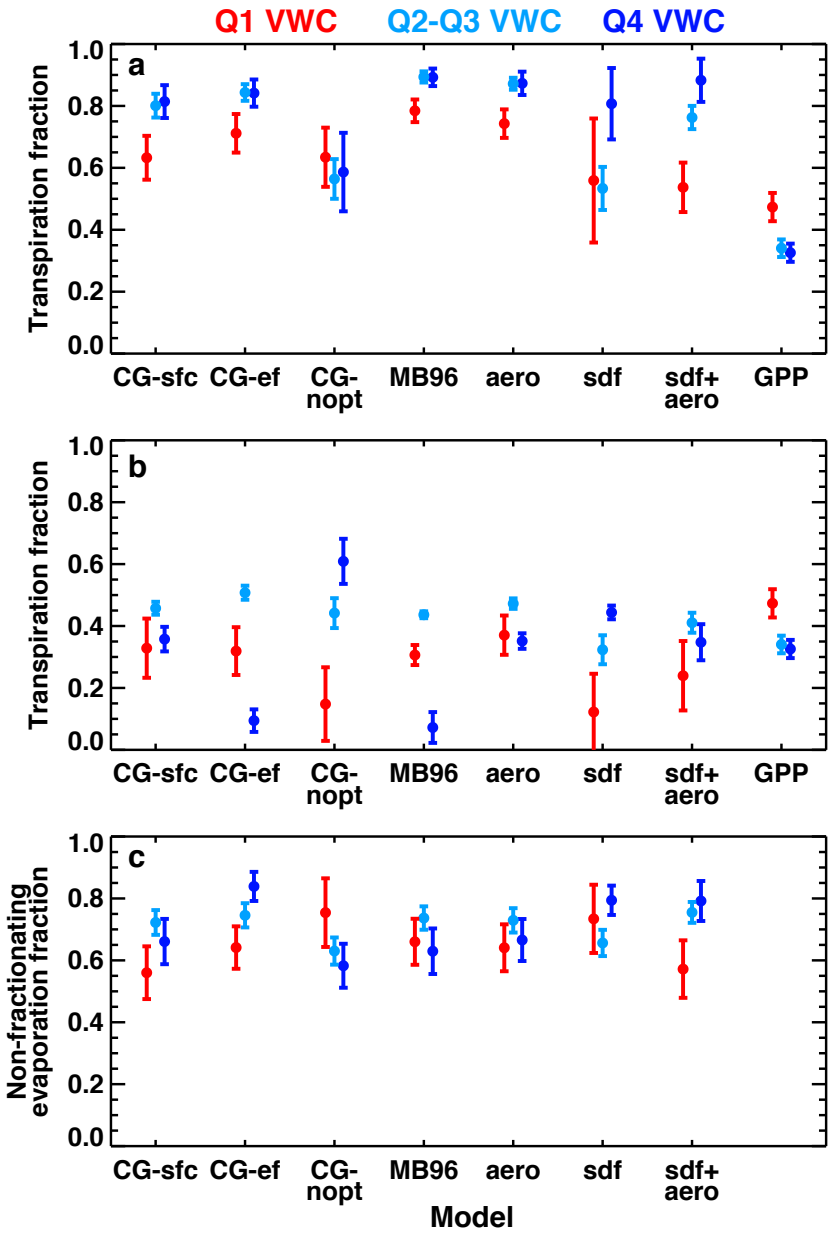

Figure 6: (a) Transpiration fraction calculated for seven different model tests (see Table 2) for lowest quartile (Q1), intermediate quartiles (Q2-Q3) and highest quartile (Q4) of total volumetric water content in the top 15 cm of the soil column, compared to GPP method, (b) Transpiration fraction for same seven model tests including a non-fractionating evaporation component, (c) Non-fractionating evaporation fraction. Note that the fractionating evaporation fraction (not plotted here) is simply 1 minus the non-fractionating evaporation fraction plotted in (c). The GPP method predicts a transpiration fraction of 0.38 ± 0.08, while the average of all models shown here is 0.67 ± 0.08 for (a) and 0.43 ± 0.03 for (b) where non-fractionating evaporation is included in the calculation. Non-fractionating evaporation in (c) makes up 58-84 % of the total evaporation under wet (Q4) conditions, and 56-75 % of the total evaporation under dry (Q1) conditions.

To resolve the mismatch with the GPP method, we introduce a partitioning approach in which some portion of the total evaporation results from near complete evaporation of soil water as the soil dries. A complete removal of the source water pool will result in evaporation from that pool being net non-fractionating, as by mass balance all of the liquid will now be in the vapor phase. This contrasts with conventional assumptions that evaporation is subject to both kinetic and equilibrium fractionation, and that all non-fractionating contribution comes from transpiration. In the new approach, we divide evaporation into two hypothetical parts which differ in the degree to which fractionation is expressed, and re-write equation (5) as:

$$R_{ET} = f_T R_T + (1 - f_T)\left[f_{EF} R_{E,f} + (1 - f_{EF}) R_{E,nf}\right] \qquad (18)$$

where f_{EF} is the fraction of evaporation flux that is fractionating, $R_{E,f}$ is the isotope ratio of this fractionated evaporation flux, and $R_{E,nf}$ is the isotope ratio of a new term – the non-fractionating evaporation flux. $R_{E,f}$ corresponds to R_E from equation (6). As in equation (5), R_T is the isotopic ratio of the non-fractionating transpiration flux, calculated as the weighted average of the soil column water isotope ratios corresponding to approximate rooting depths of plants at the BAO site, and f_T is the transpiration fraction. We assume that $R_{E,nf}$ corresponds to the isotopic ratio of the evaporation front (above which evaporation may be assumed to be almost complete), and therefore equation (18) can be used to find f_T and f_{EF} values that minimize the error between the modeled and observed isotopic ratio of evapotranspiration flux. The location of the evaporation front corresponds to where maximum soil moisture values are seen in the 0 to 1 m depth profile.

To perform the error minimization, a "cost" is defined:

$$Error = \frac{(ET\_Dexcess_{model} - ET\_Dexcess_{obs})^2}{(\sigma_{Dexcess})^2} + \frac{(A_{model} - A_{obs})^2}{(\sigma_A)^2} \qquad (19)$$

where A = (δD+8δ^{18}O)/2, and σ is the variance due to natural variability (temporal standard deviation of measurements) and measurement error. A combination of D_{excess} and the A parameter are used to emphasize the equal interest in both kinetic and equilibrium processes. The results of this approach are plotted in Figure 6b&c, where the non-fractionating evaporation fraction is simply (1-f_{EF}). Three key results emerge: (a) f_T values overall are lower for all wetness quartiles for all models, (b) several models now match the GPP method for magnitude of f_T values predicted under wetter conditions, and (c) some non-fractionating contribution has now been re-assigned to evaporation. The inclusion of non-fractionation reconciles f_T estimates under dry conditions for models which previously did not match GPP estimates (CG-sfc, MB96, AERO), but not for models which already explicitly accounted for weaker kinetic fractionation (CG-nopt, SDF, SDF+AERO). This has implications for diagnosing mechanistic controls on isotope ratios under different soil moisture conditions.

3.4 Evaluation of net ecosystem flux

Using a bulk flux approach, a net ecosystem kinetic fractionation factor can be derived which provides a complementary estimate of the relative contribution from non-fractionating turbulent exchange versus fractionating diffusive processes. It should be noted that comparing equation (3) and equation (6), we see that equilibrium fractionation could be incorporated into the R_{eff} term. We use equation (4) to calculate the effective kinetic fractionation factor (ε_{k-eff}) as latent heat flux-weighted 3-day running means. Figure 7 shows these values plotted as $\varepsilon_{k-eff} = (\alpha_{k-eff} - 1) * 1000$, as a function of soil moisture and binned by the friction velocity u_*, which is a measure of near surface turbulence measured at the height of the sonic anemometer (10 m). Under high soil moisture conditions in all u_* regimes, the effective kinetic fractionation factor is

indistinguishable from $\varepsilon_{k-eff} = 0$. This implies that exchange processes controlled by temperature-based equilibrium fractionation must dominate over kinetic processes under near saturation conditions. For low u_* regimes under all wetness conditions, the system is also characterized by conditions where equilibrium fractionation dominates. It should be noted that evaporation is low overall under low u_* and dry conditions (i.e. soil moisture quartile Q1). For dry conditions with high u_*, where a high vapor pressure deficit demand is expected to drive water out of the soil, ε_{k-eff} values are -6.99 ± 3.39‰ for δ^{18}O. There is too much error to derive robust estimates of ε_{k-eff} values from δD. The source of this error may lie in the kinetic effect being relatively small for δD compared to equilibrium effects. Nonetheless, a value of -6.99‰ suggests some contribution from sub-surface kinetic diffusion limitation, and results in a value of $n = 0.25$ for δ^{18}O. While in agreement with the process-based optimal estimate given above, it should be noted that this is much lower than typically assumed for ecosystem fluxes (c.f., Merlivat, 1978; Allison et al., 1983; Lee et al., 2009), and instead is indicative of non-fractionating processes contributing more to evaporation fluxes than previously thought, similar to results from Figure 6. As shown above, the use of an n value of around 0.2 in parameterizing kinetic fractionation appears to perform well in capturing some of the physical exchange associated with sub-surface diffusion and the SDF model.

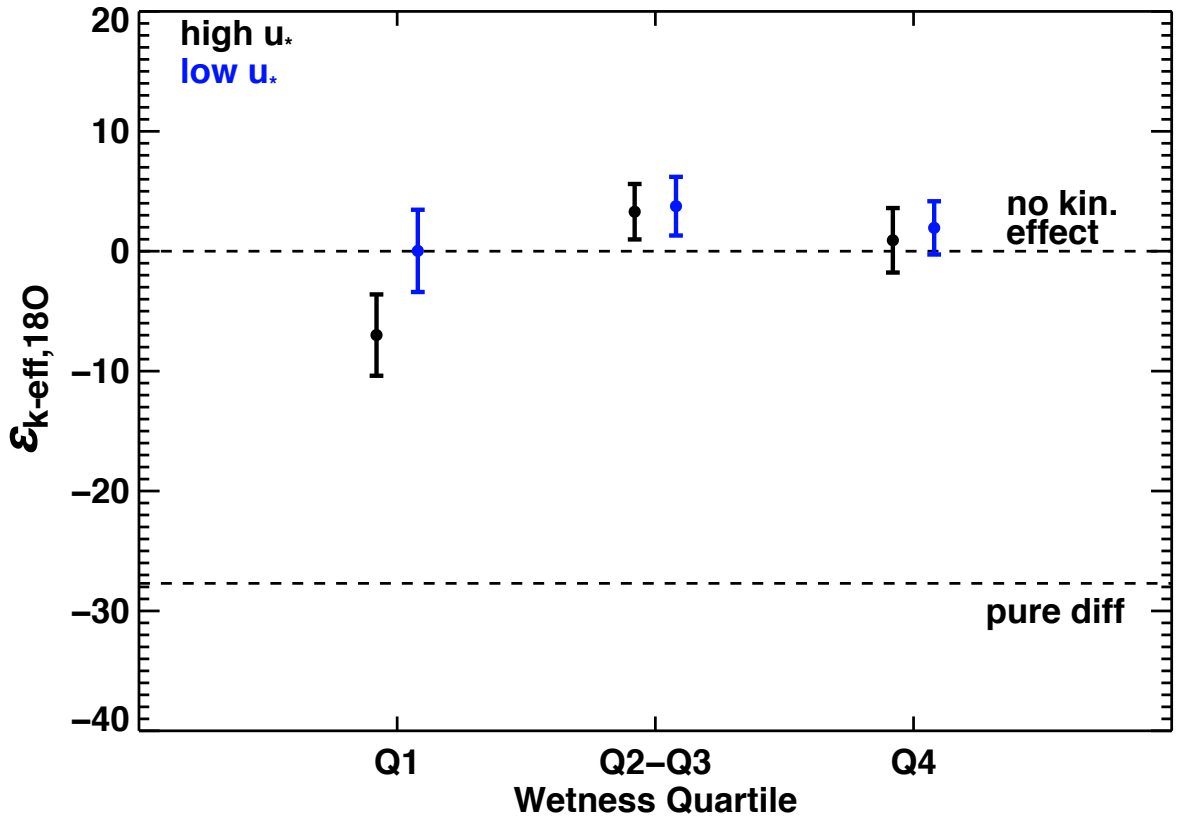

Figure 7: Effective kinetic fractionation factors evaluated under dry to wet conditions under high u_* ($u_* \geq 0.25$) and low u_* ($u_* < 0.25$) regimes for $H_2{}^{18}O$. Under high soil moisture conditions in all u_* regimes, the effective kinetic fractionation factor is indistinguishable from $\varepsilon_{k-eff} = 0$. For dry conditions with high u_*, where a high vapor pressure deficit demand is expected to drive water out of the soil, ε_{k-eff} values are -6.99 ± 3.39‰ for $\delta^{18}O$, which results in a value of $n = 0.25$.

Figure 8 shows a probability distributions of isotope ratios in vapor, evapotranspiration flux, rain and soil for the growing season from May through October, and offers a climatological context for an average "ecosystem kinetic fractionation" in this semi-arid ecosystem. This extended summer period excludes snow events. Using an average 10 m air temperature, the expected liquid equivalent isotope ratio is calculated by applying equilibrium fractionation to the 8.4 m vapor isotope values. This is shown on Figure 8 as the arrow α_{eq}, which corresponds to a 9.8 ‰ enrichment for $\delta^{18}O$ and 74.9 ‰ enrichment for δD. The total fractionation is the difference

between the soil and vapor isotope delta values, which is a 15.2 ‰ for δ^{18}O and 79.0 ‰ enrichment for δD (α_{total}). The net effective kinetic fraction (α_{k-eff}) is shown graphically as the difference between the total fractionation and the temperature-dependent equilibrium fractionation. This corresponds to -5.4 ‰ for δ^{18}O and -4.2 ‰ for δD, which equate to n values of 0.194 and 0.168 for δ^{18}O and δD respectively. Here, on the climatological time scale, we again find support for weaker kinetic fractionation contributions to the total evapotranspiration flux.

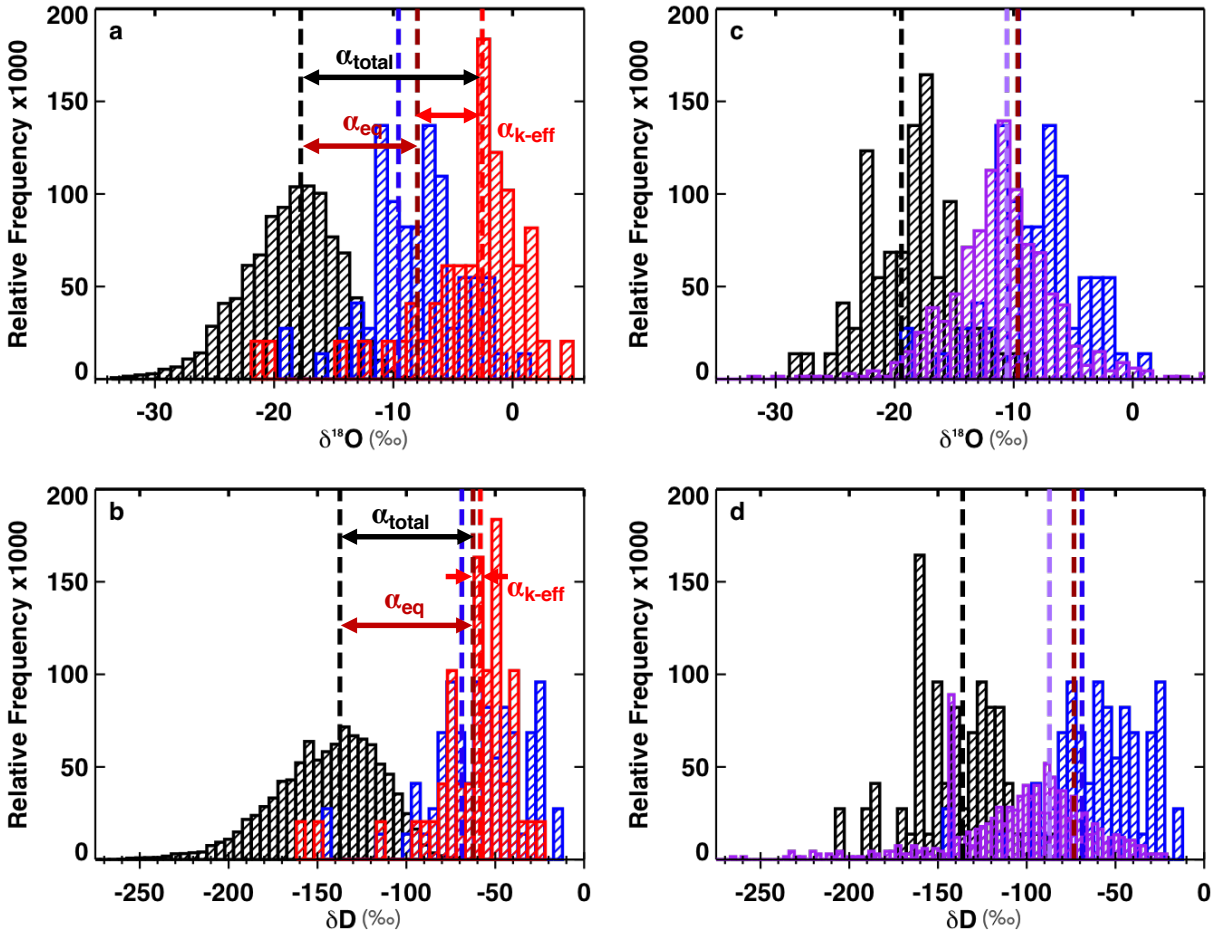

Figure 8: Histograms showing climatology of water isotope ratios in vapor (black), surface soil layer (red), precipitation (blue) and evapotranspiration flux (purple) for (a,c) δ^{18}O and (b,d) δD for May-Oct 2012-2015. Dashed lines represent weighted means of the plotted quantities, brown dashed line is the liquid-equivalent ($\delta_{liq-eqv}$) of the sampled vapor subject to only equilibrium fractionation. Vapor shown in c & d is sub-set to match rain events, and is weighted by precipitation to illustrate the equilibrium fractionation effect on

rainy days compared to all days (a & b). a & b allow for calculation of an 'ecosystem kinetic fractionation' (α_{k-eff}). The offset between $\delta_{liq-eqv}$ and mean precipitation is indistinguishable in c & d, while in a & b the interaction of soil water with vapor brings $\delta_{liq-eqv}$ into disequilibrium with precipitation and shifts it towards equilibrium with soil water on seasonal timescales.

The determination of an effective ecosystem kinetic fractionation is more robust for $\delta^{18}O$ versus δD, due to (a) comparable magnitude of kinetic and equilibrium effect for $H_2{}^{18}O$ compared to HDO when the kinetic fractionation is small compared to the equilibrium fractionation, and (b) lower uncertainty in $\delta^{18}O$ measurements versus δD. Figure 8 also illustrates a tighter coupling between soil and vapor δD values, with temperature-dependent equilibrium fractionation accounting for 94.7% of the total fractionation for δD compared to 64.3% for $\delta^{18}O$.

Figures 8c & d show that the liquid-equivalent isotope ratio of the ambient vapor during rain events (brown dashed line) is indistinguishable from the weighted mean value of the precipitation at this site (blue dashed line); $\delta_{\text{difference}}$ is -0.09 ‰ for $\delta^{18}O$ and -4.6 ‰ for δD. If the vapor associated with precipitation is composed from air masses accompanying the precipitation, with the precipitation values being set by condensation from this vapor, a closer correspondence between the precipitation and liquid-equivalent vapor values during rain events would be expected. In Figures 8a & b, the $\delta_{\text{difference}}$ between weighed mean of vapor during all days (rainy and non-rainy) and weighted mean of precipitation is +1.6 ‰ for $\delta^{18}O$ and +6.3 ‰ for δD. This observed offset can be explained by the return of precipitation water to the atmosphere from the soil, where evaporation brings the vapor into disequilibrium with the precipitation, while nudging the vapor closer to equilibrium with soil water. The stronger equilibrium fractionation shown in Figures 8a & b, which includes vapor from all days, supports the hypothesis that the atmospheric vapor is recharged by soil evaporation on seasonal timescales. Finally, if all precipitation were simply to

be returned to the atmosphere via evapotranspiration, we would expect the weighted mean of the evapotranspiration to be close to that of rainfall. Any offset here is likely explained by soil recharge and runoff.

4. Discussion and Conclusions

Profile observations of stable water vapor isotope ratios in the atmospheric surface layer coupled to soil column water isotope ratios offer insight into the mechanisms dominating energy and water exchange at the land surface under different wetness regimes. At the semi-arid BAO site, soil water isotope ratio values are set predominantly by evapotranspiration acting in two ways: (a) near complete removal of all precipitation working to set the seasonal mean isotope ratio of vapor, and (b) isotopic exchange between near-surface vapor and dry soils bringing soil isotope ratios to near equilibrium. Depth-resolved soil water isotope ratio data highlight significant sub-surface vapor diffusion contributions to surface flux from dry unsaturated soils.

Despite its common use, it is found that the Craig-Gordon (CG) model in which evaporation is assumed to derive from near surface soil water does not reproduce observations (Figure 5). The biggest discrepancies arise from the choice of the kinetic fractionation factor α_k, which in turn is a statement on the lack of constraint on diffusive versus non-fractionating (or weakly kinetic) exchange. Using a simple two-stream approach, where evapotranspiration is divided into non-fractionating transpiration and fractionating evaporation an average transpiration fraction (f_T) value of 0.67 ± 0.06 is found for all model tests. However, Table 2 shows the spread obtained for evaluating f_T from different modeling approaches and it can be seen that using modified parameters based on either soil wetness alone (MB96) or aerodynamic resistances alone (AERO) are inadequate. If one assumes that all non-fractionating flux is associated with transpiration in the

set of different models considered herein, the average annual f_T values obtained are in the range of 57-86%, with the lowest values evident in models that include vapor diffusion within the soil matrix or assume evaporation from the evaporation front is associated with weaker kinetic fractionation (Figure 6). Indeed, comparing $f_T$values derived from isotope-based methods with an independent method based on gross primary productivity (GPP), a match in values obtained with the CG-nopt, SDF and SDF+AERO models under dry conditions provides reassurance that these models are consistently capturing the mechanisms of water exchange in dry environments.

Results from bulk flux and isotope climatology approaches for estimating net kinetic isotopic fractionation at BAO indicate that the basic assumption of evaporation always being fractionating is incorrect. This conclusion arises from the optimal selection of an effective kinetic fractionation factor based on an exponent of $n \sim 0.2$-0.25, which is lower than typical assumed for n (Figures 7 & 8). The consequence of this on the traditional ET partitioning problem is that it is likely that a portion of the flux assigned to transpiration (traditionally assumed non-fractionating) is better assigned to evaporation, and therefore isotope partitioning methods likely overestimate the true transpiration fraction unless proper accounting of subsurface processes is made. If one includes a non-fractionating evaporation component in the total flux estimate from isotope-based models, 58-84% of evaporation during wetter conditions and 56-75% during drier conditions is found to be non-fractionating. Importantly, this reconciles the mismatch in f_T values with the GPP method, where f_T values of 0.38 ± 0.08 calculated for all wetness conditions now overlap with f_T values of 0.43 ± 0.03 from modified isotopic models with non-fractionating evaporation (Table 3). Figure 6 shows that inclusion of an evaporation pool which is not fractionating (following equation 18) is more important from the modeling perspective under saturated conditions. Inclusion of a non-fractionating evaporation fraction brings f_T values for Q2-Q4 wetness quartiles more in line with

the GPP method. Importantly though, since the original f_T values derived for SDF and SDF+AERO under dry conditions match the GPP method, adding a non-fractionating component to these particular models may artificially lower f_T values predicted by these particular models under dry conditions.

Model	$f_{T,wet}$	$f_{T,med}$	$f_{T,dry}$	$f_{T,all}$
CG-nopt	0.61 ± 0.07	0.44 ± 0.05	0.15 ± 0.12	0.40 ± 0.23
SDF	0.45 ± 0.06	0.34 ± 0.05	0.12 ± 0.12	0.30 ± 0.16
SDF + AERO	0.35 ± 0.05	0.38 ± 0.03	0.24 ± 0.10	0.33 ± 0.09
GPP	0.33 ± 0.03	0.34 ± 0.03	0.47 ± 0.05	0.38 ± 0.08

Table 3. Transpiration fractions calculated for different soil wetness regimes after incorporating non-fractionating contribution to evaporation. Error values are quoted as 1 standard deviation error on the estimates.

There are four possible origins of the weak kinetic fractionation observed: (1) the system is at equilibrium, (2) the system is dominated by pure turbulence, (3) the system is at steady state, or (4) the evaporation of water at the evaporation front is nearly complete and therefore there is no net fractionation. Scenario 1 is not the likely explanation as there would be no evaporation under equilibrium conditions, and easily rejected based on observed fluxes. Scenario 2 is also not likely as observations show the source of evaporation is almost always below the surface (Figure 3) and there is effectively no turbulence in soil. Diffusive processes are important for sub-surface transport, as is evident in the D_{excess} of residual soil water and the shallower slopes of the upper soil layers on a δD-δ^{18}O plot (Figure 4). Scenario 3 could be true in cases where the evaporation front is the primary source for evaporation and the lack of observed fractionation is similar to the steady state explanation for transpiration. Scenario 4 is supported by results which show strong

and near complete drying of the upper levels of soil in the days following summer precipitation events.

The traditional use of stable water isotope ratios to partition evapotranspiration is rooted in the assumption that evaporation is fractionating whereas steady state transpiration is not. This may be the case in near-saturated environments where water availability is not limiting, however in dry environments such as semi-arid grasslands where water may be removed entirely from the soil column, greater care is needed. Isotope ratio data from the targeted closure experiment described here suggest that a portion of evaporation can be non-fractionating in a manner similar to that more frequently reserved for describing transpiration, which would yield a positive bias in the derived transpiration fraction. Therefore, appropriate modifications to account for evaporation processes must be included in isotope-based approaches seeking to estimate partitioning in drier environments.

CHAPTER III

Rain re-evaporation modeled using stable water isotope observations in vapor and precipitation coupled to disdrometer measurements at a midlatitude 300-m tall-tower site

1. Introduction

A key feature of convective boundary layer moisture cycling is the degree of recycling and remoistening from evaporating raindrops, which can have a direct influence on heat and moisture budgets (Emanuel et al., 1994). Evaporating raindrops have also been linked to the formation and maintenance of downdrafts in storm systems (Bony et al., 2008; Emanuel, 1991). However, the degree to which rain evaporation contributes to moisture recycling is uncertain (van der Ent et al., 2010; Worden et al., 2007). Land-atmosphere interactions play a crucial role in moderating continental moisture fluxes (Koster et al., 2004; Seneviratne et al., 2013), however, climate models simulating these interactions show a wide range of possible outcomes (Guo et al., 2006; Koster et al., 2006; Wei & Dirmeyer, 2010). Water vapor feedbacks are especially important in arid and semi-arid regions of the world, where water recycling and the associated greenhouse effect of water vapor can be very sensitive to humidity changes (Eltahir, 1998; Risi, Bony, Vimeux, Frankenberg, et al., 2010).

The relative roles of transport, mixing and phase changes which contribute to boundary layer moisture dynamics during precipitation events can be difficult to separate with bulk moisture fluxes alone. Stable water isotope ratios of rain and water vapor, δD and δ^{18}O, are a useful tool to investigate hydrological cycle processes (Dansgaard, 1953, 1964; Gat, 2000). At regional scales, knowledge of isotope ratios of fluxes has helped assess continental rainfall recycling (Risi, Bony, Vimeux, Frankenberg, et al., 2010) and mechanisms controlling remoistening of the troposphere

(Berkelhammer et al., 2012; Gat & Airey, 2006; Noone, 2012; Stump et al., 2014). At global scales, water isotope ratios have been used to explore global land-atmosphere interactions (Good et al., 2015; Hoffmann et al. 2000; Werner et al., 2011), and to reconstruct past environmental conditions such as ambient temperature and relative humidity (Helliker & Richter, 2008). However, interpreting isotope records of past climate requires a detailed understanding of underlying moisture transport and exchange processes. Dominant controls on $\delta^{18}O$ are variable between proxy sites and include local precipitation amount variability together with changes in regional hydrology, the initial evaporative source, degree of rain-out during transit and atmospheric mixing (e.g., Hendricks et al., 2000; Jones et al., 2016; Jouzel et al., 1997; Yoshimura, 2015).

Latitudinal and seasonal differences in the isotopic composition of precipitation can be related to air mass source (Berkelhammer et al., 2012; Buenning et al., 2012; Dansgaard, 1953, 1964; Sjostrom & Welker, 2009; Vachon et al., 2010). The $\delta^{18}O$ in precipitation ($\delta^{18}O_p$) integrates changes in atmospheric circulation from source to the site of rainout (Brown et al., 2008; Crawford et al., 2016). In addition to the stable isotopic compositions δD and $\delta^{18}O$, deuterium excess signatures ($D_{excess} = \delta D - 8\delta^{18}O$) have been used to interpret specific changes such as sub-cloud evaporation and continental recycling (Aemisegger et al., 2014; Conroy et al., 2016; Crawford et al., 2013; Froehlich et al., 2008; Kong et al., 2013). Because the diffusivity of $H_2{}^{18}O$ differs from that of HDO, D_{excess} is particularly sensitive to kinetically fractionating processes and can therefore provide information about conditions under which these processes dominate over equilibrium fractionation (Gat & Gonfiantini, 1981; Mook, 2001). During evaporation of falling raindrops, strong gradients in relative humidity can result in vapor and rain phases not reaching isotopic equilibrium, which would result in a D_{excess} signal reflecting kinetic processes. In general, observational evidence suggests that sub-cloud evaporation results in a more negative D_{excess} value

while continental recycling results in a more positive D_{excess} value. However, it remains unclear if the simple theory is adequate to describe the real physical mechanism in nature.

Large changes in isotopic values can also exist within a rain shower or between showers of different types, intensities or water yields (Coplen et al., 2008; Lee et al., 2007; Muller et al., 2015; Rindsberger et al., 1990). Raindrops start out with an isotopic signature imprinted by the in-cloud processes where rain originally formed (Bolin, 1959; Bolot et al., 2013; Friedman, 1962; Kurita et al., 2011; Lee et al., 2009), but isotopic exchange between falling raindrops and ambient vapor can theoretically result in equilibration between the raindrops and boundary layer vapor (Lee & Fung, 2008; Stewart, 1975; Rozanski et al., 1993) while rain falling through a unsaturated atmosphere can undergo evaporative enrichment (Dansgaard, 1964; Gat et al., 1994). Isotope ratio information therefore provides a mechanistic way to trace process-level interactions between vapor and precipitation.

Satellite observations of vapor δD have been used to improve representations of evaporation, large-scale mixing and deep convection in atmospheric general circulation models (Berkelhammer et al., 2012; Frankenberg et al., 2009, 2013; Galewsky et al., 2016; Noone, 2012), however, these observations are incomplete as there is no observational verification that they should work for raindrop populations or for special situations such as downdrafts. For example, if all small raindrops evaporate, there should be no net fractionation associated with this process as all the water mass in raindrops is simply moved into vapor phase. Similarly, rain in equilibrium with vapor associated with a downdraft should show no kinetic enrichment, because both isotope signatures reflect the equilibrium cloud condensation conditions under which the raindrops were initially formed. The well-known "amount effect" for tropical precipitation (Dansgaard, 1964; Rozanski et al., 1993), where higher precipitation rates are associated with lower isotope ratios, is

hypothesized to be the result of several processes including condensation, downdraft moisture recycling, mesoscale organization, regional circulation and rain evaporation (e.g., Conroy et al., 2016, and references therein). It is therefore important to understand the effect of these processes on isotope ratios in order to correctly interpret modern and paleoclimate proxy records which are traditionally interpreted on the basis of the amount effect.

A tall-tower site is the ideal location to study boundary layer moisture cycling because coupled measurements of water and vapor isotope ratios at multiple heights allow us to examine the processes controlling the exchange between rain and vapor under differing boundary layer humidity and precipitation conditions to be sampled. In addition, instruments that measure drop size information enable us to interpret the isotope ratios in terms of physical changes in raindrops at different heights to test prevailing microphysical theory. This analysis seeks to: (1) describe the different synoptic scales and conditions under rainfall occurrences at BAO for individual precipitation events and at seasonal scales, (2) evaluate the degree to which raindrops are in equilibrium with vapor, both at the surface and at 300 m (the top of the tall-tower); a difference in equilibration at the two heights is a measure of the degree to which rain evaporation contributes to moisture recycling, and (3) provide an evaluation of existing approaches to determine fractionation processes in raindrops and whether these approaches are valid for observations of drop populations. Using the tower observations, we contrast the shortcomings of assuming average drop sizes (Stewart, 1975) or drop populations (Lee & Fung, 2008), and evaluate expected equilibration associated with different size distributions. Results indicate a strong degree of equilibrium between rain and vapor at seasonal scales, but event-scale observations highlight an overall lower degree of equilibration and an important lack of equilibration for downdrafts in convective systems versus stratiform drizzle events. We demonstrate the need to account for complete evaporation of smaller

raindrop populations during certain events, which leads to a weaker than expected overall fractionation.

2. Methods

2.1 Field site and measurement techniques

Measurements were made at the 300-m- tall Boulder Atmospheric Observatory (BAO) tower site in Erie, Colorado (40.050N, 105.003W, 1584 m a.s.l.). For more site details and operational history, the reader is referred to the website http://www.esrl.noaa.gov/psd/technology/bao/site/ and to Wolfe & Lataitis (2018). In addition to meteorological, flux and soil moisture and temperature measurements, a Picarro L2120-i water vapor isotope analyzer, capable of measuring $^{2}H/^{1}H$ and $^{18}O/^{16}O$, was installed in a temperature-controlled laboratory on-site. Stable isotope values are expressed in permil units (‰) and are referenced to the international standard Vienna Standard Mean Ocean Water (VSMOW):

$$\delta\ (‰) = \left(\frac{R}{R_{std}} - 1\right) \times\ 1000 \qquad (1)$$

where R is the isotopic ratio of the sample (e.g. D_{spl}/H_{spl} or $^{18}O_{spl}/^{16}O_{spl}$) and R_{std} is the isotopic ratio of the standard VSMOW [$R_{std}(D) = 1.558\text{x}10^{-4}$, $R_{std}(^{18}O) = 2.005\text{x}10^{-3}$].

Deuterium excess, "D_{excess}", is defined as:

$$D_{excess} = \delta\text{D} - 8*\delta^{18}\text{O} \qquad (2)$$

and is a useful diagnostic for tracing kinetic processes. For raindrops falling through a sub-saturated atmosphere, lighter isotopes are preferentially evaporated, which results in more negative D_{excess} values in rain and, by mass balance, more positive D_{excess} values in vapor. Figure 1 illustrates two different regimes under which rainfall can change isotopes ratios. For rain falling through

higher humidities, at lower temperatures and with a higher rain rate, there is likely to be less evaporation and consequently exchange with ambient vapor is the main mechanism controlling the isotopic signature of rainfall. If that vapor happens to be from the cloud where the rain was formed, as in the case of a downdraft, then the vapor and precipitation isotope signatures are expected to reflect the condensation processes by which the rain originally formed. For rain falling through lower ambient humidity, at higher temperatures or with a lower rain rate, evaporation of raindrops is likely to occur. During evaporation, microphysical considerations predict that smaller drops will evaporate faster, leaving a larger proportion of large drops reaching the ground (Salamalikis et al., 2016). In addition, HDO evaporates preferentially from a raindrop compared to $H_2{}^{18}O$ because of lower mass dependent diffusivity and therefore the residual D_{excess} in rainfall is expected to be lower, with a corresponding positive anomaly in the vapor phase.

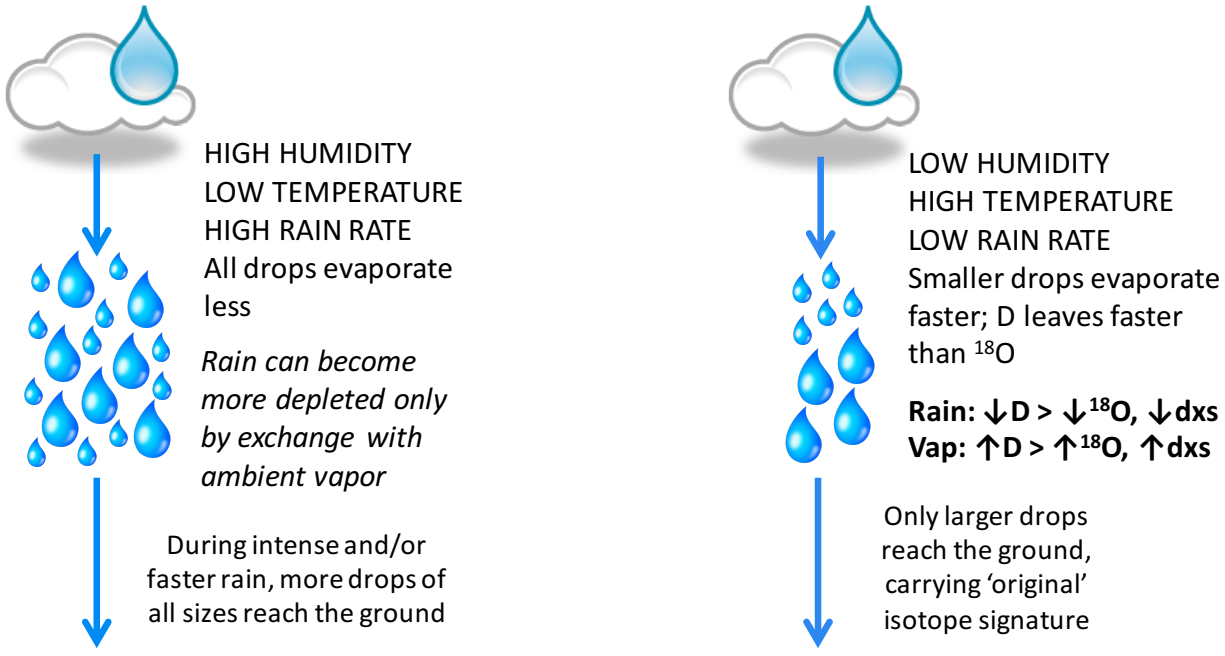

Figure 1: Schematic representations of how raindrop distribution, evaporation, humidity, temperature and rain rate could control observed isotope ratio values. Smaller drops evaporate faster because they have greater curvature and less connections between water molecules and require greater vapor pressure to prevent evaporation.

2.1.1 Stable isotope ratio measurements

Isotope ratios in water vapor were measured sequentially at eight heights (0.43 m, 0.88 m, 1.94 m, 3.94 m, 8.40 m, 100 m, 200 m, 300 m) at approximately 0.5 Hz. The design of the measurement system is similar to that of Berkelhammer et al. (2016a, 2016b) and Tremoy et al. (2011), and a description of the measurements can be found in Kaushik et al. (2018). Briefly, the sampling interval was 10 minutes for each of the eight sample lines. The last 5 minutes of data from each inlet were used to construct mean values to avoid memory effects (Bailey et al., 2015; Berkelhammer et al., 2016a). Isotopic measurements were calibrated with reference to VSMOW by introducing a pair of secondary standard waters, chosen to bracket observations, approximately every 6 hours using the commercially available Standards Delivery Module from Picarro Inc. Following Bailey et al. (2015) and Berkelhammer et al. (2016a, 2016b), isotopic data were also corrected for humidity-dependent isotope bias and instrument drift, and specific humidity was calibrated using a dew point generator. After calibration and corrections, average standard errors for the 5-minute blocks of vapor measurements were 0.49‰ for δD and 0.07‰ for δ^{18}O. All secondary standards used in the field and in the laboratory below were tied to the International Atomic Energy Agency scale with mass spectrometer determinations at the Stable Isotope Laboratory, Institute of Arctic and Alpine Research, Boulder, CO.

Precipitation at the site was monitored from May 2012-June 2013 using an automated evaporation-proof rain collector adapted from a design (Coplen et al., 2008). The automated collector is capable of collecting rain samples at frequencies of ~ 0.5 Hz during intense downpours. A maximum of 96 samples can be collected in this Precipitation Isotope Sequential Sampling

Robot and allows observation of intra-storm variations in stable water isotope ratios. From June 2013 onwards, bulk precipitation samples were collected at the site approximately weekly using a 1-liter separatory funnel collector with ~150 ml mineral oil filled in to prevent evaporation of collected rain water. Liquid samples were analyzed following the procedure given by Noone et al. (2013). Isotope ratios of the resultant liquid samples were measured on a laboratory Picarro L2120i water isotope analyzer using a LEAP PAL autosampler system. Observed standard deviations for liquid samples were 0.16‰ for δD and 0.06‰ for δ^{18}O.

2.2 Modeling rain re-evaporation

2.2.1 Rainfall equilibration

Falling raindrops will tend towards equilibrium relative to the ambient vapor they are exposed to (Lee & Fung, 2008; Stewart, 1975). If we consider rain falling through the 300 m height of the tower, the isotopic value of rain collected at the surface can be considered to be a mix of equilibrated and non-equilibrated rain where fractional equilibration is given by f_{equil}. Therefore the predicted value of rain at the surface is given as:

$$R_{rain,obs}\ or\ R_{rain,calc} = f_{equil} * \left(R_{rain,eq}\right) + \left(1 - f_{equil}\right) * R_{rain,noeq} \quad (3)$$

where $R_{\text{rain,obs}}$ is the isotope ratio of rain sampled at the surface collector, $R_{\text{rain,calc}}$ is the expected isotope ratio of rain sampled at the surface collector, f_{equil} is the fraction of the rain that is equilibrated with vapor, $R_{\text{rain,eq}}$ is the isotope ratio of surface rain that is at equilibrium with the surface vapor after falling through the height of the tower (calculated using the 10-m air temperature) and $R_{\text{rain,noeq}}$ is the isotope ratio of rain collected at 300 m which we assume has not equilibrated with ambient vapor. Data from 300 m and the surface are used to calculate values of expected f_{equil} from equation (3) for all rain events for which we have bulk rain samples at both the

top and bottom of the tower. This calculation is also performed for $R_{rain,calc}$ for a distribution of f_{equil} for each rain event, corresponding to the distribution in raindrop sizes obtained for that rain event. Raindrop sizes are measured by Parsivel disdrometers at the surface and at 300-m, and weighted by the liquid water content in each bin size class. The difference between $R_{rain,calc}$ and $R_{rain,obs}$ is then plotted against drop size to see the effect of changing size distributions on f_{equil}, which gives an indication of how well this simple model is capturing equilibration through the height of the tower.

2.2.2 Modeling raindrop-vapor exchange

Droplet evaporation is usually described by diffusive mass loss following Fick's Law applied to spherical drops, and a similar expression can be written for isotopologues. If a drop is large or if the atmospheric layer is shallow, partial equilibration may occur. We calculated this partial equilibration as the ratio between the time needed for the raindrop to equilibrate if the drop is exposed to saturated ambient vapor, and the time needed for the raindrop to fall through the atmospheric layer depth of interest (Nusbaumer et al., 2017). The e-folding equilibration time is based on Stewart (1975) and Lee & Fung (2008):

$$\tau_e = \frac{\alpha_e r^2 \rho_{H2O} R_{H2O} T}{3 f_v D_{ia} e_s} \qquad (4)$$

where α_e is the equilibrium fractionation factor, r is the raindrop radius (m), ρ_{H2O} is the density of liquid water (kg m^{-3}), R_{H2O} is the gas constant for water vapor (J K^{-1} kg^{-1}), T is the air temperature (K), D_{ia} is the diffusivity of isotopic water vapor in air (m^2 s^{-1}), e_s is the saturation vapor pressure (Pa) at temperature T and f_v is a ventilation factor calculated as:

$$f_v = \begin{cases} 0.78 + 0.308\,x, & x \geq 1.4 \\ 1 + 0.108x^2, & x < 1.4 \end{cases} \qquad (5)$$

$$x = Re^{1/2} Sc^{1/3} \qquad (6)$$

where Re is the Reynold's number and Sc is the Schmidt number. The formulae for these are given by Pruppacher and Klett (1997):

$$Re = \frac{2r\rho V_{rain}}{\mu} \quad (7)$$

$$Sc = \frac{\mu}{\rho D_{dia}} \quad (8)$$

where ρ is the density of air (kg m^{-3}), V_{rain} is the vertical fall velocity of the rain drop in m s^{-1} (equation 12 below), and μ is the viscosity of air in kg m^{-1} s^{-1}, calculated from Rodgers and Yau (1989) as:

$$\mu = (1.72 * 10^{-5}) \left(\frac{T}{273}\right)^{1.5} \left(\frac{393}{T+120}\right) \quad (9)$$

The diffusion of isotopic water vapor in air is calculated as:

$$D_{ia} = (2.11 * 10^{-5}) \left(\frac{D}{D_i}\right) \left(\frac{T}{273.15}\right)^{1.94} \left(\frac{101325}{P}\right) \quad (10)$$

where P is the air pressure in Pa. The time scale for the drop to fall through a vertical layer (τ_f) is calculated as:

$$\tau_f = \frac{\Delta z}{V_{rain}} \quad (11)$$

where Δz = 300 m (i.e. the distance from the top of the tower to the ground). The fall velocity V_{rain} is assumed to be equal to the terminal velocity, resulting from gravitational acceleration balancing non-linear drag, and is calculated using:

$$V_{rain} = V_{terminal} = \sqrt{\frac{4}{3}\frac{2gr\rho_{H2O}}{C_d\rho_a}} \quad (12)$$

where g is gravity (9.8 m s^{-2}), r is the raindrop radius (m), ρ_{H2O} is the density of liquid water (kg m^{-3}), ρ_a is the density of air (kg m^{-3}), C_d is the drag coefficient, set to be 0.6 (Straka, 2009). The fractional equilibration (f_{equil} as in section 2.2.1) is then given by:

$$f_{equil} = 1 - e^{-\frac{\tau_f}{\tau_e}} \quad (13)$$

f_{equil} is calculated for all drop size distributions and is mass-weighted by the liquid water content in each bin to compute an average f_{equil}:

$$f_{equil,average} = \frac{\sum(f_{equil} * \frac{4}{3}\pi r^3 N)}{\sum(\frac{4}{3}\pi r^3 N)} \qquad (14)$$

where r is the raindrop radius (m), and N is the number of raindrops observed in a particular size bin. $f_{equil,average}$ is then used in equation (3) to find $R_{rain,calc}$ and compare it to $R_{rain,obs}$.

3. Results

3.1 Climatology of isotope ratios in precipitation and vapor

At this midlatitude semi-arid field site, the average summer (June-July-August) mixing ratio of water was 8.42 g/kg compared to 2.50 g/kg in the winter (December-January-February). The summer to winter difference was much larger than inter-annual variability, which was 1.4 g/kg for summer and 0.3 g/kg for winter. Seasonality in water vapor isotope ratios is principally controlled by air mass source and continental recycling of moisture. The difference in transport history contributes to lower water isotope ratio values in the winter, and higher values in the summer (Figure 2a) with summer moisture being predominantly advected from warmer southerly and south-westerly sources, namely the Gulf of Mexico and the eastern Pacific. Winter moisture is associated with flow from the colder Arctic and the north-western Pacific (Figure 3). Source vapor regions have previously been shown to be influential on seasonal isotope ratio values in the eastern US (Sjostrom & Welker, 2009; Vachon et al., 2010). Assuming a typical wintertime moisture pathway sourced over ocean water of 10 °C in the North Pacific, and a summertime transport pathway with ocean temperature near 25 °C in the Gulf of Mexico, one might expect a difference in the isotope ratio of source region water vapor of around 15 ‰ in HDO and 1.3 ‰ in

$H_2{}^{18}O$ simply from the 15 °C difference in equilibrium fractionation that occurs during evaporation. The remaining difference between summer and winter isotope values must be sourced in local effects such as evaporation.

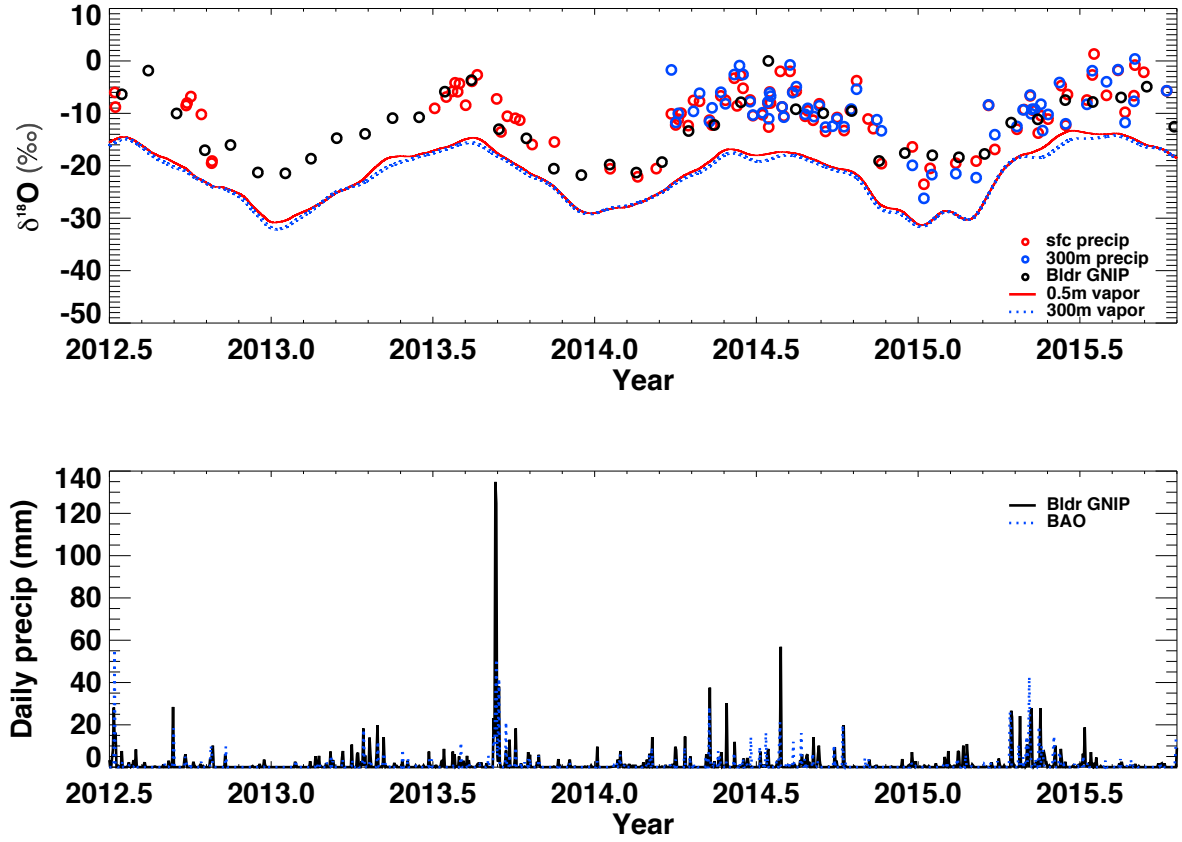

Figure 2: (a) Precipitation and vapor isotope $\delta^{18}O$ ratios at the Boulder Atmospheric Observatory (BAO) site at the surface and 300 m, and Boulder Global Network of Isotopes in Precipitation (GNIP) observations, from mid-2012 through 2015. Vapor isotope ratios are plotted as 30-day running means. (b) Daily precipitation amount for the two stations.

The Boulder Global Networks of Isotopes in Precipitation (GNIP) site is located ~23 km due west of the BAO tall-tower site, at the Foothills of the Rocky Mountains. Precipitation isotope ratio values show slightly more negative values at Boulder GNIP ($\delta^{18}O_{Bldr\text{-}GNIP}$ = -9.95 versus $\delta^{18}O_{BAO}$ = -8.73, $\delta D_{Bldr\text{-}GNIP}$ = -66.99 versus δD_{BAO} = -56.93 for May-October). This could be partly due to generally higher rainfall amounts at Boulder GNIP compared to BAO (Figure 2), but

may also reflect an east-west gradient in moisture recycling through increased rain evaporation at the more arid BAO site (a similar trend was observed in citizen science Water Spotters samples collected across an east-west transect gradient, described in Appendix A).

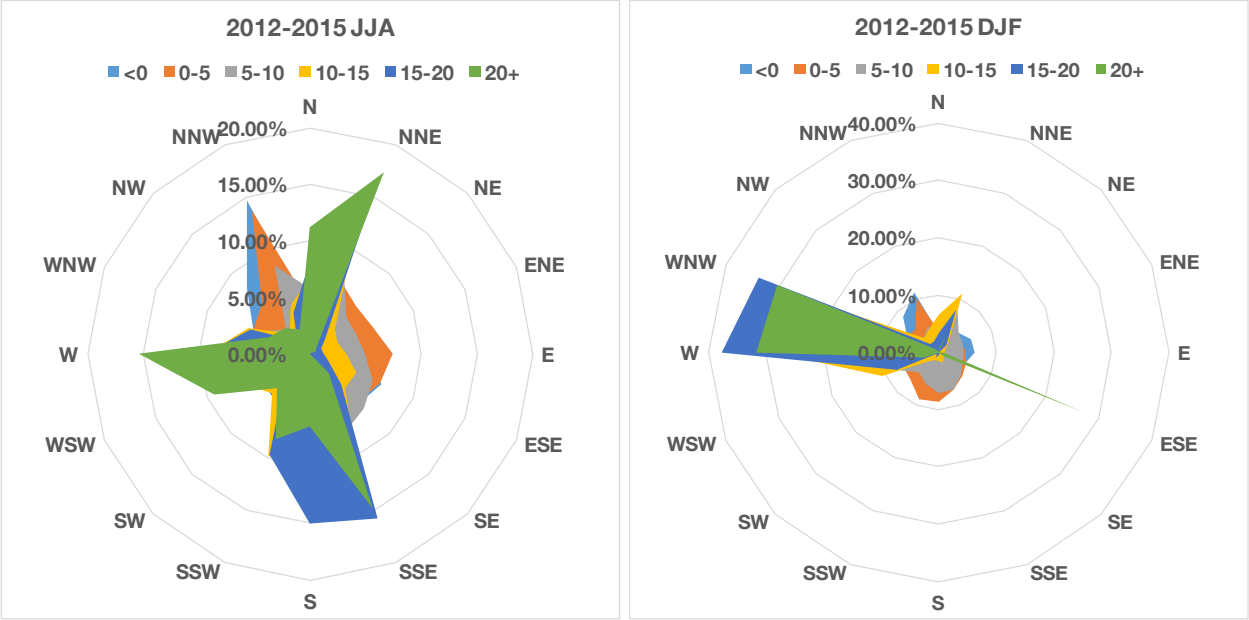

Figure 3: Predominant wind directions at BAO during summer (JJA) and winter (DJF).

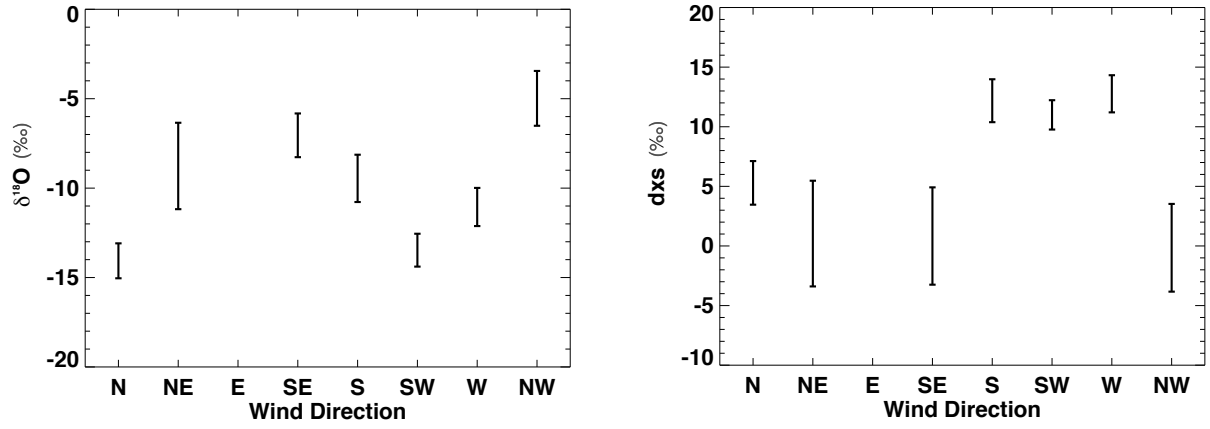

Figure 4: Precipitation isotope ratios for $\delta^{18}O$ and D_{excess} binned by wind direction for all samples collected.

Figure 3 suggests a difference between air mass source regions in summer (JJA) and winter (DJF). Precipitation isotopes binned by wind direction give an indication of the condensation history associated with air masses as they travel towards BAO (Figure 4). South to westerly moisture is associated with higher D_{excess} values, indicative of a predominantly ocean source, while lower D_{excess} values for other wind directions could be associated with regionally depleted vapor being cycled into the air masses as they pass over continental areas. The regional effect of rain falling under sub-saturated conditions in a semi-arid environment can be seen in Figure 5, which shows δD and δ^{18}O isotope ratios of precipitation and the local meteoric water line slopes for summer (May-October) and winter (November-April). Distinctly lower slopes during summer are indicative of post-condensational exchange and a higher degree of evaporation during more arid summer conditions (Salamalikis et al., 2016). Higher slopes during winter are likely due to precipitation falling as snow and continental recycling combined with reduced evaporation (Gat, 1996, and references therein). Slopes for the Boulder GNIP station are shown in addition to seasonal BAO observations and exhibit higher values than at BAO, likely because of more evaporation influence at the BAO site. Inter-annual variability is also clearly evident at BAO, with higher slopes during the summer of 2013, which was significantly wetter than other years (evident in total rainfall amounts in Figure 2 and soil moisture observations from Figure 3 in Chapter II). 2013 also included a record rainfall event where ~180 mm of rain were recorded at BAO between September 9 and 16.

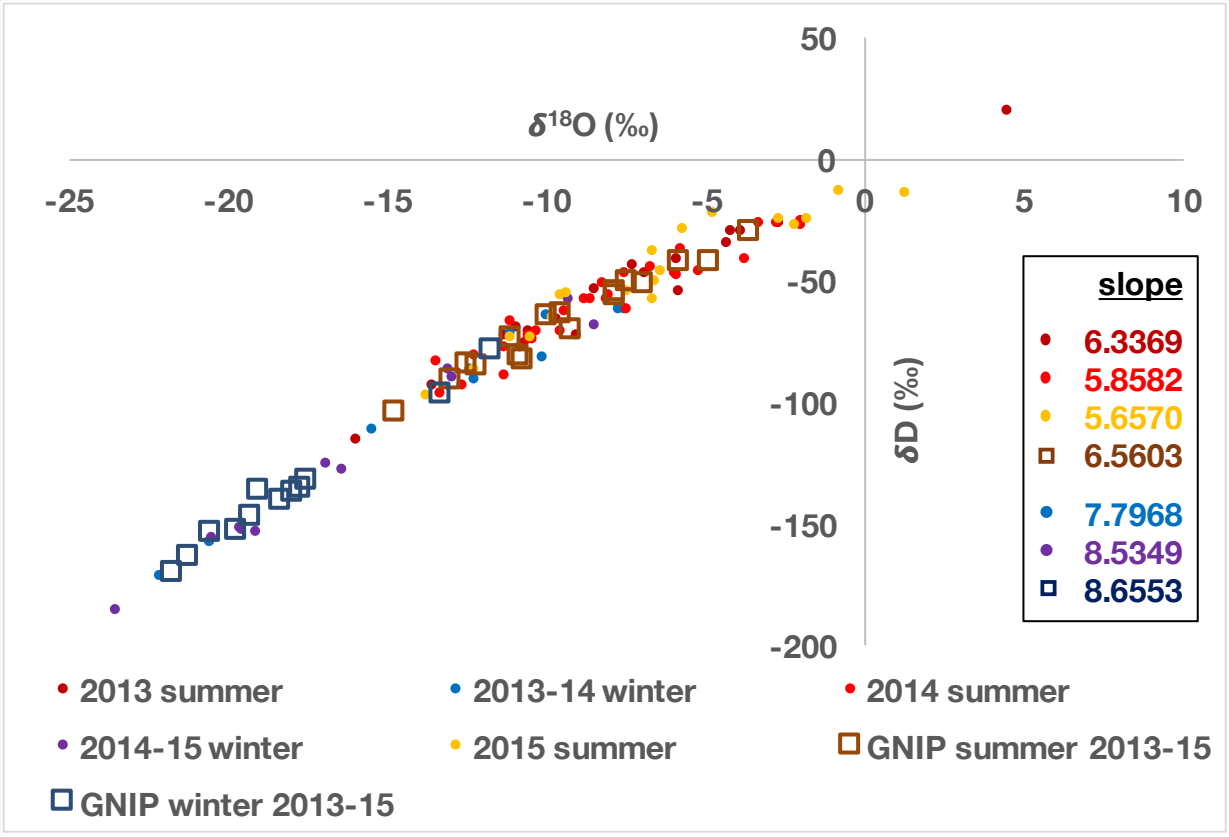

Figure 5: Stable isotope ratios (δD and δ^{18}O) of precipitation sampled from 2013-2015. Summers (May-Oct) and winters (Nov-Apr) and meteoric water line slopes corresponding to these periods in different years are indicated in different colors. The slope of the local meteoric water line is 7.09, indicating a trend towards evaporative enrichment at the BAO site. Distinctly lower slopes are seen for summer periods versus winter periods.

Observations of summer rainfall isotope ratios being influenced by evaporation are corroborated by correlations of isotope ratios with standard meteorological variables (relative humidity, rain rate, temperature), where the only significant relationship ($p < 0.001$) was found for isotope ratios and 2 m relative humidity ($R^2 = 0.23$ for δ^{18}O and $R^2 = 0.43$ for D_{excess}). The strong influence of local surface humidity on D_{excess} isotope ratios is a signal of sub-cloud evaporation (Crawford et al., 2016) and is an indication of regional seasonal control on isotope ratio values.

3.2 Event-based observations of precipitation and vapor isotope ratios

Figure 6 shows the probability distribution of isotope ratios in precipitation and vapor sub-sampled during precipitation events from 2014-2015. On the climatological scale, liquid-equivalent isotope ratio values at the surface corresponding to 8.5 m vapor equilibrated at 10 m ambient temperature appear indistinguishable from weighted mean precipitation isotope ratios (Figure 6 a & b). This indicates that, on average, surface precipitation and vapor are in equilibrium on seasonal time scales. However, a closer examination of similar observations from 300-m-height observations shows a disequilibrium between the liquid-equivalent and precipitation isotope ratios (Figure 6 c & d). The different in equilibration at the two different heights suggests a stronger kinetic effect at 300 m, which is likely related to rain evaporation processes. Parsivel raindrop size distribution data shows a greater amount of small drops at 300 m and larger drops at the surface (Figure 7). This could indicate a shift in water mass from many small drops at 300 m, undergoing evaporation, to larger drops being left at the surface, where smaller drop populations have evaporated completely.

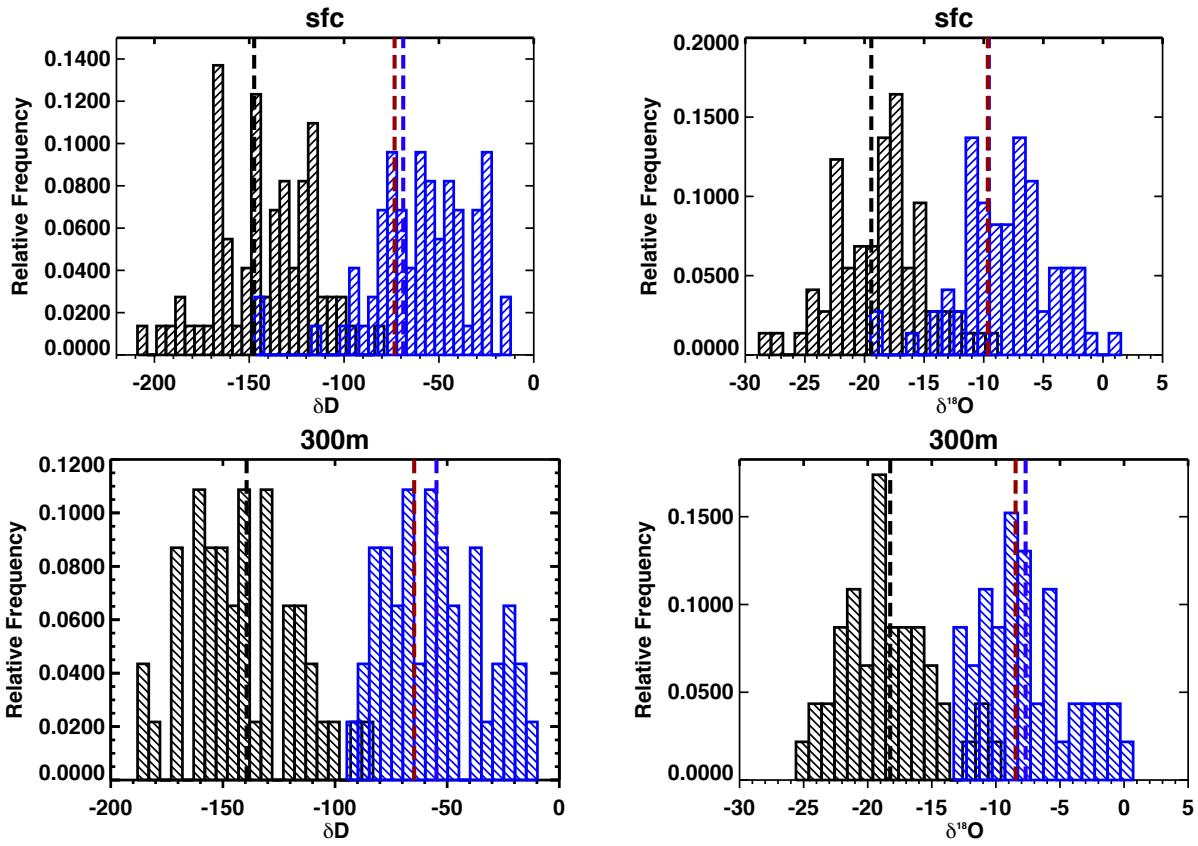

Figure 6: Histograms showing water isotope ratios in vapor (black) and precipitation (blue) for (a,c) δD and (b,d) δ^{18}O for May-Oct 2014-2015 at (a,b) surface and (b,d) 300 m. Dashed lines represent weighted means of the plotted quantities, brown dashed line is the liquid-equivalent ($\delta_{liq-eqv}$) of the sampled vapor subject to only equilibrium fractionation at ambient temperature. Vapor is sub-set to match rain events, and is weighted by precipitation to illustrate the equilibrium fractionation effect on rainy days.

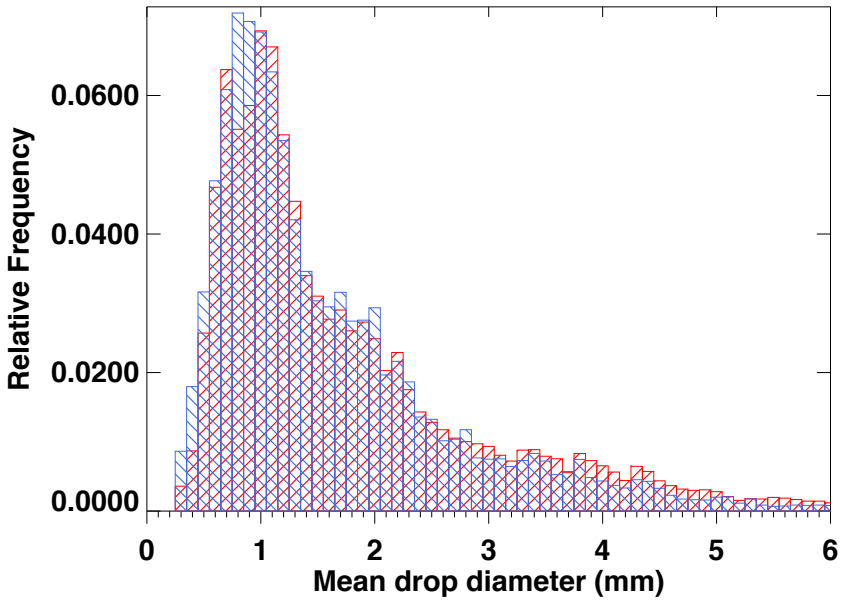

Figure 7: Histogram of drop size distributions from Parsivel instrument for May-October 2014 and 2015. Blue indicates the 300m Parsivel data, red indicates the surface Parsivel data.

Evidence for evaporative kinetic effects during individual rain events is illustrated in Figure 8. Here, intra-event samples of four precipitation events from 2012 show how isotope ratios evolve at this semi-arid site. Previous studies have connected the "U-shape" of the intra-event $\delta^{18}O$ isotope ratios as being due to frontal and convective rainfall events (Celle-Jeanton et al., 2004; Coplen et al., 2008). In three cases during July and September, there is a tendency for the D_{excess} values to trend towards ~10-12 ‰ by the end of the rain event. During the October rain event, D_{excess} also increased during the course of the rain event but stabilized around 5 ‰. The less positive D_{excess} values at the beginning of rain events in July are a reflection of the sub-saturated environment into which rain initially falls. Evaporation of falling rain would result in more negative D_{excess} values in rain (as D is lost faster than ^{18}O) and this evaporation is stronger at the beginning of rain events when the atmospheric relative humidity can be as low as 60-70%. Towards the end of the rain event, relative humidity at BAO reached 90-95% and therefore less

rain evaporation would be expected towards the tail end of rain events. In addition, rain has also undergone exchange with ambient vapor to reach partial equilibrium.

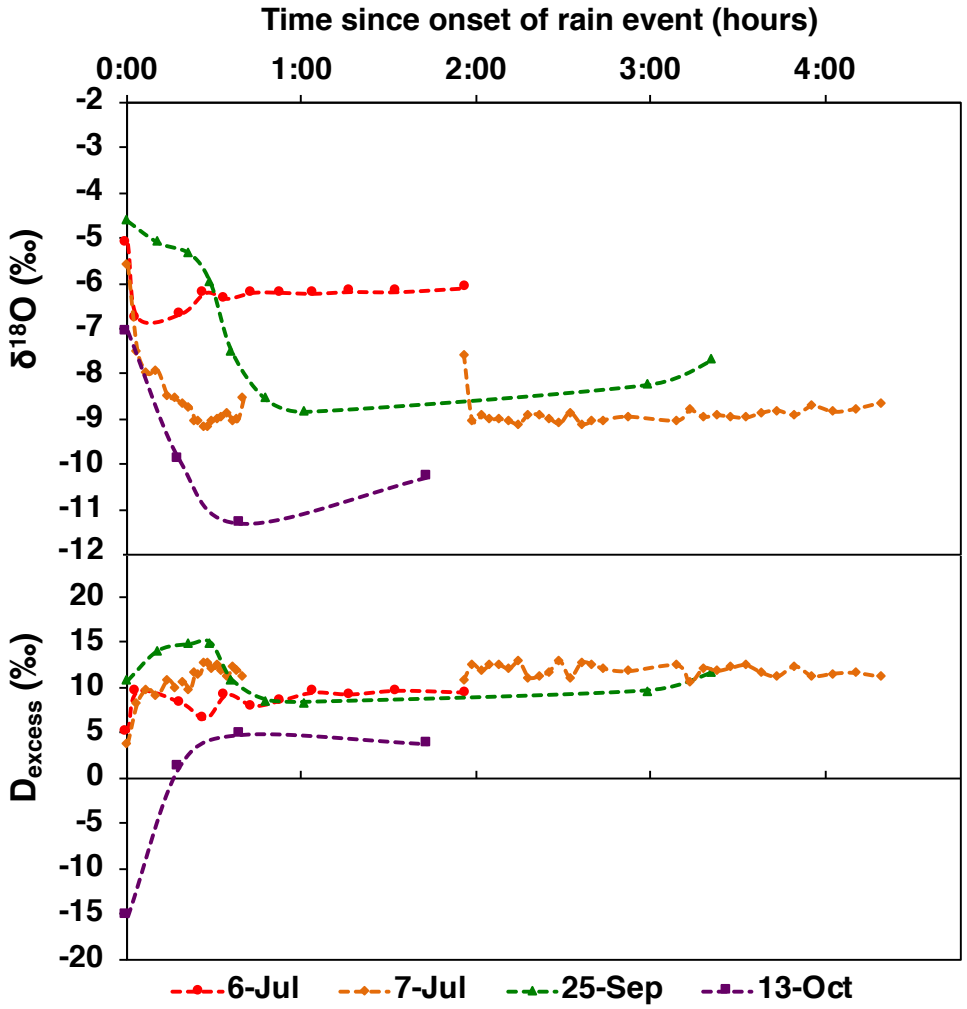

Figure 8: Intra-event samples from four precipitation events during summer 2012, collected with an evaporation-proof Precipitation Isotope Sequential Sampling Robot.

Figure 9 provides more detail about the two rain events from July 2012 shown in Figure 8. For the July 6 event, rainfall amounts were lower and relative humidity at the onset of the rain event was ~80 % at 10 m and ~60-70% at 300 m. Less positive D_{excess} values are consistent with rain falling through a sub-saturated atmosphere and likely undergoing evaporation. In plotting the liquid-equivalent of the vapor isotope ratios, there is little correspondence between these values

and the rain isotope ratios, showing a lack of equilibration of rain with vapor during this event. For the July 7 event, however, synoptic conditions were different. A temperature drop is seen, likely associated with a gust front, in addition to a spike in relative humidity up to 90-95% at both 10 m and 300 m at the onset of the rain event. While a characteristic "U-shape" is seen here as well, there is much closer correspondence between the liquid-equivalent isotope ratio and the rain values, in δD and δ^{18}O and also in D_{excess} towards the tail end of the event. This is likely indicative of a synoptic situation in which the vapor being sampled during this rain storm is the same vapor that the rain was formed from inside storm clouds (through equilibrium fractionation during condensation), and a downdraft brought both rain and vapor together into the boundary layer during this event.

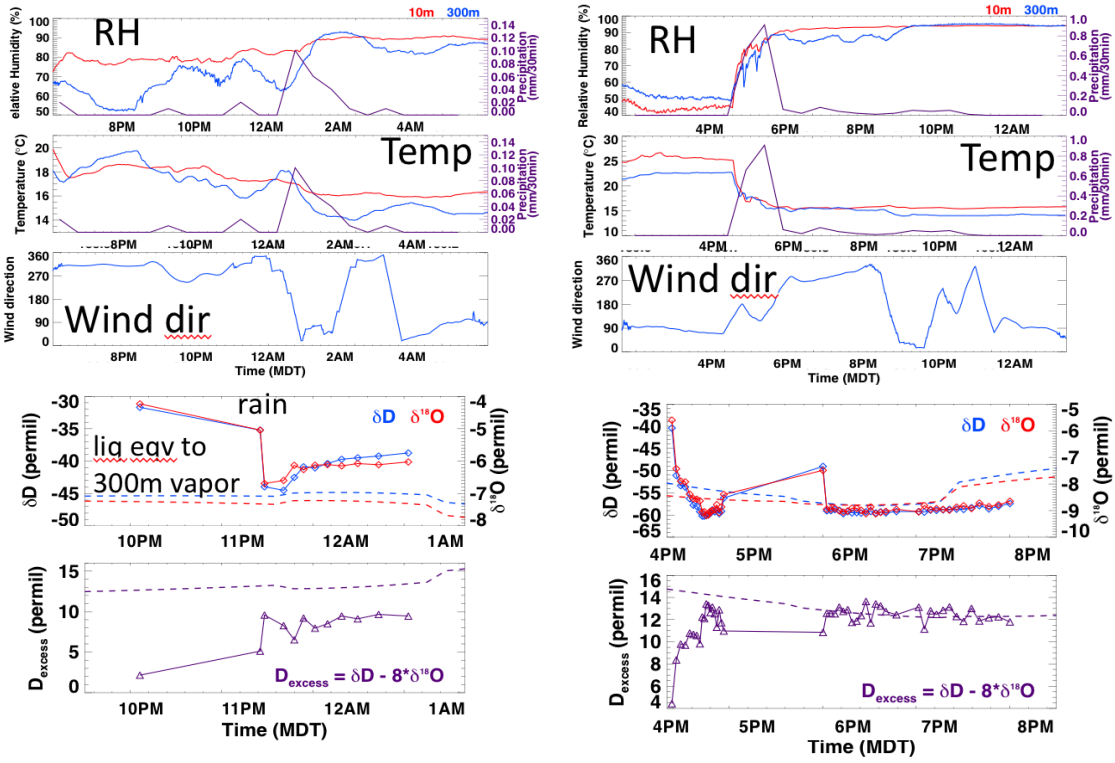

Figure 9: Data collected for two rain events on 6-Jul (left) and 7-Jul (right) which illustrate how intra-event isotope ratios evolve during different synoptic conditions.

Parsivel disdrometer drop size measurements can be used in conjunction with isotope ratio values to corroborate some of these synoptic tendencies. Unfortunately, at BAO, there were no simultaneous intra-event precipitation sampler measurements at the same time as Parsivel instruments were deployed. Nevertheless, Parsivel data subset for bulk rain sample collections can be used for inference about large-scale controls on isotope ratios. For example, Figure 10 shows the mass distribution of water content by raindrop diameter in surface precipitation events sub-set by D_{excess} values of less than and greater than 10. D_{excess} values of 10 and higher are indicative of convective-type events, where there are more drops of all sizes, and hence more water mass in all drop size bins, especially the large drop sizes. D_{excess} values of less than 10 would be evidence of rain undergoing significant evaporation, and under these synoptic conditions there are less drops of all sizes, and in particular less larger drops, with total proportional mass being shifted to smaller drop classes. Smaller drop populations < 0.4 mm diameter also disappear completely, i.e. they are likely undergoing complete evaporation before they reach the surface Parsivel station.

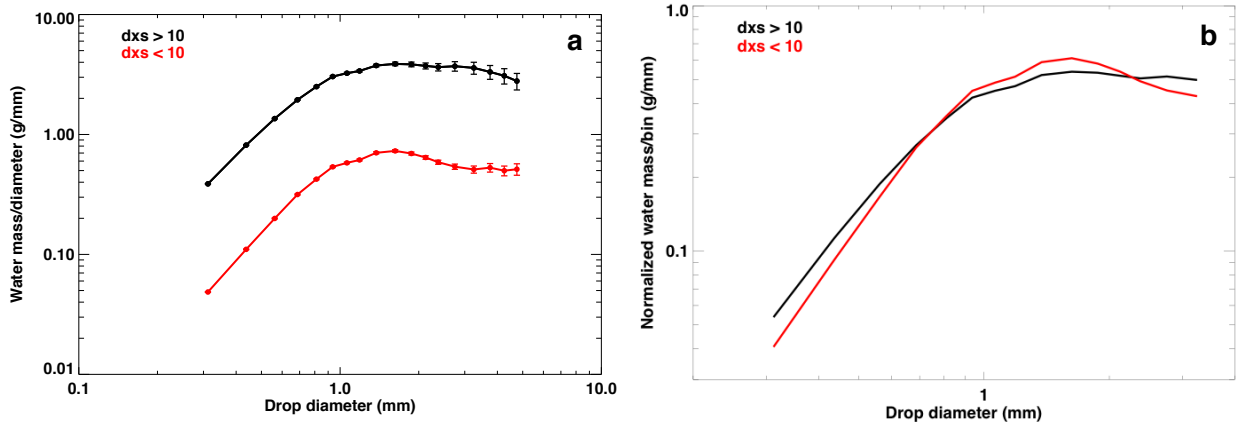

Figure 10: Water mass binned by drop diameter and sub-set for rain events where precipitation $D_{excess} > 10$ ($n = 29$) and $D_{excess} < 10$ ($n = 44$). Where $D_{excess} > 10$, relative humidity during rain events was 82.4 ± 13.4 % compared to 69.8 ± 19.8 % for $D_{excess} < 10$. (a) Absolute values of water mass per bin diameter, (b) Water mass normalized by total event rainfall amount.

The degree of equilibration (given by $f_{equil,average}$) is plotted in Figure 11 as a function of surface precipitation D_{excess} and observed mean raindrop diameter. Observed equilibration fraction is 0.16 ± 0.03 for $D_{excess} > 10$ and 0.10 ± 0.01 for $D_{excess} < 0$. A lower degree of equilibration for $D_{excess} < 0$ could be a result of drops undergoing more evaporation in a sub-saturated environment. Lower degree of equilibration is also associated with larger drops, consistent with the fact that the fall time for larger drops is much smaller than the e-folding time for equilibration. Smaller drops fall more slowly and are therefore likely to undergo more equilibration by the time they fall through the height of the tower. For $D_{excess} < 0$, lower equilibration may also be observed if all small drops are being evaporated completely, leaving only the larger drops behind which undergo less equilibration.

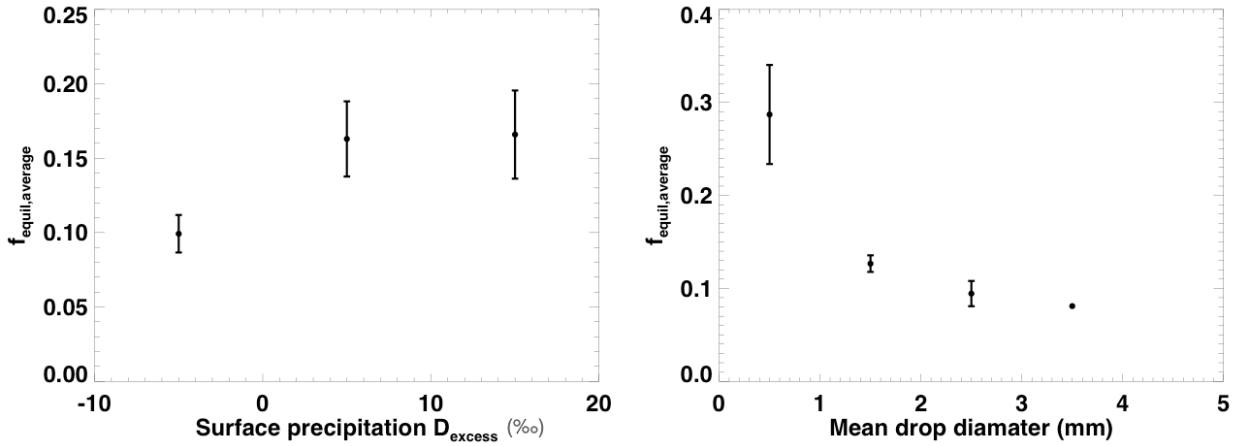

Figure 11: $f_{equil,average}$ (equilibration fraction weighted by mass distribution of drop sizes) as a function of surface precipitation D_{excess} values and mean raindrop diameter.

3.3 Modeling below-cloud processes

The relationship between vapor and precipitation highlights equilibrium fractionation, which was shown to be the dominant control on seasonal climatology of surface isotope ratios (Figure 6). Figure 12 illustrates this relationship, in which precipitation samples were equilibrated

using an average ambient temperature. Significant relationships were found at both the surface and 300 m stations (R^2 = 0.82 and 0.71, respectively, for the surface and 300 m). The lower correlation for the 300 m station indicates that equilibrium effects have a lesser role to play in determining the vapor-rain phase offset, with a likely larger role for kinetic fractionation during evaporation of raindrops.

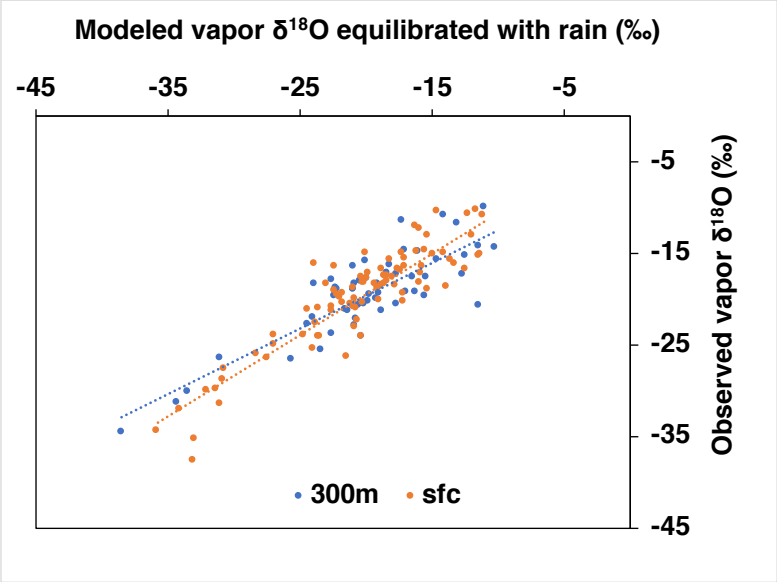

Figure 12: Modeled isotope $\delta^{18}O$ ratios of vapor equilibrated with rain using average ambient temperature plotted against observed $\delta^{18}O$ vapor isotope ratios; vapor was sub-set for when precipitation occurred and includes all precipitation samples collected from 2014-2015. Linear regression fits for the 'sfc' and '300m' station are y = 0.89x -1.55 (R^2 = 0.82) and y = 0.72x -5.22 (R^2 = 0.71) respectively.

When the precipitation dataset is subset for summer-only events, however, the correlations drop to 0.52 for the surface station, indicating that temperature equilibration only explains about half of the isotope ratio variance. Following equation (14), we re-calculated the modeled isotope ratio values with $f_{equil,average}$ using the full drop-size distribution observed during summer rainfall events. Results of these correlations are shown in Figure 13, where a significant improvement is seen in the ability to correct predict the observed rain isotopes ratios (R^2 = 0.92). Importantly, this

improved model not only captures the single isotope ratios well, but also substantially improves the prediction of D_{excess} (R^2 = 0.88 versus 0.22 without accounting for weighting by drop-size distribution), which is traditionally a more difficult isotope parameter to match.

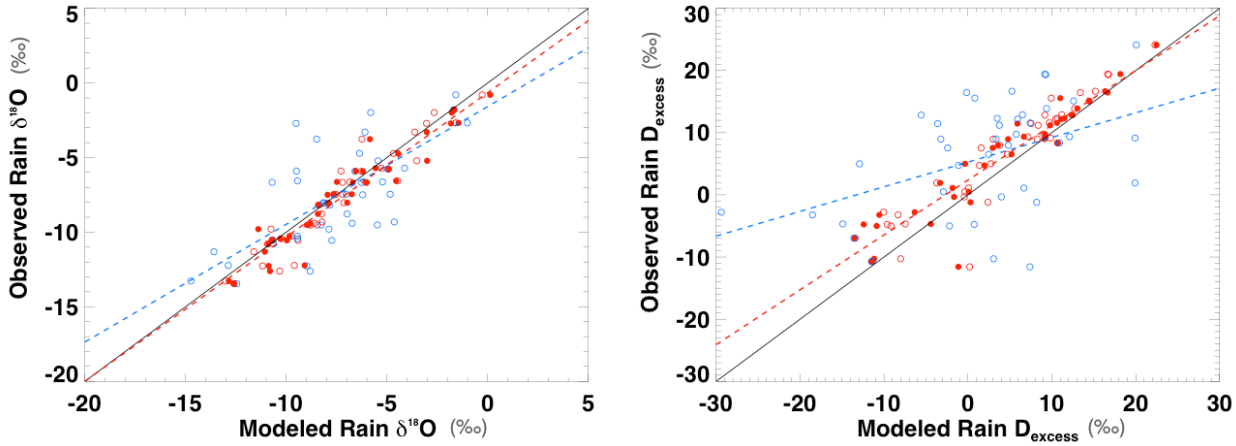

Figure 13: Observed versus modeled isotope ratios with equilibration at ambient temperature and $f_{equil,average}$ explicitly calculated using drop size distribution & weighted by mass water content in each bin. Data is subset for summer only (May-Oct). Black line shows 1:1 fit. Blue dashed line is the linear regression fit for model with temperature equilibration only (R^2 = 0.52 for $\delta^{18}O$ and R^2 = 0.22 for D_{excess}, respectively); red dashed line is the linear regression fit including drop size distribution in calculation of kinetic fractionation (R^2 = 0.92 for $\delta^{18}O$ and R^2 = 0.88 for D_{excess}, respectively).

4. Discussion and Conclusions

Precipitation isotope ratios at BAO show characteristic signatures for rain falling in a semi-arid environment (Crawford et al., 2016; Kong et al., 2013). In addition to information about source trajectories and condensation history, there is evidence of local evaporation contributing to isotope ratio signals, especially in summer months (Figure 5). The agreement between weighted mean precipitation and temperature-equilibrated vapor when raining (Figure 6) is an indication either of vapor values being initially set by precipitation or precipitation being formed alongside regional vapor. This could be reflected in the D_{excess} signals in Figure 4, where $D_{excess} \sim 10$ is indicative of an ocean source, but $D_{excess} < 10$ indicates evaporative processes have contributed to the isotopic

signature observed (Gat, 1996).

Evolution of the isotopic signatures for rain events with differing humidity, downdraft and temperature characteristics reveal that the initial isotopic signature is set by the air mass source, and there is a tendency towards a final D_{excess} value of 10 by the end of the storm for intra-event samples (Figures 8). However, the degree of equilibration observed (i.e. how close the rain samples are to matching the liquid-equivalent of the vapor) depends strongly on the relative humidity characteristics during the rain event (Figure 9). Furthermore, local evaporation effects strongly influence the D_{excess} value of bulk rain samples (reflected by the lower slopes in figure 5), and an examination of drop size distributions during rain events with different isotopic signatures reveals a shift in the drop populations from larger and more plentiful drops when $D_{excess} \geq 10$ to less drops overall and smaller populations disappearing entirely when $D_{excess} < 10$.

The intensity of post-condensational exchange processes such as diffusion and rain re-evaporation is strongly correlated with precipitation rate and mean raindrop size. Smaller raindrops lead to a greater degree of isotopic exchange, which results in the surrounding vapor having a more depleted isotopic value compared to a Rayleigh distillation curve (Worden et al., 2007). The precipitation water isotope value was correspondingly more enriched. However, complete evaporation of small drop populations could result in no fractionation at all if all the rain is simply moved into vapor form through mass conservation. This could result in an overall weaker kinetic fractionation associated with the ensemble of drop populations, which is consistent with temperature equilibration explaining 50% or higher of the correlation between observed and modeled precipitation values and also higher correlations between observed and modeled precipitation at the surface station versus the 300 m station.

Another reason for the approximate agreement with temperature equilibration alone is that

the rain could already be in equilibrium with the vapor, with both being part of a downdraft preceding and during a rain event. During the more intense convection associated with downdrafts, raindrops do not have time to come to a new equilibrium with surface vapor and retain the original "cloud signal" (Figures 6 & 9). Observations that deviate from simple Rayleigh-type processes could be alternatively explained by evaporation occurring near equilibrium, which would result in precipitation and vapor D_{excess} values being around 10. Since many of the precipitation samples collected at BAO have a D_{excess} value of less than 10, this indicates that an additional enrichment process is likely occurring, namely selective evaporation of smaller drop populations between 300 m and the surface.

With the advent of satellite isotope ratio measurements, there is a need for a more complete understanding and verification of the processes that should be included in climate models and the parameterizations associated with them. Satellites also only measure isotope ratios in vapor, and several studies have leveraged these measurements in conjunction with ground-based precipitation collections from the Global Network of Isotopes in Precipitation (GNIP) to assess tropical precipitation controls. However, these studies lack the raindrop size measurements necessary to complete the picture. A tall tower is an excellent location for ground-based validation of boundary layer moisture recycling as we can simultaneously measure vapor, rain and drop size distributions through a 300 m profile of the boundary layer. Explicit inclusion of drop distribution observations brings existing microphysical models in much better agreement with observations.

CHAPTER IV

CONCLUSIONS

The goals of this thesis were to examine the process-level controls on stable water isotope ratio values with an eye to using simple models to evaluate parameterizations that are important for larger scale climate models that seek to use these isotope ratios as diagnostic tracers for the water cycle. Land-atmosphere interactions are a key component of climate models and have been identified as being a large source of error in predicting future hydroclimate (Berg et al., 2016; Pitman et al., 2009; Wei et al., 2017). In addition, soil moisture and associated feedbacks are important drivers of the water cycle (Berg et al., 2015; Seneviratne et al., 2010, 2013) and it is vital to understand the mechanisms involved in transporting water through soil and into the atmosphere. In order to constrain boundary layer moisture budgets, one must also evaluate the contribution of rain evaporation and its connection with microphysical and larger scale synoptic processes driving rainfall (Conroy et al., 2016).

1. Findings

Analysis of isotope-enabled land surface model schemes reveals a shortcoming in existing model frameworks, where all the non-fractionating evapotranspiration flux is incorrectly assigned solely to transpiration. We find that a significant component of evaporation in dryland ecosystems could potentially be non-fractionating as well, through the complete mass transfer of water from the liquid into the vapor phase. Separating evaporation into two theoretically distinct "pools", where one undergoes fractionation and one does not, enables isotope-based methods to be reconciled with an isotope-independent method based on gross primary productivity. This is a potentially key development in the successful use of water isotope ratios for partitioning surface latent heat flux, and would help correct source apportionment for future hydroclimate predictions

where land use change may result in significantly different effects on transpiration versus evaporation.

Stable water isotope ratios also provide a window into seasonality and where air masses originate, as well as provide information about condensation history and event-based rainfall dynamics. At specific sites, they can be used along with profile measurements to evaluate below-cloud processes such as rain evaporation, which plays a key role in remoistening the boundary layer. Results presented in this thesis demonstrate that temperature equilibration plays a key role at longer time scales, and that using observed drop size distributions greatly enhances the predictive power of existing model schemes. The degree of rain-vapor equilibration sheds light on the mechanisms and isotope ratios expected for a particular type of rain event.

2. Perspectives

The use of stable water isotope ratios as tracers to evaluate land surface processes is steadily expanding. The National Ecological Observatory Network is a recently funded National Science Foundation initiative which seeks to collect meteorological, biological and isotopic measurements at sites across the United States. These sites are "strategically selected to represent different regions of vegetation, landforms, climate and ecosystem performance" (https://www.neonscience.org/observatory). While the cavity ring-down laser technology is now readily available for carrying out the desired isotopic measurements, these continental-scale datasets must be treated with appropriate checks and calibrations before sweeping conclusions are drawn from isotopic inferences. These checks must include accounting for missing processes such as sub-surface vapor movement and correct applications of fractionations in different environments. While our results show that an "ecosystem-level kinetic fractionation factor" can be derived for semi-arid environments, this must first be tested using data from other semi-arid

environments and the analysis then extended to other types of vegetated environments to verify continent-wide application of this principle.

An interesting question that arises from land surface studies is the degree to which carbon cycling is controlled primarily through hydrological drivers. In particular, there are several carbon-based tracers that could be leveraged alongside water isotope tracers – namely isotopologues of carbon dioxide and methane, and carbonyl sulfide. This thesis has demonstrated some of the challenges in realizing the potential usefulness of water isotope tracers for latent heat flux partitioning, and has demonstrated the ways in which carbon dioxide measurements can be paired with isotope measurements to check process-based source apportionment. A natural extension to this would be to identify whether the process-level mechanisms highlighted are also applicable to carbon fluxes and the partitioning of carbon between respiration and photosynthesis. This could be extremely important in vulnerable ecosystems such as high-latitude and high-altitude permafrost. Observed increasing seasonal amplitudes of carbon fluxes at sites across Alaska have been attributed to terrestrial biogeochemical interactions (Graven et al., 2013), but climate models are not constrained well enough to replicate limited observations and this leads to large uncertainties in future predictions. Hydrological controls in the form of summer melt, snow cover dynamics and an evolving landscape could be key to a better understanding of carbon exchange.

On the rain evaporation front, there is an expanding network of satellite instrumentation which can carry out isotopic measurements, and there is huge potential for these data to be analyzed alongside data from the NASA and Japan Aerospace Exploration Agency Global Precipitation Measurement (GPM) mission, which seeks to measure raindrop sizes from space. These measurements will be key to evaluating microphysical schemes in climate models that use water isotope ratios as tracers for convective processes. Ground-based instrumentation in

"campaign mode" will necessarily be a part of validating the satellite measurements, and again checks and calibrations will be key. Results from this thesis highlight ways in which these data could be used to validate water cycle processes from the land surface up to exchange processes in the boundary layer and shed light on the microphysical controls that could be expected in coupling raindrop measurements to satellite-derived water isotope ratios.

Finally, no science endeavor is complete without dissemination of that knowledge to the public, and the outreach program we ran ("Water Spotters") enabled me to do just that at local schools in the St. Vrain Valley School District. In addition to the technical and logistical details of coordinating and deploying weather stations and rain collectors and organizing sampling routines, I was able to educate Coloradan students about how isotopes tell us where their water comes from. The citizen science data gathered are also scientifically useful as they provide a 30 km east-west transect of isotope ratios for a full annual cycle from the foothills of the Rockies in Lyons all the way to Firestone in Weld County, providing the necessary information to construct a spatial uncertainty parameter for use in isotope-enabled climate models.

BIBLIOGRAPHY

Aemisegger, F., Pfahl, S., Sodemann, H., Lehner, I., Seneviratne, S. I., & Wernli, H. (2014). Deuterium excess as a proxy for continental moisture recycling and plant transpiration. *Atmospheric Chemistry and Physics*, *14*(8), 4029–4054. https://doi.org/10.5194/acp-14-4029-2014

Allison, G. B., Barnes, C. J., & Hughes, M. W. (1983). The distribution of deuterium and 18O in dry soils 2. Experimental. *Journal of Hydrology*, *64*(1–4), 377–397. https://doi.org/10.1016/0022-1694(83)90078-1

Bailey, A., Noone, D., Berkelhammer, M., Steen-Larsen, H. C., & Sato, P. (2015). The stability and calibration of water vapor isotope ratio measurements during long-term deployments. *Atmospheric Measurement Techniques*, *8*(10), 4521–4538. https://doi.org/10.5194/amt-8-4521-2015

Barkan, E., & Luz, B. (2007). Diffusivity fractionations of H216O/H217O and H216O/H218O in air and their implications for isotope hydrology. *Rapid Communications in Mass Spectrometry : RCM*, *21*, 2999–3005. https://doi.org/10.1002/rcm

Barnes, C. J., & Allison, G. B. (1984). The distribution of deuterium and 18O in dry soils. 3. Theory for non-isothermal water movement. *Journal of Hydrology*, *74*(1–2), 119–135. https://doi.org/10.1016/0022-1694(84)90144-6

Barnes, C. J., & Allison, G. B. (1988). Tracing of water movement in the unsaturated zone using stable isotopes of hydrogen and oxygen. *Journal of Hydrology*, *100*(1–3), 143–176. https://doi.org/10.1016/0022-1694(88)90184-9

Berg, A., Lintner, B. R., Findell, K., Seneviratne, S. I., Denhurk, B. Van, Ducharne, A., & Gentine, P. (2015). Interannual coupling between summertime surface temperature and

precipitation over land: Processes and implications for climate change. *Journal of Climate*, *28*(3), 1308–1328. https://doi.org/10.1175/JCLI-D-14-00324.1

Berg, A., Sheffield, J., & Milly, P. C. D. (2016). Divergent surface and total soil moisture projections under global warming. *Geophysical Research Letters*. https://doi.org/10.1002/2016GL071921

Berkelhammer, M., Hu, J., Bailey, A., Noone, D. C., Still, C. J., Barnard, H., & Turnipseed, A. (2013). The nocturnal water cycle in an open-canopy forest. *Journal of Geophysical Research Atmospheres*, *118*(17), 10225–10242. https://doi.org/10.1002/jgrd.50701

Berkelhammer, M., Noone, D. C., Steen-larsen, H. C., Bailey, A., Cox, C. J., Neill, M. S. O., & White, J. W. C. (2016). Surface-atmosphere decoupling limits accumulation at Summit, Greenland. *Science Advances*, *2*(April), 1–10.

Berkelhammer, M., Noone, D. C., Wong, T. E., Burns, S. P., Knowles, J. F., Kaushik, A., & Williams, M. W. (2016). Convergent approaches to determine an ecosystem's transpiration fraction. *Global Biogeochemical Cycles*, *30*(6), 933–951. https://doi.org/10.1002/2016GB005392

Berkelhammer, M., Risi, C., Kurita, N., & Noone, D. C. (2012). The moisture source sequence for the Madden-Julian Oscillation as derived from satellite retrievals of HDO and H2O. *Journal of Geophysical Research Atmospheres*, *117*(3), 1–20. https://doi.org/10.1029/2011JD016803

Berkelhammer, M., Stott, L., Yoshimura, K., Johnson, K., & Sinha, A. (2012). Synoptic and mesoscale controls on the isotopic composition of precipitation in the western United States. *Climate Dynamics*, *38*(3–4), 433–454. https://doi.org/10.1007/s00382-011-1262-3

Bolin, B. (1959). *On the use of tritium as a tracer for water in nature. Proc. 2nd U.N. Conf.*

Peaceful Uses of Atomic Energy (Vol. 18).

Bolot, M., Legras, B., & Moyer, E. J. (2013). Modelling and interpreting the isotopic composition of water vapour in convective updrafts. *Atmospheric Chemistry and Physics*, *13*(16), 7903–7935. https://doi.org/10.5194/acp-13-7903-2013

Bony, S., Risi, C., & Vimeux, F. (2008). Influence of convective processes on the isotopic composition ($d^{18}O$ and dD) of precipitation and water vapor in the tropics: 1. Radiative-convective equilibrium and Tropical Ocean-Global Atmosphere-Coupled Ocean-Atmosphere Response Experiment. *Journal of Geophysical Research Atmospheres*, *113*(19), 1–21. https://doi.org/10.1029/2008JD009942

Bowling, D. R., Baldocchi, D. D., & Monson, R. K. (1999). Dynamics of isotopic exchange of carbon dioxide in a Tennessee deciduous forest. *Global Biogeochemical Cycles*, *13*(4), 903–922. https://doi.org/10.1029/1999gb900072

Braud, I., Bariac, T., Biron, P., & Vauclin, M. (2009a). Isotopic composition of bare soil evaporated water vapor. Part I: RUBIC IV experimental setup and results. *Journal of Hydrology*, *369*, 1–16. https://doi.org/10.1016/j.jhydrol.2009.01.034

Braud, I., Bariac, T., Biron, P., & Vauclin, M. (2009b). Isotopic composition of bare soil evaporated water vapor. Part II: Modeling of RUBIC IV experimental results. *Journal of Hydrology*, *369*(1–2), 17–29. https://doi.org/10.1016/j.jhydrol.2009.01.038

Braud, I., Bariac, T., Gaudet, J. P., & Vauclin, M. (2005). SiSPAT-Isotope, a coupled heat, water and stable isotope (HDO and H 218O) transport model for bare soil. Part I. Model description and first verifications. *Journal of Hydrology*, *309*(1–4), 277–300. https://doi.org/10.1016/j.jhydrol.2004.12.013

Brown, D., Worden, J., & Noone, D. (2008). Comparison of atmospheric hydrology over

convective continental regions using water vapor isotope measurements from space. *Journal of Geophysical Research Atmospheres*, *113*(15), 1–17. https://doi.org/10.1029/2007JD009676

Brutsaert, W. (1975). A theory for local evaporation (or heat transfer) from rough and smooth surfaces at ground level. *Water Resources Research*, *11*(4), 543–550. https://doi.org/10.1029/WR011i004p00543

Brutsaert, W. (1982). *Evaporation into the atmosphere*. Kluwer Academic Publishers. https://doi.org/10.1007/978-94-017-1497-6

Buenning, N. H., Stott, L., Yoshimura, K., & Berkelhammer, M. (2012). The cause of the seasonal variation in the oxygen isotopic composition of precipitation along the western U.S. coast. *Journal of Geophysical Research Atmospheres*, *117*(17), D18114. https://doi.org/10.1029/2012JD018050

Cappa, C. D., Hendricks, M. B., DePaolo, D. J., & Cohen, R. C. (2003). Isotopic fractionation of water during evaporation. *Journal of Geophysical Research*, *108*(D16), 4525. https://doi.org/10.1029/2003JD003597

Celle-Jeanton, H., Gonfiantini, R., Travi, Y., & Sol, B. (2004). Oxygen-18 variations of rainwater during precipitation: Application of the Rayleigh model to selected rainfalls in Southern France. *Journal of Hydrology*, *289*(1–4), 165–177. https://doi.org/10.1016/j.jhydrol.2003.11.017

Conroy, J. L., Noone, D., Cobb, K. M., Moerman, J. W., & Konecky, B. L. (2016). Paired stable isotopologues in precipitation and vapor: A case study of the amount effect within western tropical Pacific storms. *Journal of Geophysical Research: Atmospheres*, *121*(7), 3290–3303. https://doi.org/10.1002/2015JD023844

Coplen, T. B., Neiman, P. J., White, A. B., Landwehr, J. M., Ralph, F. M., & Dettinger, M. D. (2008). Extreme changes in stable hydrogen isotopes and precipitation characteristics in a landfalling Pacific storm. *Geophysical Research Letters*, *35*(21), 1–5. https://doi.org/10.1029/2008GL035481

Craig, H., & Gordon, L. (1965). *Deuterium and oxygen 18 variations in the ocean and the marine atmosphere*. *Stable Isotopes in Oceanographic Studies and Paleotemperatures*. Retrieved from http://yncenter.sites.yale.edu/sites/default/files/shen_jing_jan_2013.pdf

Crawford, J., Hollins, S. E., Meredith, K. T., & Hughes, C. E. (2016). Precipitation stable isotope variability and subcloud evaporation processes in a semi-arid region. *Hydrological Processes*. https://doi.org/10.1002/hyp.10885

Crawford, J., Hughes, C. E., & Parkes, S. D. (2013). Is the isotopic composition of event based precipitation driven by moisture source or synoptic scale weather in the Sydney Basin, Australia ? *Journal of Hydrology*, *507*, 213–226. https://doi.org/10.1016/j.jhydrol.2013.10.031

Dansgaard, W. (1953). The abundance of 18O in atmospheric water and water vapour. *Tellus*, *5*(4), 461–469. https://doi.org/10.1111/j.2153-3490.1953.tb01076.x

Dansgaard, W. (1964). Stable isotopes in precipitation. *Tellus*, *16*(4), 436–468. https://doi.org/10.3402/tellusa.v16i4.8993

Dawson, T. E. (1996). Determining water use by trees and forests from isotopic, energy balance and transpiration analyses: the roles of tree size and hydraulic lift. *Tree Physiology*, *16*, 263–272. https://doi.org/10.1093/treephys/16.1-2.263

Dubbert, M., Cuntz, M., Piayda, A., Maguás, C., & Werner, C. (2013). Partitioning evapotranspiration - Testing the Craig and Gordon model with field measurements of

oxygen isotope ratios of evaporative fluxes. *Journal of Hydrology*, *496*, 142–153. https://doi.org/10.1016/j.jhydrol.2013.05.033

Eltahir, E. A. B. (1998). A soil moisture-rainfall feedback mechanism 1. Theory and observations. *Water Resources Research*, *34*(4), 765–776.

Emanuel, K. A., Neelin, D. J., & Bretherton, C. S. (1994). On large-scale circulations in convecting atmospheres. *Quarterly Journal of the Royal Meteorological Society*, *120*(519), 1111–1143. https://doi.org/10.1256/qj.03.151

Emanuel, K. A. (1991). A Scheme for Representing Cumulus Convection in Large-Scale Models. *Journal of the Atmospheric Sciences*. https://doi.org/10.1175/1520-0469(1991)048<2313:ASFRCC>2.0.CO;2

Ent, R. J. Van Der, Savenije, H. H. G., Schaefli, B., & Dunne, S. C. S. (2010). Origin and fate of atmospheric moisture over continents. *Water Resources Research*, *46*, 1–12. https://doi.org/10.1029/2010WR009127

Farquhar, G. D., & Cernusak, L. A. (2005). On the isotopic composition of leaf water in the non-steady state. *Functional Plant Biology*, *32*(4), 293–303. https://doi.org/10.1071/FP04232

Farquhar, G. D., & Lloyd, J. (1993). Carbon and oxygen isotope effects in the exchange of carbon dioxide between terrestrial plants and the atmosphere. In *Stable Isotopes and Plant Carbon-water Relations*. https://doi.org/10.1016/B978-0-08-091801-3.50011-8

Frankenberg, C., Wunch, D., Toon, G., Risi, C., Scheepmaker, R., Lee, J. E., & Worden, J. (2013). Water vapor isotopologue retrievals from high-resolution GOSAT shortwave infrared spectra. *Atmospheric Measurement Techniques*, *6*(2), 263–274. https://doi.org/10.5194/amt-6-263-2013

Frankenberg, C., Yoshimura, K., Warneke, T., Aben, I., Butz, A., Deutscher, N., & Röckmann,

T. (2009). Dynamic processes governing lower-tropospheric HDO/H2O ratios as observed from space and ground. *Science (New York, N.Y.)*, *325*(5946), 1374–7. https://doi.org/10.1126/science.1173791

Friedman, I. (1962). Water-Vapor Exchange between a Water Droplet and Its Environment, *57*.

Froehlich, K., Kralik, M., Papesch, W., Rank, D., Scheifinger, H., & Stichler, W. (2008). Deuterium excess in precipitation of Alpine regions - moisture recycling. *Isotopes in Environmental and Health Studies*, *44*(1), 61–70. https://doi.org/10.1080/10256010801887208

Galewsky, J., Steen-Larsen, H. C., Field, R. D., Worden, J., Risi, C., & Schneider, M. (2016). Stable isotopes in atmospheric water vapor and applications to the hydrologic cycle. *Reviews of Geophysics*, *54*(4), 809–865. https://doi.org/10.1002/2015RG000512

Gat, J. R., Bowser, C. J., & Kendall, C. (1994). The contribution of evaporation from the Great Lakes to the continental atmosphere: estimate based on stable isotope data.pdf. *Geophysical Research Letters*, *21*(7), 557–560.

Gat, J. R. (1996). Oxygen and hydrogen isotopes in the hydrologic cycle. *Annual Reviews in Earth and Planetary Sciences*, *24*(1), 225–262.

Gat, J. R. (2000). Atmospheric water balance-the isotopic perspective. *Hydrological Processes*, *14*(8), 1357–1369. https://doi.org/10.1002/1099-1085(20000615)14:8<1357::AID-HYP986>3.0.CO;2-7

Gat, J. R. (2008). The isotopic composition of evaporating waters – review of the historical evolution leading up to the Craig – Gordon model. *Isotopes in Environmental and Health Studies*, *44*(1), 5–9. https://doi.org/10.1080/10256010801887067

Gat, J. R., & Airey, P. L. (2006). Stable water isotopes in the atmosphere/biosphere/lithosphere

interface: Scaling-up from the local to continental scale, under humid and dry conditions. *Global and Planetary Change*, *51*(1–2 SPEC. ISS.), 25–33. https://doi.org/10.1016/j.gloplacha.2005.12.004

Gat, J. R., & Gonfiantini, R. (1981). *Stable isotope hydrology*.

Gehrels, J. C., Peeters, J. E. M., De Vries, J. J., & Dekkers, M. (1998). The mechanism of soil water movement as inferred from 18O stable isotope studies. *Hydrological Sciences Journal*, *43*(March 2015), 579–594. https://doi.org/10.1080/02626669809492154

Good, S. P., Soderberg, K., Wang, L., & Caylor, K. K. (2012). Uncertainties in the assessment of the isotopic composition of surface fluxes: A direct comparison of techniques using laser-based water vapor isotope analyzers. *Journal of Geophysical Research Atmospheres*, *117*(15), 1–22. https://doi.org/10.1029/2011JD017168

Graven, H. D., Keeling, R. F., Piper, S. C., Patra, P. K., Stephens, B. B., Wofsy, S. C., & Bent, J. D. (2013). Enhanced seasonal exchange of CO2 by northern ecosystems since 1960. *Science (New York, N.Y.)*, *341*(September), 1085–9. https://doi.org/10.1126/science.1239207

Griffis, T. J., Sargent, S. D., Lee, X., Baker, J. M., Greene, J., Erickson, M., & Hu, N. (2010). Determining the Oxygen Isotope Composition of Evapotranspiration Using Eddy Covariance. *Boundary-Layer Meteorology*, *137*(2), 307–326. https://doi.org/10.1007/s10546-010-9529-5

Guo, Z., Dirmeyer, P. A., Koster, R. D., Bonan, G., Chan, E., Cox, P., & Yamada, T. (2006). GLACE: The Global Land–Atmosphere Coupling Experiment. Part II: Analysis. *Journal of Hydrometeorology*, 611–625. https://doi.org/10.1175/JHM510.1

Gupta, P., Noone, D., Galewsky, J., Sweeney, C., & Vaughn, B. V. (2009). Demonstration of

high-precision continuous measurements of water vapor isotopologues in laboratory and remote field deployments using wavelength-scanned cavity ring-down spectroscopy (WS-CRDS) technology. *Rapid Communications in Mass Spectrometry : RCM*, *23*, 2534–2542. https://doi.org/10.1002/rcm

Haverd, V., & Cuntz, M. (2010). Soil-Litter-Iso: A one-dimensional model for coupled transport of heat, water and stable isotopes in soil with a litter layer and root extraction. *Journal of Hydrology*, *388*(3–4), 438–455. https://doi.org/10.1016/j.jhydrol.2010.05.029

Haverd, V., Cuntz, M., Griffith, D., Keitel, C., Tadros, C., & Twining, J. (2011). Measured deuterium in water vapour concentration does not improve the constraint on the partitioning of evapotranspiration in a tall forest canopy, as estimated using a soil vegetation atmosphere transfer model. *Agricultural and Forest Meteorology*, *151*(6), 645–654. https://doi.org/10.1016/j.agrformet.2011.02.005

Helliker, B. R., & Richter, S. L. (2008). Subtropical to boreal convergence of tree-leaf temperatures. *Nature*, *454*(7203), 511–514. https://doi.org/10.1038/nature07031

Helliker, B. R., Roden, J. S., Cook, C., & Ehleringer, J. R. (2002). A rapid and precise method for sampling and determining the oxygen isotope ratio of atmospheric water vapor. *Rapid Communications in Mass Spectrometry*, *16*(10), 929–932. https://doi.org/10.1002/rcm.659

Henderson-Sellers, A., Fischer, M., Aleinov, I., McGuffie, K., Riley, W. J., Schmidt, G. A., & Irannejad, P. (2006). Stable water isotope simulation by current land-surface schemes: Results of iPILPS Phase 1. *Global and Planetary Change*, *51*(1–2 SPEC. ISS.), 34–58. https://doi.org/10.1016/j.gloplacha.2006.01.003

Henderson-Sellers, A., McGuffie, K., Noone, D., & Irannejad, P. (2004). Using Stable Water Isotopes to Evaluate Basin-Scale Simulations of Surface Water Budgets. *Journal of*

Hydrometeorology, *5*(5), 805–822. https://doi.org/10.1175/1525-7541(2004)005<0805:USWITE>2.0.CO;2

Hendricks, M.B., DePaolo, D.J., & Cohen, R. C. (2000). Space and time variation of d18O and dD in precipitation: Can paleotemperature be estimated from ice cores?, *14*(3), 851–861. https://doi.org/10.1029/1999GB001198

Hoffmann, G., Jouzel, J., & Masson, V. (2000). Stable water isotopes in atmospheric general circulation models. *Hydrological Processes*, *14*(8), 1385–1406. https://doi.org/10.1002/1099-1085(20000615)14:8<1385::AID-HYP989>3.0.CO;2-1

Horita, J., Rozanski, K., & Cohen, S. (2008). Isotope effects in the evaporation of water: a status report of the Craig-Gordon model. *Isotopes in Environmental and Health Studies*, *44*(1), 23–49. https://doi.org/10.1080/10256010801887174

Horita, J., & Wesolowski, D. J. (1994). Liquid-vapor fractionation of oxygen and hydrogen isotopes of water from the freezing to the critical temperature. *Geochimica et Cosmochimica Acta*, *58*(16), 3425–3437. https://doi.org/10.1016/0016-7037(94)90096-5

Hu, Z., Wen, X., Sun, X., Li, S., Li, L., Yu, G., & Lee, X. (2014). Partitioning of evapotranspiration through oxygen isotopic measurements of water pools and fluxes in a temperate grassland. *Journal of Geophysical Research: Biogeosciences*, *119*(3), 358–371. https://doi.org/10.1002/2013JG002367

Jones, M. D., Cuthbert, M. O., Leng, M. J., McGowan, S., Mariethoz, G., Arrowsmith, C., & Cross, I. (2016). Comparisons of observed and modelled lake d18O variability. *Quaternary Science Reviews*, *131*, 329–340. https://doi.org/10.1016/j.quascirev.2015.09.012

Jouzel, J., Alley, R. B., Cuffey, K. M., Dansgaard, W., Grootes, P., Hoffmann, G., & White, J. (1997). Validity of the temperature reconstruction from ice cores. *Journal of Geophysical*

Research, *102*(C12), 26471–26487.

Kanner, L. C., Buenning, N. H., Stott, L. D., Timmerman, A., & Noone, D. (2014). The role of soil processes in d18O terrestrial climate proxies. *Global Biogeochemical Cycles*, *28*, 239–252. https://doi.org/10.1002/2013GB004742.Received

Keeling, C. D. (1958). The Concentration and Isotopic Abundances of Carbon Dioxide in the Atmosphere. *Geochemistry Geophysics Geosystems*, *13*(2), 322–334. https://doi.org/10.1111/j.2153-3490.1960.tb01300.x

Kong, Yanlong, Pang, Z., & Froehlich, K. (2013). Quantifying recycled moisture fraction in precipitation of an arid region using deuterium excess. *Tellus, Series B: Chemical and Physical Meteorology*, *65*, 1–8. https://doi.org/10.3402/tellusb.v65i0.19251

Koster, R. D., Chang, Y., Wang, H., & Schubert, S. D. (2016). Impacts of local soil moisture anomalies on the atmospheric circulation and on remote surface meteorological fields during boreal summer: A comprehensive analysis over North America. *Journal of Climate*, *29*(20), 7345–7364. https://doi.org/10.1175/JCLI-D-16-0192.1

Koster, R. D., Dirmeyer, P. A., Guo, Z., Bonan, G., Chan, E., Cox, P., & Yamada, T. (2004). Regions of Strong Coupling Between Soil Moisture and Precipitation. *Science*, *305*(5687), 1138–1140. https://doi.org/10.1126/science.1100217

Koster, R. D., Guo, Z., Dirmeyer, P. A., Bonan, G. B., Chan, E., Cox, P. M., & Yamada, T. (2006). GLACE: The Global Land – Atmosphere Coupling Experiment. Part I: Overview. *Journal of Hydrometeorology*, *7*, 611–625. https://doi.org/http://dx.doi.org/10.1175/JHM511.1

Kurita, N., Noone, D., Risi, C., Schmidt, G. A., Yamada, H., & Yoneyama, K. (2011). Intraseasonal isotopic variation associated with the Madden-Julian Oscillation. *Journal of*

Geophysical Research Atmospheres, *116*, D24101. https://doi.org/10.1029/2010JD015209

Lai, C. T., & Ehleringer, J. R. (2011). Deuterium excess reveals diurnal sources of water vapor in forest air. *Oecologia*, *165*(1), 213–223. https://doi.org/10.1007/s00442-010-1721-2

Lee, J.-E., & Fung, I. (2008). "Amount effect" of water isotopes and quantitative analysis of post-condensation processes. *Hydrological Processes*, *22*, 1–8. https://doi.org/10.1002/hyp

Lee, J.-E., Fung, I., DePaolo, D. J., & Henning, C. C. (2007). Analysis of the global distribution of water isotopes using the NCAR atmospheric general circulation model. *Journal of Geophysical Research*, *112*(D16), 1–14. https://doi.org/10.1029/2006JD007657

Lee, J. E., Pierrehumbert, R., Swann, A., & Lintner, B. R. (2009). Sensitivity of stable water isotopic values to convective parameterization schemes. *Geophysical Research Letters*, *36*(23), 1–5. https://doi.org/10.1029/2009GL040880

Lee, X., Griffis, T. J., Baker, J. M., Billmark, K. A., Kim, K., & Welp, L. R. (2009). Canopy-scale kinetic fractionation of atmospheric carbon dioxide and water vapor isotopes. *Global Biogeochemical Cycles*, *23*(1), 1–15. https://doi.org/10.1029/2008GB003331

Lee, X., Smith, R., & Williams, J. (2006). Water vapour 18O/16O isotope ratio in surface air in New England, USA. *Tellus, Series B: Chemical and Physical Meteorology*, *58*(4), 293–304. https://doi.org/10.1111/j.1600-0889.2006.00191.x

Limm, E. B., Simonin, K. A., Bothman, A. G., & Dawson, T. E. (2009). Foliar water uptake: A common water acquisition strategy for plants of the redwood forest. *Oecologia*, *161*(3), 449–459. https://doi.org/10.1007/s00442-009-1400-3

Mathieu, R., & Bariac, T. (1996a). A numerical model for the simulation of stable isotope profiles in drying soils. *Journal of Geophysical Research*, *101*(D7), 12685. https://doi.org/10.1029/96JD00223

Mathieu, R., & Bariac, T. (1996b). An Isotopic Study (2 H and 18 O) of Water Movements in Clayey Soils Under a Semiarid Climate. *Water Resources Research*. https://doi.org/10.1029/96WR00074

Maxwell, R. M., & Condon, L. E. (2016). Connections between groundwater flow and transpiration partitioning. *Science*, *353*(6297), 377–380. https://doi.org/10.1126/science.aaf7891

Melayah, A., Bruckler, L., & Bariac, T. (1996). Modelling the transport of water stable isotopes in unsaturated soils under natural conditions. *Water Resources Research*, *32*(7), 2047–2054.

Merlivat, L. (1978). The dependence of bulk evaporation coefficients on air-water interfacial conditions as determined by the isotopic method. *Journal of Geophysical Research*, *83*(C6), 2977. https://doi.org/10.1029/JC083iC06p02977

Merlivat, L., & Jouzel, J. (1979). Global Climatic Interpretation of the Deuterium-Oxygen 18 Relationship for Precipitation, *84*(9), 5029–5033.

Miller, J. B., & Tans, P. P. (2003). Calculating isotopic fractionation from atmospheric measurements at various scales. *Tellus, Series B: Chemical and Physical Meteorology*, *55*(2), 207–214. https://doi.org/10.1034/j.1600-0889.2003.00020.x

Mook, W. G. (2001). V1 - Introduction - Theory , methods, review. *Environmental Isotopes in the Hydrological Cycle - Principles and Applications*, *1*, 1–165.

Muller, C. L., Baker, A., Fairchild, I. J., Kidd, C., & Boomer, I. (2015). Intra-Event Trends in Stable Isotopes: Exploring Midlatitude Precipitation Using a Vertically Pointing Micro Rain Radar. *Journal of Hydrometeorology*, *16*(1), 194–213. https://doi.org/10.1175/JHM-D-14-0038.1

Munksgaard, N. C., Davies, K., Wurster, C. M., Bass, A. M., & Bird, M. I. (2013). Field-based

cavity ring-down spectrometry of $\delta^{13}C$ in soil-respired CO_2. *Isotopes in Environmental and Health Studies*, *49*(2), 232–42. https://doi.org/10.1080/10256016.2013.750606

Newberry, S. L., Prechsl, U. E., Pace, M., & Kahmen, A. (2017). Tightly bound soil water introduces isotopic memory effects on mobile and extractable soil water pools. *Isotopes in Environmental and Health Studies*, *53*(4), 368–381. https://doi.org/10.1080/10256016.2017.1302446

Noone, D. (2012). Pairing measurements of the water vapor isotope ratio with humidity to deduce atmospheric moistening and dehydration in the tropical midtroposphere. *Journal of Climate*, *25*(13), 4476–4494. https://doi.org/10.1175/JCLI-D-11-00582.1

Noone, D., Risi, C., Bailey, A., Berkelhammer, M., Brown, D. P., Buenning, N., & Wolfe, D. (2013). Determining water sources in the boundary layer from tall tower profiles of water vapor and surface water isotope ratios after a snowstorm in Colorado. *Atmospheric Chemistry and Physics*, *13*(3), 1607–1623. https://doi.org/10.5194/acp-13-1607-2013

Nusbaumer, J., Wong, T. E., Bardeen, C., & Noone, D. C. (2017). Evaluating hydrological processes in the Community Atmosphere Model Version 5 (CAM5) using stable isotope ratios of water. *Journal of Advances in Modeling Earth Systems*, *9*, 949–977. https://doi.org/10.1002/2016MS000839

Oleson, K. W., Lawrence, D. M., Gordon, B., Flanner, M. G., Kluzek, E., Peter, J., & Zeng, X. (2010). Technical Description of version 4 . 0 of the Community Land Model (CLM), (April).

Pataki, D. E., Ehleringer, J. R., Flanagan, L. B., Yakir, D., Bowling, D. R., Still, C. J., Buchmann, N., Kaplan, J. O., & Berry, J. A. (2003). The application and interpretation of Keeling plots in terrestrial carbon cycle research. *Global Biogeochemical Cycles*, *17*(1), n/a-

n/a. https://doi.org/10.1029/2001GB001850

Pitman, A. J., De Noblet-Ducoudré, N., Cruz, F. T., Davin, E. L., Bonan, G. B., Brovkin, V., & Voldoire, A. (2009). Uncertainties in climate responses to past land cover change: First results from the LUCID intercomparison study. *Geophysical Research Letters*, *36*(14), 1–6. https://doi.org/10.1029/2009GL039076

Reichstein, M., Falge, E., Baldocchi, D., Papale, D., Aubinet, M., Berbigier, P., & Valentini, R. (2005). On the separation of net ecosystem exchange into assimilation and ecosystem respiration: Review and improved algorithm. *Global Change Biology*, *11*(9), 1424–1439. https://doi.org/10.1111/j.1365-2486.2005.001002.x

Riley, W. J., Still, C. J., Torn, M. S., & Berry, J. A. (2002). A mechanistic model of (H2O)-O-18 and (COO)-O-18 fluxes between ecosystems and the atmosphere: Model description and sensitivity analyses. *Global Biogeochem. Cycles*, *16*(4), 1–23. https://doi.org/ARTN 1095

Rindsberger, M., Jaffe, S., Rahamim, S., & Gat, J. R. (1990). Patterns of the isotopic composition of precipitation in time and space: data from the Israeli storm water collection program. *Tellus B*. https://doi.org/10.1034/j.1600-0889.1990.t01-2-00005.x

Risi, C., Bony, S., Vimeux, F., Chongd, M., & Descroixe, L. (2010). Evolution of the stable water isotopic composition of the rain sampled along sahelian squall lines. *Quarterly Journal of the Royal Meteorological Society*, *136*(SUPPL. 1), 227–242. https://doi.org/10.1002/qj.485

Risi, C., Bony, S., Vimeux, F., Frankenberg, C., Noone, D., & Worden, J. (2010). Understanding the Sahelian water budget through the isotopic composition of water vapor and precipitation. *Journal of Geophysical Research Atmospheres*, *115*(24), 1–23. https://doi.org/10.1029/2010JD014690

Rothfuss, Y., Biron, P., Braud, I., Canale, L., Durand, J. L., Gaudet, J. P., & Bariac, T. (2010). Partitioning evapotranspiration fluxes into soil evaporation and plant transpiration using water stable isotopes under controlled conditions. *Hydrological Processes*, *24*(22), 3177–3194. https://doi.org/10.1002/hyp.7743

Rothfuss, Y., Braud, I., Le Moine, N., Biron, P., Durand, J. L., Vauclin, M., & Bariac, T. (2012). Factors controlling the isotopic partitioning between soil evaporation and plant transpiration: Assessment using a multi-objective calibration of SiSPAT-Isotope under controlled conditions. *Journal of Hydrology*, *442–443*, 75–88. https://doi.org/10.1016/j.jhydrol.2012.03.041

Rozanski, K., Araguas-Araguas, L., & Gonfiantini, R. (1993). Isotope patterns in Modern Global Precipitation.pdf. *Climate Change in Continental Isotopic Records*, *Geophysica*. https://doi.org/10.1029/GM078p0001

Salamalikis, V., Argiriou, A. A., & Dotsika, E. (2016). Isotopic modeling of the sub-cloud evaporation effect in precipitation. *Science of the Total Environment*, *544*, 1059–1072. https://doi.org/10.1016/j.scitotenv.2015.11.072

Schlesinger, W. H., & Jasechko, S. (2014). Transpiration in the global water cycle. *Agricultural and Forest Meteorology*, *189–190*, 115–117. https://doi.org/10.1016/j.agrformet.2014.01.011

Schuepp, P. H., Leclerc, M. Y., Macpherson, J. I., & Desjardins, R. L. (1990). Footprint prediction of scalar fluxes from analytical solutions of the diffusion equation. *Boundary-Layer Meteorology*, *50*, 355–373.

Seneviratne, S. I., Corti, T., Davin, E. L., Hirschi, M., Jaeger, E. B., Lehner, I., & Teuling, A. J. (2010). Investigating soil moisture-climate interactions in a changing climate: A review.

Earth-Science Reviews, *99*(3–4), 125–161. https://doi.org/10.1016/j.earscirev.2010.02.004

Seneviratne, S. I., Wilhelm, M., Stanelle, T., Van Den Hurk, B., Hagemann, S., Berg, A., & Smith, B. (2013). Impact of soil moisture-climate feedbacks on CMIP5 projections: First results from the GLACE-CMIP5 experiment. *Geophysical Research Letters*, *40*(19), 5212–5217. https://doi.org/10.1002/grl.50956

Sjostrom, D. J., & Welker, J. M. (2009). The influence of air mass source on the seasonal isotopic composition of precipitation, eastern USA. *Journal of Geochemical Exploration*, *102*(3), 103–112. https://doi.org/10.1016/j.gexplo.2009.03.001

Small, E. E., & Kurc, S. A. (2003). Tight coupling between soil moisture and the surface radiation budget in semiarid environments: Implications for land-atmosphere interactions. *Water Resources Research*, *39*(10), 1278. https://doi.org/10.1029/2002WR001297

Soderberg, K., Good, S. P., Wang, L., & Caylor, K. (2011). Stable Isotopes of Water Vapor in the Vadose Zone: A Review of Measurement and Modeling Techniques. *Vadose Zone Journal*, *11*(3). https://doi.org/10.2136/vzj2011.0165

Stewart, M. K. (1975). Stable Isotope Fractionation Due to Evaporation and Isotopic Exchange of Falling Waterdrops: Applications to Atmospheric Processes and Evaporation of Lakes. *Journal of Geophysical Research*, *80*(9), 1133–1146.

Sutanto, S. J., Van Den Hurk, B., Dirmeyer, P. A., Seneviratne, S. I., Röckmann, T., Trenberth, K. E., & Hoffmann, G. (2014). HESS Opinions "a perspective on isotope versus non-isotope approaches to determine the contribution of transpiration to total evaporation." *Hydrology and Earth System Sciences*, *18*(8), 2815–2827. https://doi.org/10.5194/hess-18-2815-2014

Tang, J., & Riley, W. J. (2013). Impacts of a new bare-soil evaporation formulation on site,

regional, and global surface energy and water budgets in CLM4. *Journal of Advances in Modeling Earth Systems*, *5*(3), 558–571. https://doi.org/10.1002/jame.20034

Tanny, J., & Cohen, J. (2008). Revisiting the boundary layer structure used in Craig and Gordon's model of isotope fractionation in evaporation. *Isotopes in Environmental and Health Studies*, *44*(1), 11–21. https://doi.org/10.1080/10256010801887091

Tans, P. P. (1998). Oxygen isotopic equilibrium between carbon dioxide and water in soils. *Tellus, Series B: Chemical and Physical Meteorology*, *50*(2), 163–178. https://doi.org/10.1034/j.1600-0889.1998.t01-1-00004.x

Tremoy, G., Vimeux, F., Cattani, O., Mayaki, S., Souley, I., & Favreau, G. (2011). Measurements of water vapor isotope ratios with wavelength-scanned cavity ring-down spectroscopy technology: New insights and important caveats for deuterium excess measurements in tropical areas in comparison with isotope-ratio mass spectrometry. *Rapid Communications in Mass Spectrometry*, *25*(23), 3469–3480. https://doi.org/10.1002/rcm.5252

Vachon, R. W., Welker, J. M., White, J. W. C., & Vaughn, B. H. (2010). Monthly precipitation isoscapes (d18O) of the United States: Connections with surface temperatures, moisture source conditions, and air mass trajectories. *Journal of Geophysical Research Atmospheres*, *115*(21), 1–17. https://doi.org/10.1029/2010JD014105

Vargas, A. I., Schaffer, B., Yuhong, L., & Sternberg, L. da S. L. (2017). Testing plant use of mobile vs immobile soil water sources using stable isotope experiments. *New Phytologist*, *215*(2), 582–594. https://doi.org/10.1111/nph.14616

Wang, L., Caylor, K. K., Villegas, J. C., Barron-Gafford, G. A., Breshears, D. D., & Huxman, T. E. (2010). Partitioning evapotranspiration across gradients of woody plant cover:

Assessment of a stable isotope technique. *Geophysical Research Letters*, *37*(9), 1–7. https://doi.org/10.1029/2010GL043228

Wang, L., D'Odorico, P., Evans, J. P., Eldridge, D. J., McCabe, M. F., Caylor, K. K., & King, E. G. (2012). Dryland ecohydrology and climate change: Critical issues and technical advances. *Hydrology and Earth System Sciences*, *16*(8), 2585–2603. https://doi.org/10.5194/hess-16-2585-2012

Wei, J., & Dirmeyer, P. A. (2010). Toward understanding the large-scale land-atmosphere coupling in the models: Roles of different processes. *Geophysical Research Letters*, *37*(19). https://doi.org/10.1029/2010GL044769

Wei, Z., Yoshimura, K., Wang, L., Miralles, D. G., Jasechko, S., & Lee, X. (2017). Revisiting the contribution of transpiration to global terrestrial evapotranspiration. *Geophysical Research Letters*, *44*(6), 2792–2801. https://doi.org/10.1002/2016GL072235

Welp, L. R., Lee, X., Griffis, T. J., Wen, X. F., Xiao, W., Li, S., & Huang, J. (2012). A meta-analysis of water vapor deuterium-excess in the midlatitude atmospheric surface layer. *Global Biogeochemical Cycles*, *26*(3), 1–12. https://doi.org/10.1029/2011GB004246

Welp, L. R., Lee, X., Kim, K., Griffis, T. J., Billmark, K. A., & Baker, J. M. (2008). d18O of water vapour, evapotranspiration and the sites of leaf water evaporation in a soybean canopy. *Plant, Cell and Environment*, *31*(9), 1214–1228. https://doi.org/10.1111/j.1365-3040.2008.01826.x

Werner, M., Langebroek, P. M., Carlsen, T., Herold, M., & Lohmann, G. (2011). Stable water isotopes in the ECHAM5 general circulation model: Toward high-resolution isotope modeling on a global scale. *Journal of Geophysical Research Atmospheres*, *116*(15), 1–14. https://doi.org/10.1029/2011JD015681

West, A. G., Patrickson, S. J., & Ehleringer, J. R. (2006). Water extraction times for plant and soil materials used in stable isotope analysis. *Rapid Communications in Mass Spectrometry : RCM*, *20*, 1317–1321. https://doi.org/10.1002/rcm

Williams, D. G., Cable, W., Hultine, K., Hoedjes, J. C. B., Yepez, E. A., Simonneaux, V., & Timouk, F. (2004). Evapotranspiration components determined by stable isotope, sap flow and eddy covariance techniques. *Agricultural and Forest Meteorology*, *125*(3–4), 241–258. https://doi.org/10.1016/j.agrformet.2004.04.008

Wolfe, D. E., & Lataitis, R. J. (2018). Boulder Atmospheric Observatory 1977-2016: The End of an Era and Lessons Learned. *Bulletin of the American Meteorological Society*. https://doi.org/10.1175/BAMS-D-14-00145.1

Wong, T., Nusbaumer, J., & Noone, D. (2017). Evaluation of modeled land-atmosphere exchanges with a comprehensive water isotope fractionation scheme in version 4 of the Community Land Model. *Journal of Advances in Modeling Earth Systems*, *Submitted*(March). https://doi.org/10.1002/2016MS000842

Worden, J., Noone, D., & Bowman, K. (2007). Importance of rain evaporation and continental convection in the tropical water cycle. *Nature*, *445*(7127), 528–532. https://doi.org/10.1038/nature05508

Yakir, D., & Wang, X.-F. (1996). Fluxes of CO2 and water between terrestrial vegetation and the atmosphere estimated from isotope measurements. *Nature*, *380*(6574), 515–517. https://doi.org/10.1038/380515a0

Yepez, E. A., Huxman, T. E., Ignace, D. D., English, N. B., Weltzin, J. F., Castellanos, A. E., & Williams, D. G. (2005). Dynamics of transpiration and evaporation following a moisture pulse in semiarid grassland: A chamber-based isotope method for partitioning flux

components. *Agricultural and Forest Meteorology*, *132*(3–4), 359–376. https://doi.org/10.1016/j.agrformet.2005.09.006

Yepez, E. A., Williams, D. G., Scott, R. L., & Lin, G. (2003). Partitioning overstory and understory evapotranspiration in a semiarid savanna woodland from the isotopic composition of water vapor. *Agricultural and Forest Meteorology*, *119*(1–2), 53–68. https://doi.org/10.1016/S0168-1923(03)00116-3

Yoshimura, K. (2015). Stable Water Isotopes in Climatology, Meteorology, and Hydrology : A Review. *Journal of the Meteorological Society of Japan*, *93*(5), 513–533. https://doi.org/10.2151/jmsj.2015-036

Zhang, S., Wen, X., Wang, J., Yu, G., & Sun, X. (2010). The use of stable isotopes to partition evapotranspiration fluxes into evaporation and transpiration. *Acta Ecologica Sinica*, *30*(4), 201–209. https://doi.org/10.1016/j.chnaes.2010.06.003

Zhou, S., Yu, B., Huang, Y., & Wang, G. (2014). The effect of vapor pressure deficit on water use efficiency at the subdaily time scale. *Geophysical Research,* 5005–5013. https://doi.org/10.1002/2014GL060741.Received

Zimmermann, U., Ehhalt, D., & Munnich, K. O. (1967). Soil-Water Movement and Evapotranspiration: Changes in the Isotopic Composition of the Water. In *Isotopes in Hydrology* (pp. 567–585). International Atomic Energy Agency, Vienna, Austria.

APPENDIX A

Water Spotters data collection

Weather stations and evaporation-proof precipitation collectors were deployed at nine schools across the Front Range: 1. Lyons High School (Lyons, CO), 2. Blue Mountain Elementary School (Longmont, CO), 3. Eagle Crest Elementary School (Longmont, CO), 4. Westview Middle School (Longmont, CO), 5. Trail Ridge Middle School (Longmont, CO), 6. Erie Middle School (Erie, CO), 7. Centennial Elementary School (Centennial, CO), 8. Coal Ridge Middle School (Longmont, CO), 9. Mead High School (Longmont, CO). Figure 1 shows a map of the school locations relative to the BAO site.

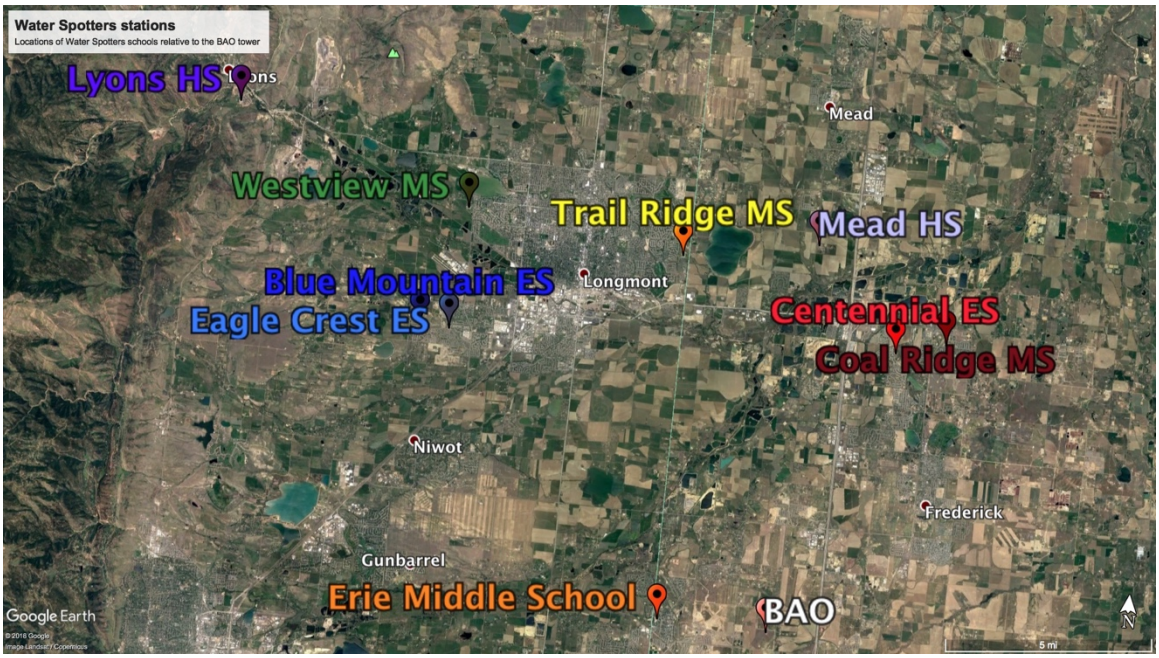

Figure 1: Locations of Water Spotters schools. Color codes match data plotted in Figure 2.

Rain samples were collected weekly by the students and teachers and mailed to the Noone laboratory for isotope analysis. Data for $\delta^{18}O$ and D_{excess} are given in the figures below, with BAO precipitation data overlaid as the dashed black line. Seasonality is evident in the collections, as with BAO, and interestingly there is an east-west difference in the isotope ratios with the

westernmost collection site (at Lyons High School) generally showing more depleted values of $\delta^{18}O$ in the summer. This is consistent with the observations for the Boulder GNIP site (at approximately the same longitude) being generally more depleted than the BAO site.

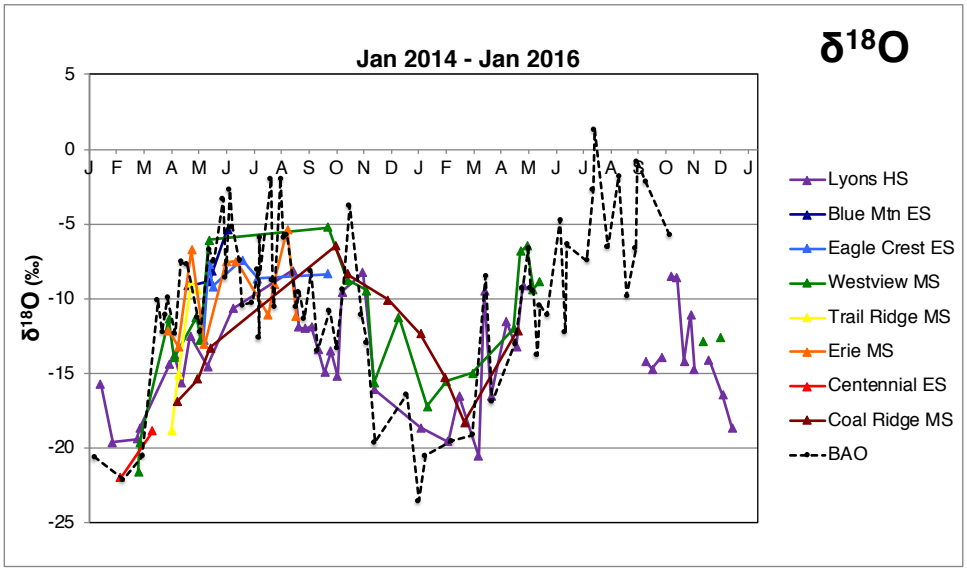

Figure 2: Precipitation $\delta^{18}O$ for samples collected from the Water Spotters schools.

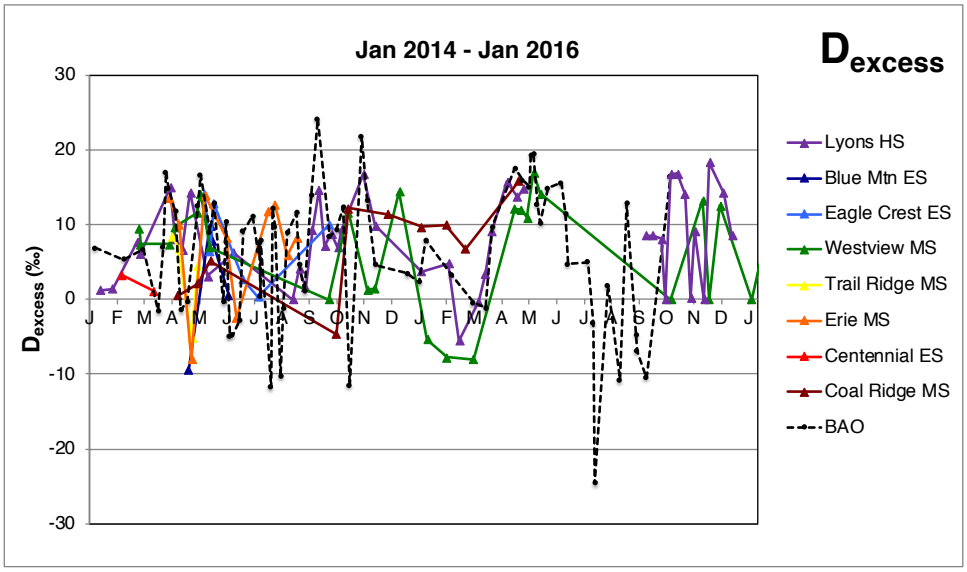

Figure 3: Precipitation D_{excess} for samples collected from the Water Spotters schools.

Meteorological data collected from the co-located weather stations provided precipitation amount information for quantifying regression fits, and Lyons HS was the only station where precipitation amount was significantly correlated to D_{excess} values ($R^2 = 0.23$, $p < 0.01$). However, as at BAO, lower precipitation amounts (likely associated with lower humidity and more evaporation) are associated with lower D_{excess} values (~5.2 ± 1.7 to 7.3 ± 1.1 ‰ associated with < 25 mm of rain) while higher precipitation amounts are associated with higher D_{excess} values (~11.7 ± 1.1 ‰ associated with > 25 mm of rain).

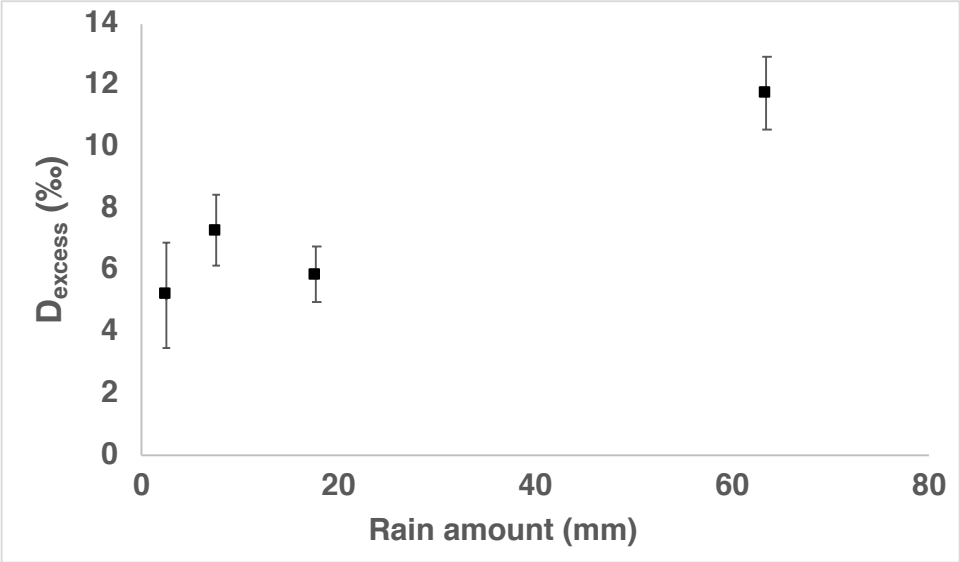

Figure 4: Observed D_{excess} in Water Spotters rain samples as a function of rain amount recorded by the co-located Davis weather stations.